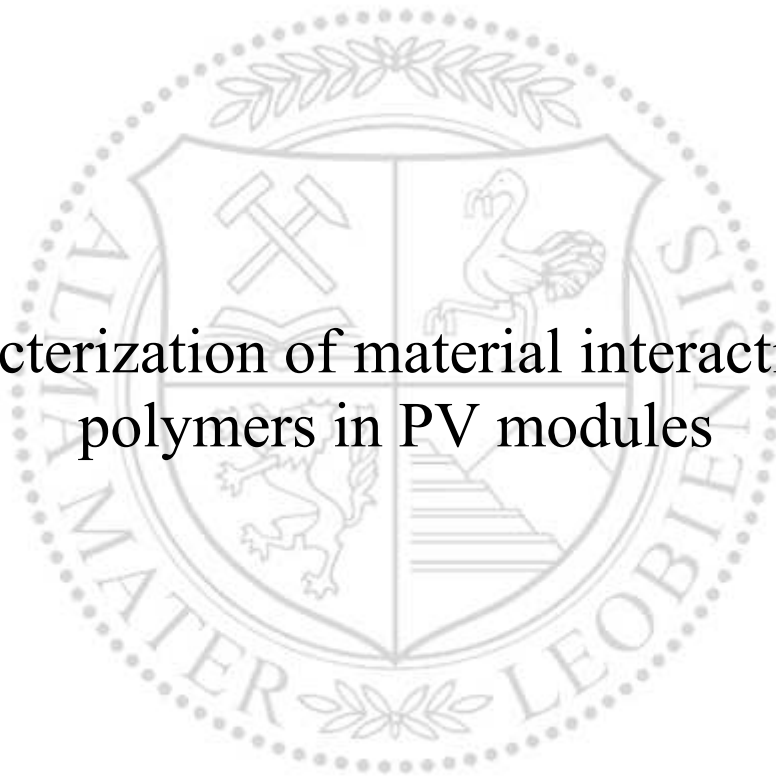Chair of Materials Science and Testing of Polymers

Doctoral Thesis

Characterization of material interactions of polymers in PV modules

Chiara Barretta

November 2022

AFFIDAVIT

I declare on oath that I wrote this thesis independently, did not use other than the specified sources and aids, and did not otherwise use any unauthorized aids.

I declare that I have read, understood, and complied with the guidelines of the senate of the Montanuniversität Leoben for "Good Scientific Practice".

Furthermore, I declare that the electronic and printed version of the submitted thesis are identical, both, formally and with regard to content.

Date 27.11.2022

_____

Signature Author
Chiara Barretta

Doctoral thesis

Characterization of material interactions of polymers in PV modules

Authored by

Chiara Barretta, M.Sc.

Submitted to

Chair of Material Science and Testing of Polymers

Montanuniversität Leoben

Leoben, Austria

Conducted at

Polymer Competence Center Leoben GmbH

Leoben, Austria

Academic Supervisor

Univ.-Prof. Dipl.-Ing. Dr.mont. Gerald Pinter

Chair of Materials Science and Testing of Polymers

Montanuniversität Leoben

Co-Supervisor

Priv.-Doz. Dipl.-Ing. Dr.mont. Gernot Oreski

Polymer Competence Center Leoben GmbH

Acknowledgements

Funding

Abstract

A photovoltaic (PV) module is a complex structure where each component has a fundamental role. The polymers that are part of a PV module are responsible for several degradation modes that happen in the field. The materials are stressed by the climatic characteristics of the surrounding environment and by the microclimate. This latter corresponds to the actual boundary conditions that the polymers in a PV module configuration experience during operation. Temperature, relative humidity, oxygen and ultraviolet (UV) radiation can strongly affect the stability of the polymers and cause their degradation. Understanding how the single factors and their combination impact on polymers on a molecular lever, transfer this knowledge to the changes that we can see on a macro scale and eventually link those changes to PV module performances is a challenging task.

The objectives of this work are to (I) define the relevant factors that characterize the polymer microclimate during the exposure in a PV module configuration, (II) identify the characteristic of the encapsulant materials that mostly change during operation and how those properties are influenced by the microclimate, (III) correlate the polymer changes to PV module performances, (IV) identify characterization methods able to effectively describe polymer changes.

After a brief introduction regarding the deployment of PV technologies and the main issues concerning reliability, a literature review is carried out to determine what the state-of-the-art is about analysis of polymer encapsulants in PV modules. In particular, the PV module reliability and above all the role of the polymer encapsulants is discussed. The second chapter gives additional information how to study reliability and compatibility of materials in PV modules, and focuses on the polymer properties that are more significant for PV applications and how to characterize them.

In the fourth chapter, the performances of the state-of-the-art encapsulant material (i.e. ethylene vinyl acetate, EVA) are compared with two newly developed materials to verify their suitability in replacing EVA. Qualitative additive analysis, characterization of thermal properties, optical properties and chemical structure are carried out to assess the impact of two artificial ageing tests on the materials performances. The results showed that UV irradiation is

the most detrimental stress factor when standalone films are exposed. A good stabilization recipe is the key factor to ensure long term stability. Additionally, a good correlation is found between the depletion of stabilizers, increase of formation of oxidation products and decrease of polymer thermal stability. The results of this study showed that the polyolefin elastomer (POE) encapsulant could be a replacement for EVA because of the very similar performances and the advantage of not producing acetic acid upon degradation.

The fifth chapter is focused on understanding how different artificial ageing tests and different microclimates influence polymer degradation and eventually PV mini-module performances using EVA as encapsulant. The polymers were extracted from three different areas of the mini-module and characterized and the electrical performances of the mini-modules were evaluated. Among the test used, the combined UV-damp heat (UV-DH) showed the most relevant impact on PV module performances, causing about 5% power loss with respect to the reference value. The power loss was mostly associated with encapsulant yellowing, caused by additive degradation. The microclimate played a fundamental role because the excess of encapsulant directly exposed to the environment experienced a much more severe degradation with respect to the material encapsulated within the mini-module.

Finally, the sixth chapter shows the effect of the microclimate on polymer degradation and PV module performances of full scale PV modules operating in two different climates for about eight years. Encapsulant samples were extracted from different areas of the PV module: from the front side, from the back side and from the back side in correspondence of the junction box. The results showed that the tropical climate had the strongest impact on the electrical performances causing power losses between 10% and 45%. The power degradation was mostly associated with corrosion of metallization and interconnections that were caused by encapsulant degradation, with formation of acetic acid, and humidity ingress. In this study, the additive analysis proved itself again to be a valid tool to better understand the mechanisms behind polymer degradation. The acetic acid production, indeed, was mostly associated with a depletion of the UV absorber that had a dramatic impact on the EVA stability. Additionally, the local higher temperatures in

correspondence of the junction box caused a non-homogeneous depletion of the primary antioxidant for the modules exposed in the tropical climate.

Kurzfassung

Ein Photovoltaik (PV)-Modul hat eine komplexe Struktur, bei der jede Komponente eine grundlegende Rolle spielt. Die Polymere, die Teil eines PV-Moduls sind, sind für mehrere Degradationsprozesse verantwortlich, die in der Praxis auftreten. Die Materialien werden durch die klimatischen Eigenschaften der Umgebung und durch das Mikroklima belastet. Letzteres entspricht den tatsächlichen Randbedingungen, denen die Polymere in einer PV-Modulkonfiguration während des Betriebs ausgesetzt sind. Temperatur, relative Luftfeuchtigkeit, Sauerstoff und ultraviolette (UV) Strahlung können die Stabilität der Polymere stark beeinflussen und deren Abbau verursachen. Es ist eine anspruchsvolle Aufgabe zu verstehen, wie sich die einzelnen Faktoren und ihre Kombination auf molekularer Ebene auf die Polymere auswirken, dieses Wissen auf die Veränderungen zu übertragen, die wir auf der Makroebene sehen können, und diese Veränderungen schließlich mit der Leistung der PV-Module in Verbindung zu bringen.

Die Ziele dieser Arbeit sind (I) die Definition der relevanten Faktoren, die das Polymer-Mikroklima während der Exposition in einer PV-Modulkonfiguration charakterisieren, (II) die Identifizierung der Eigenschaften der Verkapselungsmaterialien, die sich während des Betriebs am stärksten verändern, und wie diese Eigenschaften durch das Mikroklima beeinflusst werden, (III) die Korrelation der Polymerveränderungen mit den PV-Modulleistungen, (IV) die Identifizierung von Charakterisierungsmethoden, die in der Lage sind, Polymerveränderungen effektiv zu beschreiben.

Nach einer kurzen Einführung über den Einsatz von PV-Technologien und die wichtigsten Fragen zu ihrer Zuverlässigkeit wird eine Literaturübersicht erstellt, um den Stand der Technik bei der Analyse von Polymerverkapselungen in PV-Modulen zu ermitteln. Insbesondere wird die Zuverlässigkeit von PV-Modulen und vor allem die Rolle der Polymerverkapselungen diskutiert. Das zweite Kapitel enthält zusätzliche Informationen zur Untersuchung der Zuverlässigkeit und Kompatibilität von Materialien in PV-Modulen und konzentriert sich auf die Polymereigenschaften, die für PV-Anwendungen am wichtigsten sind, sowie auf deren Charakterisierung.

Im vierten Kapitel werden die Leistungen des modernsten Verkapselungsmaterials (d. h. Ethylenvinylacetat, EVA) mit zwei neu entwickelten Materialien verglichen, um ihre Eignung als Ersatz für EVA zu prüfen. Qualitative Additivanalysen, die Charakterisierung der thermischen Eigenschaften, der optischen Eigenschaften und der chemischen Struktur werden durchgeführt, um die Auswirkungen von zwei künstlichen Alterungstests auf die Leistungen der Materialien zu bewerten. Die Ergebnisse zeigen, dass die UV-Bestrahlung der schädlichste Stressfaktor ist, wenn die Folien alleinstehend sind. Eine gute Stabilisierungsrezeptur ist der Schlüsselfaktor für die Gewährleistung der Langzeitstabilität. Außerdem wurde eine gute Korrelation zwischen dem Abbau von Stabilisatoren, der Zunahme der Bildung von Oxidationsprodukten und der Abnahme der thermischen Stabilität des Polymers festgestellt. Die Ergebnisse dieser Studie zeigen, dass das Polyolefinelastomer (POE) ein Ersatz für EVA sein könnte, da es sehr ähnliche Eigenschaften aufweist und den Vorteil hat, dass beim Abbau keine Essigsäure entsteht.

Das fünfte Kapitel befasst sich mit der Frage, wie verschiedene künstliche Alterungstests und unterschiedliche Mikroklimas den Polymerabbau und schließlich die Leistung von PV-Mini-Modulen mit EVA als Verkapselungsmaterial beeinflussen. Die Polymere wurden aus drei verschiedenen Bereichen des Mini-Moduls extrahiert und charakterisiert, sowie die elektrischen Leistungen der Mini-Module bewertet. Unter den verwendeten Tests zeigte die kombinierte UV-Feuchtwärme (UV-DH) die größte Auswirkung auf die Leistung der PV-Module und verursachte einen Leistungsverlust von etwa 5 % im Vergleich zum Referenzwert. Der Leistungsverlust stand hauptsächlich im Zusammenhang mit der Vergilbung der Verkapselung, die durch den Abbau von Additiven verursacht wurde. Das Mikroklima spielte eine wesentliche Rolle, da der Überschuss an Verkapselungsmaterial, der direkt der Umgebung ausgesetzt war, eine viel stärkere Degradation erfuhr als das Material, das innerhalb des Mini-Moduls eingekapselt war.

Das sechste Kapitel schließlich zeigt die Auswirkungen des Mikroklimas auf den Polymerabbau und die Leistung von PV-Modulen in Originalgröße, die etwa acht Jahre lang in zwei verschiedenen Klimazonen betrieben wurden.

Verkapselungsproben wurden aus verschiedenen Bereichen des PV-Moduls entnommen: von der Vorderseite, von der Rückseite und vom Bereich der Anschlussdose. Die Ergebnisse zeigten, dass sich das tropische Klima am stärksten auf die elektrische Leistung auswirkte und Leistungsverluste zwischen 10% und 45% verursachte. Die Leistungsverschlechterung resultierte hauptsächlich aus der Korrosion der Metallisierung und der Verbindungen. Die Korrosion wurde aus den Abbau des Verkapselungsmaterials, die Bildung von Essigsäure und das Eindringen von Feuchtigkeit verursacht. In dieser Studie erwies sich die Additivanalyse erneut als nützliches Instrument, um die Mechanismen der Polymerdegradation besser zu verstehen. Die Essigsäurebildung war in der Tat meist mit einer Erschöpfung des UV-Absorbers verbunden, was sich dramatisch auf die Stabilität des EVA auswirkte. Darüber hinaus verursachten die lokal höheren Temperaturen in der Nähe der Anschlussdose einen inhomogenen Abbau des primären Antioxidationsmittels bei den im tropischen Klima exponierten Modulen.

Table of Contents

List of abbreviations

AM	Air mass
ATR	Attenuated Total Reflectance
BHT	Butylated Hydrohytoluene
BIPV	Building Integrated Photovoltaic
COVID	Coronavirus Disease
c-Si	Crystalline Silicon
DART-MS	Direct Analysis in Real Time Mass Spectrometry
DH	Damp Heat
DSC	Differential Scanning Calorimetry
EGA	Evolved Gas Analysis
EL	Electroluminescence
EVA	Ethylene Vinyl Acetate
FF	Fill factor
FT-IR	Fourier Transform Infrared
GDP	Gross Domestic Product
GHI	Global horizontal irradiance
HALS	Hindered Amine Light Stabilizers
IEA	International Energy Agency
IEC	International Electrotechnical Commission
HPLC	High performance liquid chromatography
IR	Infrared
I_{sc}	Short circuit current
LED	Light-emitting diode
LeTID	Light and elevated temperature induced degradation
LID	Light induced degradation
MS	Mass spectrometry
NIR	Near IR
NIST	National Institute of Standard and Technology
Non-OECD	Non- Organization for Economic Co-operation and Development
OECD	Organization for Economic Co-operation and Development
OI	Oxidation Index

PDMS	Polydimethylsiloxane
PE	Polyethylene
PET	Polyethylene Terephthalate
PID	Potential Induced Degradation
P_{MAX}	Maximum power point
PO	Polyolefin
POA	Plane of array
POE	PO Elastomer
PV	Photovoltaic
PVB	Polyvinyl Butyral
RD&D	Research, Development and Demonstration
RH	Relative humidity
R_S	Series resistance
T_5	Temperature corresponding to 5% weight loss
T_{40}	Temperature corresponding to 40% weight loss
TC	Thermal cycle
TD-GC/MS	Thermal Desorption Gas Chromatography coupled to Mass Spectrometry
T_g	Glass transition temperature
TGA	Thermogravimetric Analysis
T_m	Melting temperature
T_{mod}	Module temperature
TPO	Thermoplastic PO
TPSE	Thermoplastic silicon elastomer
TS	Technical specification
UV	Ultraviolet
UV-Vis-NIR	Ultraviolet-Visible-Near Infrared
V_{OC}	Open circuit voltage
W_P	Watt peak
WVTR	Water Vapor Transmission Rate
YI	Yellowness Index

1 Introduction

The energy demand has largely grown over the past decades and it is expected to further increase of about 50% by 2050 [1]. In particular, it is forecasted that in the next years fast developing countries, especially in Asia, will drive the growth of energy consumption [1]. Improvement of life quality conditions and urbanization in fast developing countries have contributed to the increase of energy demand [2]. In Organization for Economic Co-operation and Development (OECD) countries, such as many countries in Europe and United States, the increase of energy consumption's rate has slowed down in the last 10-12 years and in some cases even decreased. On the other hand, in non-OECD countries, such as China or India, the global electricity consumption has rose with a rate higher than the increase of the global population, Figure 1.1 [3].
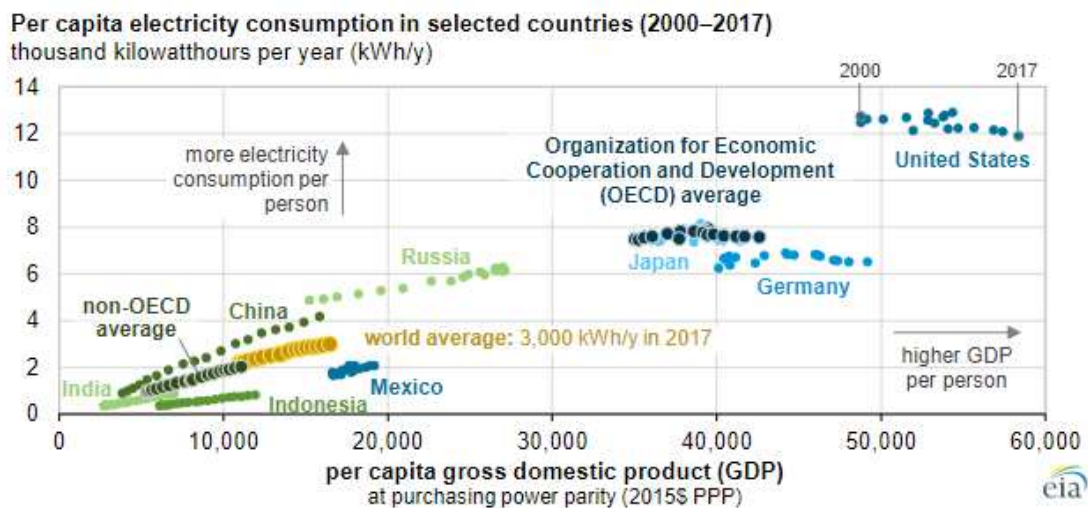
Figure 1.1: Per capita energy consumption versus per capita gross domestic product (GDP) in selected countries from 2000 to 2017 [3].

The decrease of energy demand of 5.3%, in Europe [4], can be seen also as a positive result of increasing efforts in research towards improving efficiency [5]. Additionally, the mix of sources producing electricity has shifted over the years towards renewable resources and especially towards photovoltaic [4]. Figure 1.2 shows towards which areas International Energy Agency (IEA) countries directed their investments in the last 45 years, between 1974 and 2019. If in 1974 almost 75% of the funding for Research, Development and Demonstration (RD&D) was directed towards nuclear energy, nowadays it is

possible to see how the value has decreased to about 22%. At the same time, more and more interest, and therefore investments, are focused on cross-cutting, renewable energies and improvement of energy efficiencies. Additionally, in the last two decades, particular attention was given to hydrogen, fuel cells and storage solutions.
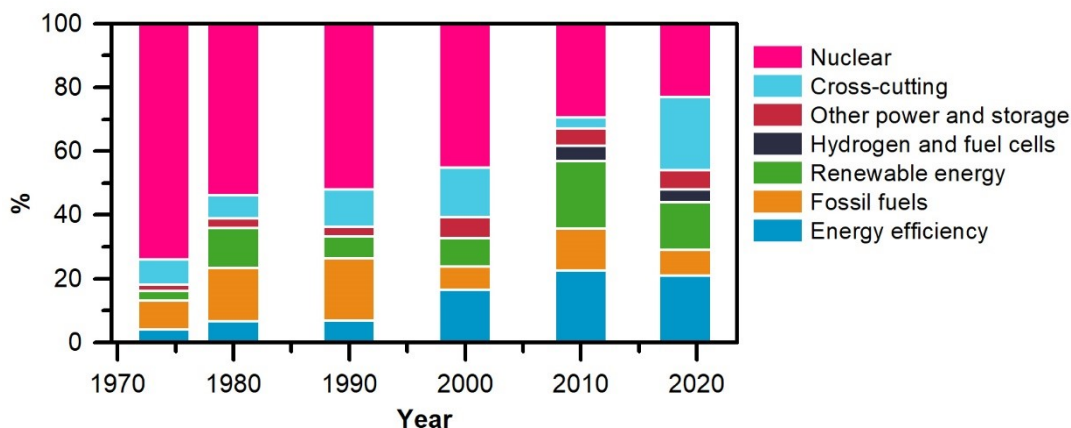
Figure 1.2: Evolution of IEA total public energy RD&D by technology, 1974-2019, re-drawn from [5].

In this framework, it is forecasted that there will be a boost towards electricity produced from renewable resources and that will be the main source of electricity in 2050, overcoming the electricity produced by means of non-renewable resources [2]. Figure 1.3 represents the evolution of the energy mix over the last 10 years, on the left side, and how the electricity generation by source has changed during 2019, on the right side.
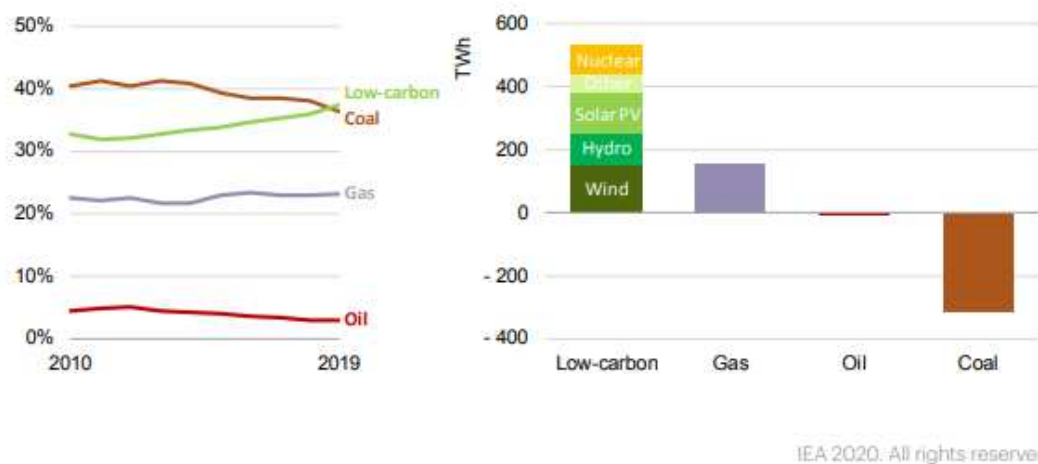
Figure 1.3: Global power mix over time and year-on-year change in electricity generation by source in 2019 [4].

Fossil fuels have seen a general decrease in their consumption towards electricity generation in the last 20 years, only natural gas has experienced a slight increase. At the same time, the production of electricity by means of low carbon sources (such as renewables) was boosted.

The year 2020 will be remembered as the year of the spread of the Coronavirus Disease (COVID)-19 pandemic. Beside the tremendous impact on world population's health and economy, the COVID-19 pandemic has had a significant impact on energy demand and relative impact of energy sources in electricity production. The strict confinement measures, indeed, caused a strong decrease of the energy demand (20% or more [6]), which partially recovered when the restrictive measures were eased [7]. However, the electricity consumption has reached the same values as in 2019 in September/October 2020, before confinement measures were adopted again in several countries resulting in a new decrease of energy demand [7]. In this framework, the importance of renewable sources was highlighted because the whole electricity production saw a shift towards renewables thanks to their low operating costs compared to fossil fuels and priority access to the grid [7].

In the last 10 years, the cumulative photovoltaic installation increased exponentially from 70.4 GW (2011) to 758.9 GW (2020) with a share of electricity production in 2019 at about 3.7% worldwide [8]. Europe had the lead of the annual photovoltaic (PV) installation until 2012, when China began to take over and rapidly overcome the European annual PV installation capacity [9]. In 2020, the five leading countries for cumulative PV capacity were China (accounting for the 33.4%), followed by USA (12.3%), Japan (9.4%), Germany (7.1%) and India (6.2%) [8]. Similarly, PV module production takes place nowadays especially in China (71%), South Korea (6%) and Malaysia (6%), with Europe accounting for only the 2% of the PV production share [9].

Since when the PV technology was established, the most widely produced PV technology was based on c-Si solar cells. Over the years, of course, many different technologies were developed, such as thin films, organic photovoltaics and recently perovskites, but none of them has so far been able to replace c-Si based PV modules. About 95% of the PV modules produced on 2020 were based on crystalline silicon technology [10]. The ratio between mono- and multi-crystalline silicon was not always the same, with mono- prevailing over multi-

from the 1980s until the early 2000s until when the trend was inverted. From 2017 on, the trend has shifted again towards mono-crystalline based PV modules, which corresponds nowadays to about the 65% of the PV module produced. Over the years, the development of the c-Si PV technology was accompanied by the development of the so-called *packaging materials* constituting the PV module itself. Different polymers, as result of industrial and technological material development, reached the market and were used as encapsulants and backsheets in modules.

For many years, the state-of-the art PV module configuration was characterized by an ethylene copolymer-based encapsulant, namely Ethylene Vinyl Acetate (EVA), and backsheet with a Polyethylene Terephthalate (PET) core layer laminated between two layers of fluorinated polymers. However, since the introduction of the EVA as encapsulant, which replaced silicone-based materials, the problem of the long-term reliability of the packaging materials has become a key factor in the assessment of the reliability of the whole technology. Corrosion of metallization and interconnections as well as discoloration of the EVA encapsulants are only two of the most common issues related to the use of this material. Even though significant steps forward in understanding degradation mechanisms of EVA and improvements in its formulations have been made there are still problems connected to the use of this encapsulant as packaging materials. Additionally, nowadays there is significant attention on the environmental impacts and the recyclability of the PV modules. Improving the impact often means increasing the lifetime of the modules, together with applying specific module design concepts able to facilitate the recycling process, recovery of valuable materials or end of life scenarios more sustainable than landfilling. From this point of view, it becomes vitally important to use materials that are able to withstand operating periods of 40 years of more and, alternatively, to develop materials that can replace the current most widely used EVA, being competitive in terms of costs and with better long-term performances.

1.1 Structure of the thesis

The work is structured into the following chapters:

1. Introduction.

2. State of the Art: Analysis of polymer encapsulants in PV modules.
3. Experimental methods and analytical techniques used to describe polymer degradation.
4. Comparison of performances of newly developed PV encapsulants exposed to different artificial ageing tests.
5. Artificial ageing of PV mini-modules laminated with EVA as encapsulant and exposed to different artificial ageing tests.
6. Analysis of degradation of EVA encapsulant in PV modules operating in different climates.
7. Summary.

In the **introduction**, a brief overview regarding energy demand and the role of PV technologies as a renewable source for electricity production is discussed. Additionally, information regarding PV reliability issues are given.

The **second chapter** describes the state of the art regarding polymer materials used as encapsulants in PV applications, the degradation mechanisms of polymers ageing within a PV module configuration and the effects of polymers degradation on the module itself. The focus of this chapter is to describe the typical procedures used to describe polymer degradation in PV, the main characterization methods and analytical techniques applied, their advantages and their limitations.

The main experimental methods and analytical techniques used to describe polymer degradation are described in the **third chapter**.

The performances of two newly developed encapsulants compared to the state-of-the-art EVA encapsulant are described in the **fourth chapter**. Standalone materials thermally pre-treated were subjected to two different weathering tests, with and without ultraviolet (UV) radiation. The changes in additive composition, optical and thermal properties, chemical structure (investigated by means of Thermal Desorption Gas Chromatography coupled to Mass Spectrometry (TD-GCMS), Ultraviolet-Visible-Near Infrared (UV-Vis-NIR) spectroscopy, Differential Scanning Calorimetry (DSC), Thermogravimetric Analysis (TGA) and Fourier Transform Infrared (FT-IR) spectroscopy, respectively) of the analyzed polymers are monitored throughout the exposure to artificial weathering tests and discussed. A novel approach is presented to

derive information of oxidation induction time/dose from TGA measurements that well correlate with results obtained by using oxidation indices.

To better simulate what actually happens within a standard module configuration, PV mini-modules were laminated using EVA as encapsulant and exposed to artificial ageing tests (Damp Heat (DH), UV and UV-DH combined tests). The electrical performances of the mini-modules before and after the exposure to the artificial ageing tests are described in the **fifth chapter**. Additionally, the impact of changes in material properties with changes in PV power generation is discussed.

The **sixth chapter** deals with the analysis of EVA encapsulant withdrawn from full-scale modules that were in operation in different locations, corresponding to different climates. The material properties and electrical performances of modules exposed in Germany and in the Caribbean are compared to the material characteristics of a module that was stored in the dark and considered as reference. The objective of this chapter is to evaluate the influence of the different climates on materials changes and their effects on the power generated. Additionally, the EVA encapsulant object of the investigation was withdrawn from different areas of the module, thus allowing to get information regarding the impact of the microclimate.

Finally, a comparison between the information learned with the different sample configurations and the conclusions are presented in the **seventh chapter**.

1.2 References

[1]   IEA - International Energy Agency, *Electricity demand and renewables generation growth, 2010-2019.* [Online]. Available: https://www.iea.org/data-and-statistics/charts/electricity-demand-and-renewables-generation-growth-2010-2019 (accessed: Dec. 6 2020).

[2]   EIA - U.S. Energy Information Administration, *EIA projects nearly 50% increase in world energy usage by 2050, led by growth in Asia.* [Online]. Available: https://www.eia.gov/todayinenergy/detail.php?id=42342 (accessed: Dec. 6 2020).

[3]   EIA - U.S. Energy Information Administration, *Global electricity consumption continues to rise faster than population.* [Online]. Available: https://www.eia.gov/todayinenergy/detail.php?id=44095 (accessed: Dec. 6 2020).

[4]   IEA - International Energy Agency, "Global Energy Review 2019: The latest trends in energy and emissions in 2019," IEA - International Energy Agency, Paris, 2020. Accessed: Dec. 6 2020. [Online]. Available: https://www.iea.org/reports/global-energy-review-2019

[5]   IEA - International Energy Agency, "Energy Technology RD&D Budgets: Overview," Paris, Apr. 2020. Accessed: Dec. 6 2020. [Online]. Available: https://www.iea.org/reports/energy-technology-rdd-budgets-2020

[6]   IEA - International Energy Agency, "Global Energy Review 2020: The impacts of the Covid-19 crisis on global energy demand and CO2 emissions," IEA - International Energy Agency, Paris, 2020. Accessed: Dec. 6 2020. [Online]. Available: https://www.iea.org/reports/global-energy-review-2020

[7]   IEA - International Energy Agency, "Covid-19 impact on electricity," IEA - International Energy Agency, Paris, Nov. 2020. Accessed: Dec. 6 2020. [Online]. Available: https://www.iea.org/reports/covid-19-impact-on-electricity#changes-in-electricity-mix

[8]   A. Jäger-Waldau, I. Kaizuka, J. Donosco, A. Detollenaere, and G. Masson, "Snapshot of Global PV Markets 2021," Report IEA-PVPS T1-39:2021, Apr. 2021. Accessed: Feb. 14 2022. [Online]. Available: https://iea-pvps.org/snapshot-reports/snapshot-2021/

[9]   G. Masson and I. Kaizuka, "IEA PVPS Trends in Photovoltaic Applications 2020," IEA PVPS, 2020. [Online]. Available: https://iea-pvps.org/wp-content/uploads/2020/11/IEA_PVPS_Trends_Report_2020-1.pdf

[10]   Fraunhofer Institute for Solar Energy Systems, ISE, *Photovoltaics Report, updated 24 February 2022* (accessed: March 13th 2022).

2 State-of-the-Art: Analysis of polymer encapsulants in PV modules

2.1 PV module reliability

A common crystalline silicon (c-Si) PV module is a multilayer structure, as shown in Figure 2.1, constituted by different layers. Each layer has to withstand environmental stresses and maintain the desired properties during the entire lifetime of the PV module.

1. Front-sheet
2. Encapsulant
3. c-Si solar cells
4. Encapsulant
5. Back-sheet
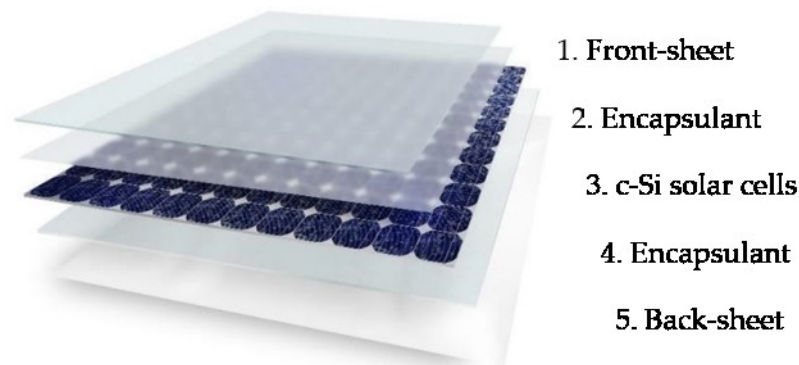
Figure 2.1: c-Si PV module stack configuration.

PV modules can fail at various phases of their lifetime. The so-called *infant failures* take place during the early stages of the PV module's lifetime and are the most frequent. They might be due to bad installation or flaws and involve in particular junction boxes, string interconnections, glass breakage and loose frames [1]. During operation, due to the effect of UV radiation, temperature and humidity, polymers can degrade and affect the performances of the modules causing, in extreme cases even failures (*mid-life failures*).

Polymers (encapsulant and backsheets) are considered responsible for 9% of failures that can happen during medium and long term operation [1]. The most common degradation modes observable due to polymer degradation are corrosion of cells and interconnects, discoloration of encapsulant and backsheets, delamination, snail trails, potential induced degradation (PID), backsheet cracks and chalking [2–5]. Delamination processes might take place at different interfaces, i.e. between the different PV modules components (glass / encapsulant, encapsulant / cell, encapsulant / interconnections, encapsulant / backsheet and so on) as well as between the backsheet layers, in case of laminated backsheets.

Eventually, at late stages of PV module's lifetime, there is again a rise of failure rates that are due to a further increase of the extent of existing degradation phenomena. The modules reach the end of the lifetime when the power output is no longer acceptable and/or when a safety issue occurs.

2.2 EVA as encapsulant in PV: advantages and limitations

EVA is an ethylene copolymer characterized by the presence of ethylene and vinyl acetate moieties, as shown in Figure 2.2, usually in the range of 28 wt.% and 33 wt.%. Upon the exposure to high temperature, UV irradiation and humidity, a complex scheme of photo-oxidation reactions takes place, as can be seen in Figure 2.3.
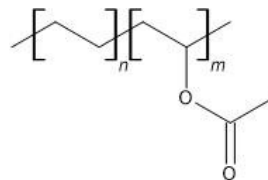
Figure 2.2: Molecular structure of EVA.
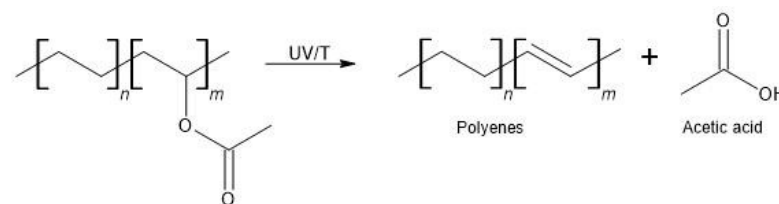
Norrish II reaction - Deacethylation
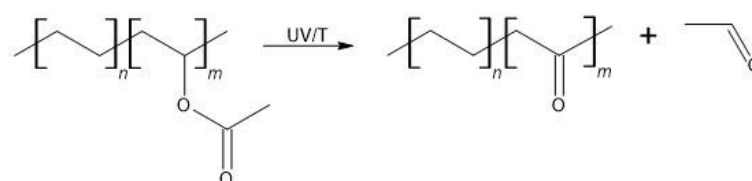
Norrish III reaction - Formation of ketones and aldehydes
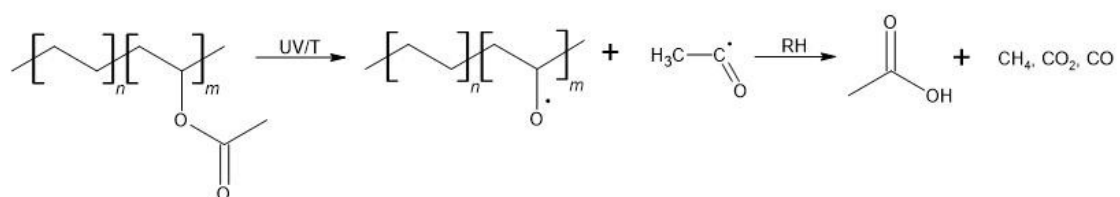
Norrish I reaction - Hydrolysis

Figure 2.3: Reaction scheme of EVA degradation [6].

Deacetylation results in acetic acid formation and it is followed by oxidation with development of hydroxyl/hydroperoxides, ketones, α-β unsaturated carbonyl groups, conjugated dienes, lactones and several vinyl types [7, 8]. Eventually, breakdown of the man polymer chain takes place. Formation of unsaturation by deacetylation makes EVA even more susceptible to further oxidation processes [6]. Acetic acid is a relevant issue for the reliability of the whole PV module because it reduces the pH of the surrounding environment and will catalyze corrosion processes of metallization and interconnections [9–11]. Corrosion causes an increase of series resistance of the module and consequent decrease in power output [12]. Additionally, acetic acid can lead to delamination at the glass-cell interface [13, 14]. Delamination further influences module performances because it facilitates moisture ingress with consequent additional increase of series resistance with time [15]. Potential induced degradation (PID) is a degradation mode that affects PV modules and one of the causes of its occurrence is addressed as the encapsulation material. In general, PID is related to transport of sodium ions from the glass through the encapsulant that penetrate the front junction of solar cells producing module degradation upon the exposure to voltage stress [16]. Acetic acid, additionally, enhances the compatibility of EVA with Na$^+$ ions, favoring PID effects [5, 16]. A recent study [17] showed that multiple mechanisms are connected with the PID phenomena and that mainly two types of PID exist. They are the polarization type (PID-p), the shunting type (PID-s), and especially the PID-p might be strongly influenced by encapsulant's resistivity.

The most well-known PV degradation mode associated to EVA degradation is its discoloration. Discoloration is an important issue, not only because of its aesthetic effects, but mainly because it reduces the light transmitted towards the solar cells and affects, decreasing, the power generated by the module. Discoloration of EVA of different extent (from yellow to brown) has been often observed in the field [18–22]. Many hypotheses have been developed in research regarding the causes of EVA discoloration, and they will be described more in depth in section 2.6.1., dealing with optical properties of encapsulants.

2.3 From EVA to newly developed encapsulants

An encapsulant material has to provide the following functions [6]:

- Structural support to the PV modules components during its whole lifetime, from production to disposal;
- Optimal optical coupling ensuring transmittance values above 90% and a maximum loss < 5% after 20 years;
- Protection from environmental stress factors, including exposure to pollutants and hazardous substances;
- Electrical insulation to protect the PV module's components, as well as for safety reasons.

In the early stages of the development of the PV technologies, PDMS based materials were the most widely used encapsulants for their intrinsic stability. The dissociation energy necessary to cleave Si–O bonds is indeed higher (~108 kcal mol^{-1}) than the energy needed to cleave C–C bonds, typical of polyolefin based encapsulants (~83 kcal mol^{-1}) [23]. In the 1960s and 1970s Polydimethylsiloxane (PDMS) based encapsulants were replaced by EVA thanks to the balance of acceptable reliability performances and low costs. Many materials have been developed as PV encapsulants and their most interesting properties are listed in Table 2.1.

Over the years EVA has become the market leader for typical glass-backsheet module configuration, whereas Polyvinyl Butyral (PVB) has taken the leadership over glass-glass modules, especially in building integrated photovoltaic (BIPV) applications [2]. Significant improvement of the formulation of the EVA itself led to the overcoming of issues such as PID [24], e.g. PID-free EVA are nowadays common materials on the market. Additionally, new EVA formulations (e.g. EVA with white fillers, used on the back side of the module) claim to increase the amount of light reflected from the back side of the modules and therefore increase the power generated [25, 26]. However, now it seems that the trend is again shifting towards different materials other than EVA.

Table 2.1: PV encapsulants and their main properties [5, 16, 27–32].

Encapsulant	Polymer type	Glass Transition Temperature	Processing Temperature	Volume Resistivity	Water Vapor Transmission Rate (WVTR)	Young's modulus	Refractive index (n)
		°C	°C	Ω*cm	g m^{-2} day^{-1}	MPa	-
EVA	Elastomer	−40 to 34	140-160	10^{14}	34	≤ 68	1.48-1.49
POE (polyolefin elastomer)	Elastomer	−50 to -40	140-160	10^{15}-10^{16}	3.30	≤ 30	1.49
PDMS	Elastomer	≤ −100	80 (casting process)	10^{14}-10^{15}	130-200	≤ 10	1.38-1.58
PVB	Thermoplastic	−12 to +20	140-160	10^{10}-10^{12}	40.05	≤ 11	1.48
Ionomer	Thermoplastic	−40 to -50	140-160	10^{16}	0.19	≤ 300	1.49
TPO (thermoplastic polyolefin)	Thermoplastic elastomer	−60 to -40	140-160	10^{14}-10^{18}	2.85	≤ 32	1.48

The development of new polyolefin-based materials, especially, has driven the interest towards the replacement of EVA. The new materials do not present vinyl acetate moieties and therefore do not produce acetic acid upon degradation. The alternative polyolefin-based materials might be a solution to overcome the PV degradation modes mainly related to acetic acid. It is forecasted that the newly developed polyolefin (PO) based encapsulant will be about 30% for the market by 2030 [33], as shown in Figure 2.4.
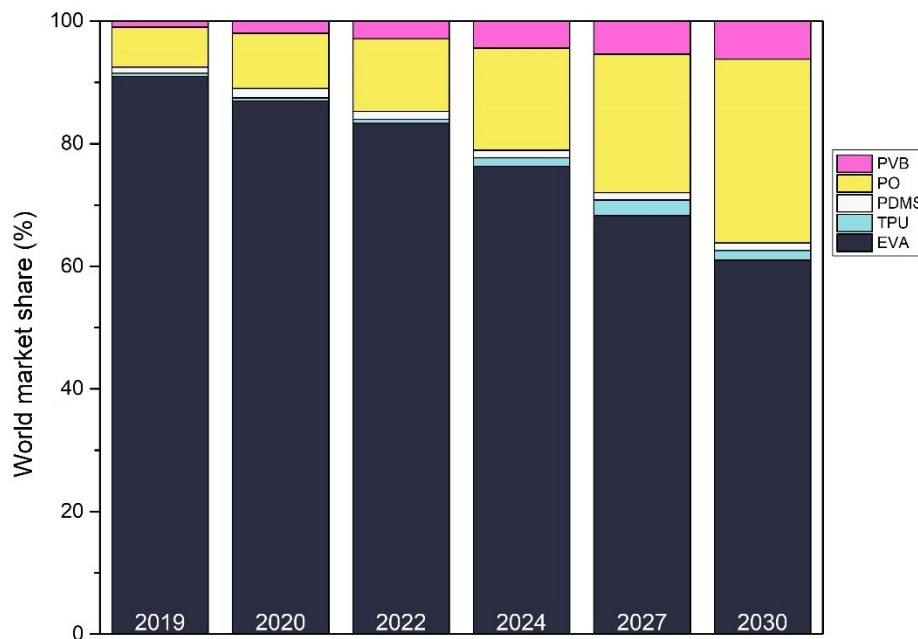
Figure 2.4: Current encapsulant market share and forecast until 2030 (reconstructed from [33]).

PO based materials, Figure 2.5, are characterized by a polyethylene backbone and acrylates, acrylic acids or n-alkanes as side groups [34].
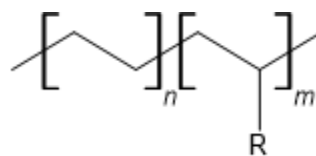
Figure 2.5: Chemical structure of a generic PO based encapsulant.

The materials mentioned above have the advantage that they can be processed with the same equipment used to produce traditional PV modules with EVA and do not require special processing equipment. However, lamination conditions need to be optimized accordingly depending on the encapsulant used [21]. POEs have melting temperature similar to EVA and might include

crosslinking agents in their formulation. In this case, processing conditions would be very similar to EVA. TPOs, instead, do not chemically crosslink; they melt at a temperature higher than EVA, but have the advantage that shorter lamination times are sufficient to ensure good adhesion between the module's components. No additional time is needed to allow the crosslinking reaction to take place. Additionally, multi-layered combinations of EVA and POE were recently developed and tested with the objective of combining the advantages that both materials can provide [25]. A layer of EVA, thanks to its superior adhesion properties is placed directly in contact with the glass, whereas the POE layer is on the side that is directly in contact with the cells. The aim of this configuration is to protect the cells, the metallization and the interconnections from the damages that might result from acetic acid production.

POE and TPO specific formulations for photovoltaic applications are on the market since a relatively short time and not enough modules using these materials are currently operating in the field. The new materials caught the attention of the academic and industrial sector [5, 35–40], but more studies are necessary and especially long-term indoor and outdoor exposure investigations are crucial to discover new degradation modes that might appear. Additionally, the effects of the long-term interaction between the new encapsulant materials and the other module components are still an open question.

2.4 Reliability assessment of polymers in PV

Currently, the qualification of c-Si PV modules follows the regulations of standardized tests such as International Electrotechnical Commission (IEC) 61215 series "Design qualification and Type Approval" [41, 42] and IEC 61730 series "Photovoltaic (PV) module safety qualifications" [43, 44]. The main purpose of these standards is to qualify new modules entering the market to be suitable for commercialization. However, the application of the standards mentioned above lacks in giving indication regarding long-term artificial testing procedures able to assess the reliability of the modules that are supposed to be exposed in the field for 25 years or even longer. Additionally, the standards do not consider the possible installation of the same module types in different climates, and therefore the influence of the different stress loads that the modules might experience throughout their lifetime. The problem of

long-term material compatibility and interaction is also not properly addressed in the standards. The described testing procedures and testing times are not appropriate to simulate degradation modes and mechanism taking place in real operation. Nevertheless, the qualification of new modules according to the existing standards allows, at least, to determine whether a product would dramatically fail in the short-term of its lifetime or not, especially because of bad module design. For all the reason mentioned above, industry and academia have been intensively working in the last years to develop testing procedures and sequences able to address and give a solution to the very relevant problem of simulating precisely what happens in the field. The series standards IEC 62788 and IEC Technical Specifications (TS) 62788 give some indications regarding testing of properties of interest of materials such as polymeric encapsulants and backsheets used in PV. However, the standards and technical specifications mentioned above do not give a comprehensive description of all the tests that might be performed on polymers to explain their behavior upon ageing.

Polymers undergo the action of internal and external stress factors that can cause changes in molecular, supermolecular or phase structure. Those alterations might lead to modifications of physicochemical processes essential during all the steps that characterize the life of a polymer: manufacturing, production, storage and operation [45]. During their lifetime, polymers can be subject to chemical as well as physical ageing processes. The main difference between them is that physical processes might be reversible, whereas chemical processes irreversibly alter the polymer's structure. Chemical processes involve mainly changes in molecular structure (such as chain scission, chain branching and crosslinking), formation of functional groups and elimination of low molecular weight products [45]. Chemical changes mainly affect optical and mechanical properties. Physical ageing processes are always the results of thermodynamically unstable states and changes in physical structure are often connected to mechanical stresses leading to cracks and/or changes in dimensions [45]. Physical ageing processes, moreover, might have effect on water absorption and diffusion as well as oxygen diffusion [45]. Physical processes are post crystallization, relaxation, separation, agglomeration, migration, extraction and loss of plasticizers [45].

Physical and chemical ageing processes are often taking place simultaneously, which complicates very much the understanding of polymer degradation behavior as well as the replication in laboratory conditions of the degradation modes observed in the field.

2.5 Design of reliability study

To analyze how polymers degrade in PV modules upon ageing it is necessary to design experiments able to reproduce known failure modes occurring during exposure. Additionally, it is of crucial importance to test materials and material combinations to assess how they behave upon the application of environmental stress factors. The current standards do not give yet satisfactory answers to these issues, as described in the previous subchapter, and relevant work is ongoing to introduce standards able to give more precise guidelines of testing procedures to apply to assess the reliability of PV materials and PV modules. The most reliable solution would be to test the modules in the real environment of application throughout their lifetime. However, it is unrealistic the idea of exposing the modules for 20-25 years in the field before assessing materials' performances and compatibility. It is, therefore, necessary to develop artificial ageing tests, procedures and sequences able to replicate what happens in the filed in a shorter time, acceptable also for industrial development.

2.5.1 Artificial simulation of real climatic conditions

One of the most challenging aspects of the long-term stability assessment is the technological possibility to simulate indoor the environmental conditions that a PV module would experience in real outdoor operation in an accelerated way. Substantial effort was put into the development of chambers able to apply several stresses simultaneously as well as test sequences that allowed to reproduce degradation modes of encapsulant and backsheets occurring outdoors [46–49].

Climate specific accelerated ageing tests have been developed by Eder et al. [50]. They considered four specific climate profiles (tropical, arid, moderate and alpine) and established 14 climate specific artificial ageing test procedures. Different testing protocols resulted in different PV modules behavior. Additionally, it is important to keep always in mind that the artificial testing

procedure that is applied to the modules needs to be designed specifically for a technology/configuration. It means, for example, that a testing procedure that works in accelerating degradation modes specific for glass/glass configuration might not be appropriate to provoke degradation modes that take place in glass/polymer backsheet configuration, because of the different microclimate.

2.5.2 Test samples

The climatic conditions have a strong impact on module behavior as well as on polymers behavior. However, the microclimate that the polymers and PV module components actually experience is the most relevant aspect that determines the occurrence and the extent of degradation modes. The polymer microclimate, namely the boundary conditions that the polymers is in contact with, depends not only on the external environmental conditions such as temperature, humidity, UV irradiance and wind, to name a few. Contingent factors e.g. overheat due to partial cell shading or higher temperature in correspondence of the junction box might trigger localized degradation modes and an inhomogeneous behavior of the materials within the module. The microclimate that the polymers experience is also different when thinking about the encapsulant on top of the cell rather than the encapsulant beneath the solar cell. Different temperature values might be achieved during operation in addition to different transport pathways for small molecules such as moisture, oxygen, polymer degradation products and pollutants. Changes in diffusion pathways for small molecules can be associated also to the occurrence of concomitant degradation modes such as cell or polymer backsheet cracks. Finally, the selection of materials that will be used for the production of the PV modules has an important impact on the microclimatic conditions that will occur within the module. For example, using a glass instead of a polymer backsheet or polymer backsheet with different transport properties towards small molecules has an important influence also on encapsulant degradation as well as on power output [51–53].

It is necessary to test specimens at different levels of complexity to assess fully the reliability of PV modules, to understand how materials interact with each other and to assess the influence of the microclimate on material behavior as well as product performances. The *levels* can be identified as follows:

- *Base materials* (e.g. polymer resins, additives, minerals for solar cells, formulations for electrically conductive adhesives, …);
- *Processed base materials* (polymer encapsulant films, polymer backsheet films, solar cells, metallic interconnections, electrically conductive adhesives, …);
- *Test laminates* (combination of two or more processed base materials);
- *Mini-modules* (containing the key components of a full-scale module, but with reduced size, multiple configurations are possible);
- *Full scale modules* (final product, including all the components).

The costs as well as the complexity increases from base materials to full scale modules. Moreover, the type of characterization tests that can be performed and the information that can be gained at each level are substantially different.
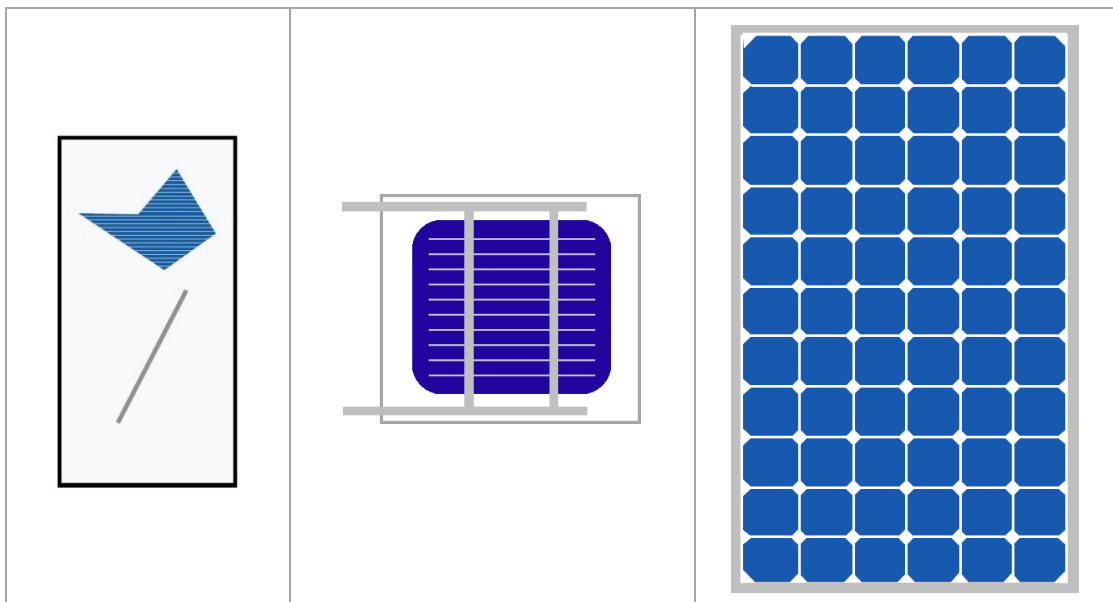
Figure 2.6: Illustration of testing samples type: test laminate (left), mini-module (middle), full scale PV module (right). The illustrations are not in scale with one another.

Generally, it is possible to distinguish between two different types of tests, i.e. destructive and non-destructive. The firsts are called *destructive* because they cause irreversible changes of material properties/structure/state/function. After the application of destructive tests, it is no longer possible to retrieve the original sample. *Non-destructive* tests, instead, do not affect in any way the original sample, which can be reused without substantial changes. A per se non-destructive test can become destructive if it is necessary to destroy the

original sample to withdraw material for further investigations. An example of destructive material testing procedure is TGA because the material undergoes thermal decomposition and its original characteristics are no longer the same. UV-Vis-NIR spectroscopy, on the contrary, allows investigating optical properties of samples without altering them.

The level of the *base materials* is characteristic of the product development phase. In this framework, different stabilization recipes for encapsulant materials, for example, can be tested to achieve the desired performances. Once the product is finalized, the level of *processed base materials* is reached.

The level of *processed base materials* is important because many information can be obtained. At this stage, intrinsic physical and chemical properties of materials such as polymer encapsulants and backsheets can be compared. It is especially useful when, for example, new materials enter the market and they have to be compared with existing materials to determine whether it might be an advantage to replace them with the new ones or not. A large number of specimens can be produced, destructive and non-destructive tests can be applied. Single materials can be also exposed to artificial ageing tests and their performances can be compared [54–56]. Additionally, testing of processed base materials can be useful to obtain material properties that can be implemented in finite element analysis simulation of relevant characteristics during operation [57, 58] and to optimize, for example, PV lamination conditions [35]. Testing of processed base materials, however, does not give any information regarding incompatibilities that might occur between different PV module components and does not consider the actual microclimate that materials experience during operation.

Test laminates (also called *coupons*) are useful to assess material compatibility and to compare interactions between different material combinations. Test laminates usually include front-sheet / encapsulant / back-sheet [51, 54, 56, 59] and often include additional components such as fragment of cells and/or metallic ribbons [60]. Non-destructive characterization methods and analytical techniques can be applied. Destructive analysis of polymers' properties can be performed only upon their destructive extraction. The test laminate configuration makes a step forward in resembling the microclimatic conditions that the materials experience within PV module stack. However, no correlating

information regarding material degradation and electrical performances can be derived. Additionally, the reduced scale of the produced samples does not entirely represent the diffusion pathways that small molecules experience in a full-scale PV module.

PV mini-modules are characterized by the presence of a frontsheet, encapsulant, solar cells, interconnections and backsheet. In addition, a frame, a junction box and the cabling might be installed, depending of the mini-module size. The PV mini-module configuration is probably the most widely used in literature and many variations exist according to the cells' size, number of cells, type of interconnections and so on. Non-destructive techniques can be applied as well as destructive techniques after the polymers' extraction. The main advantage of using a mini-module configuration with respect to the full-scale is trivially its reduced size. Testing of mini-modules sensibly reduces the costs and the complexity of testing, especially in terms of costs of material itself and space needed in the climate chambers where artificial ageing tests are performed. Material interactions and effect of different material combinations on power output can be tested. Electrical performances if mini-modules can be assessed non-destructively by means of I-V curve measurements and acquisition of electroluminescence images. In this way, it is possible to investigate changes in material properties and to assess their impact on the power generated. Additionally, specific PV module degradation modes, e.g. corrosion of interconnection and metallization, PID, Light Induced Degradation (LID) and Light and Elevated Temperature (LeTID), can be reproduced and studied.

Testing of *full-scale PV modules* requires a significant use of resources and implies a high level of complexity. The numbers of full-scale modules that are usually tested is limited with respect to the mini-modules. Normally, non-destructive characterization methods are applied, but destructive methods via materials extraction [61] are very useful to investigate the root causes of observable degradation modes. In fact, even though extracting materials from full scale modules can be a rather complex procedure, the full-scale configuration is the one that is actually operating in the field and it is the most reliable to use to entirely understand the effect of different microclimates on material degradation. Testing of mechanical loading static and dynamic on PV modules can be performed on full scale modules according to IEC 61215 and

IEC TS 62782, respectively. Recently, procedures able to derive loading conditions for reduced-scale testing were presented [49, 62].

2.6 Properties of interest and their assessment

By definition, an encapsulant material needs to have an optical transmittance above 90% and it can decrease at lowest to 85% after 20 years of operation. Needless to say, optical properties (and especially transmittance) of the encapsulants are crucial to ensure the correct functioning of the whole PV module. Worsening of optical properties often means discoloration of the encapsulant that derives from the occurrence of degradation processes involving the polymer itself or its formulation (e.g. stabilizers). Therefore, methods able to describe chemical changes taking place in the polymers are fundamental to understand the root causes behind the observed degradation.

The occurrence of chemical and physical degradation processes can have an effect on mechanical properties and morphology of polymers that might result in additional stresses for the other PV module components. The extent of the effects provoked by chemical and physical ageing processes needs to be deeply understood to avoid, for example, improper use of materials in modules designed for a specific climate zone. The next chapters will describe the most widely used characterization methods and analytical techniques able to describe ageing of polymers in PV applications. Their advantages and disadvantages will be discussed and a critical overview of the information that can be learned by applying the methods will be given.

2.6.1 Optical properties

The determination of the optical transmittance of the encapsulant material is a crucial parameter to monitor upon ageing. Decrease in encapsulant transmittance, as described in previous sections, can affect the performance of the PV module by decreasing the electrical power generated. In addition to optical transmittance of the encapsulants, according to the IEC TS 62788-2:2017 [63], optical reflectance of polymer backsheet might be also monitored to estimate its contribution to the PV module performance.

A reference solar spectrum was introduced to make the industry able to compare performances of different PV module technologies. The Air Mass

(AM) 1.5 spectrum is the industrial standard referred to the solar radiation filtrated by the atmosphere, air and dust particles, with an angle of incidence of 48.2° with respect to the zenith [64]. The total irradiance used in the industrial standard corresponds to I_e (AM1.5) = 1000 W m^{-2}. The power measured using this irradiance value and the AM1.5 spectrum is measured in Watt peak (W_p) and it is the reference power value for a module (regardless of the module technology) [64].
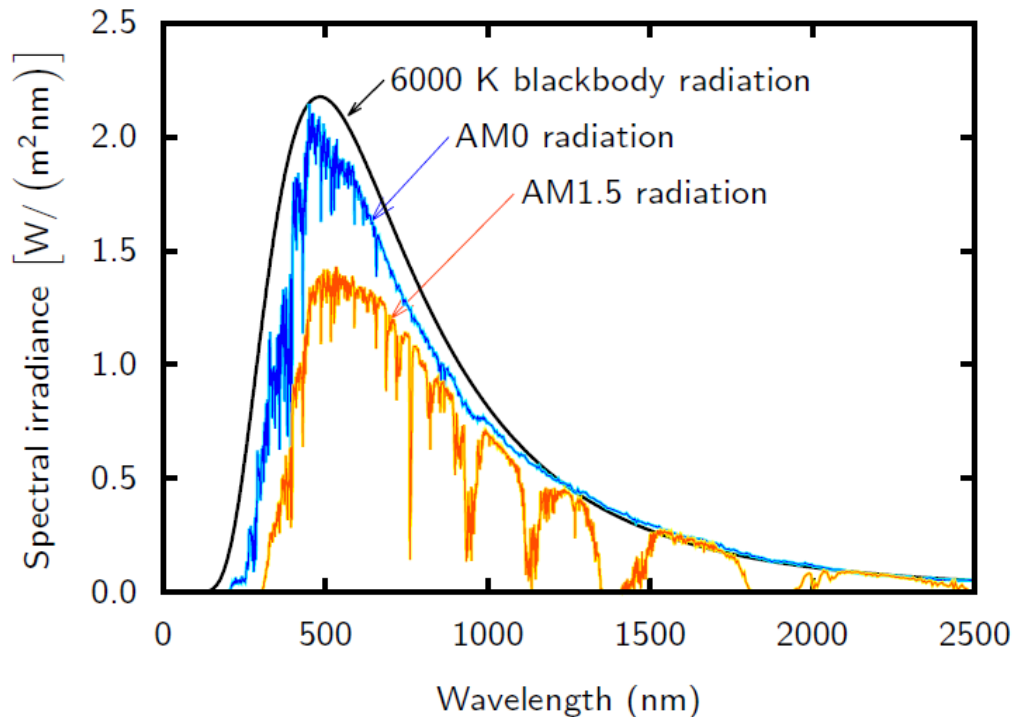
Figure 2.7: Solar spectra of black body, AM0 and AM1.5 [64].

Typically, optical reflectance and transmittance are measured using a spectrophotometer with integrating sphere, whose details and measurement procedures are described in IEC 62805−2. Solar-weighted transmission of photon irradiance, defined as *proportion of the solar spectral photon irradiance ($E_{p\lambda}$, m^{-2} s^{-1} nm^{-1}) optically transmitted through the specimen* [65] in the range of the terrestrial solar spectrum, 280 nm to 2500 nm, might also be reported. Yellowness index (YI) is an additional parameter that can be monitored over lifetime/exposure time to assess and evaluate color changes of encapsulants and polymer back-sheets. Transmission measurements are used to calculate YI values for front- and clear back-sheets, whereas reflection measurements are used for opaque sheets as well as to monitor color changes in the air-side of the backsheets [63]. Lastly, the UV cut-off wavelength (λ_{cUV}) of encapsulants can be

evaluated from transmission measurements as the value in the UV range where the transmittance equals 10% or less [65]. The presence of a UV cut-off indicates the presence of UV absorbers that have the function to protect the polymers from photo-degradation reactions.

Measurements of optical properties can be used not only to monitor changes in transmittance in the visible range, which is the most interesting for the electricity production in PV modules, but also to study the consumption/migration of stabilizers (especially antioxidants and UV absorbers) present in the polymer [35, 59]. Miller et al. [59] studied the effect of different artificial ageing tests (without and with irradiation, using different UV light sources) on glass-encapsulant-glass coupons to determine which stress factor has the most influence on decrease of transmittance. They assessed that samples that underwent artificial test with illumination experienced the most degradation. The selected light sources had also an influence on the polymer ageing behavior as well as the glasses used in the specimen setup. Discoloration of EVA does not always take place uniformly within a PV module. Pern et al. [66] reported that photodiscoloration phenomena compete with photobleaching due to the interaction between the formed chromophore species and oxygen. They observed that field exposed modules showed browning only above the cell, whereas the EVA in the free space between the cells did not show relevant discoloration. The phenomenon of photo-oxidative bleaching was reported quite frequently in literature in correspondence of strong discoloration [46, 60, 67–71]. Besides the analysis of polymer properties, UV-Vis-NIR spectroscopy can be used to determine the properties of antireflective coatings [72–74].

2.6.2 Chemical structure

Spectroscopic analytical techniques are especially useful to investigate chemical structure of materials. Molecular movements can be detected via spectroscopy and this allows material identification as well as monitoring of degradation reactions taking place during material exposure to the environment. In particular, infrared, Raman and fluorescence spectroscopy will be described in the following sections.

Fourier Transform Infrared (FT-IR) Spectroscopy

FT-IR spectroscopy, especially in ATR (attenuated total reflectance) mode has been widely used by researchers to investigate chemical changes taking place in polymers (encapsulants and backsheets) used in PV upon ageing.

The characteristics bands for a virgin EVA are at $2920\,cm^{-1}$, $2850\,cm^{-1}$, $1465\,cm^{-1}$ and $1370\,cm^{-1}$ that can be assigned to stretching and deformation vibration of methylene and ethylene groups, typical of polyethylene moieties. Additional bands at $1736\,cm^{-1}$, $1238\,cm^{-1}$ and $1020\,cm^{-1}$ can be assigned to C=O stretching vibrations and C−O−C stretching vibrations that are typical of vinyl acetate moieties [7, 75]. FT-IR spectroscopy analysis of EVA has been initially used to investigate the origin of its discoloration [76], attributed to formation of polyenic chromophores. Later studies [7] attributed discoloration of EVA with formation of α, β-unsaturated carbonyl product originated by breakdown of hydroperoxides. In the same study, a step forward in understanding synergistic and antagonistic effects of stabilization substances is made. Hindered amine light stabilizers (HALS) in combination with a phenol/phosphite antioxidant showed the best performances. Jin at al. [8] demonstrated that EVA with higher VA content are more prone to degradation. VA units are more vulnerable to environmental stress factors and can form hydroperoxides or unstable radicals leading to further degradation. Chain scission is found being the main degradation mechanism taking place upon UV irradiation. Ottersböck et al. [54] studied encapsulants (EVA and TPO) laminated in a glass-encapsulant-backsheet coupon configuration and analyzed in transmittance mode the penetration depth of oxidation upon artificial ageing exposure. They observed that for an EVA film, the extent of oxidation increased with longer exposure times and that higher OI values were found in the surface layers.

FT-IR spectroscopy has the advantage that is a very simple and fast characterization method and it allows getting many information regarding chemical changes taking place in the material. FT-IR ATR spectra of different EVA samples are showed in Figure 2.8. The spectra related to the two materials exposed to artificial ageing tests are the green spectrum and the red spectra. The two materials were extracted from mini-module samples that were exposed to DH test (85 °C and 85% relative humidity, R.H.) for 12000 hours and 1600 thermal cycles (TC), respectively. The sample exposed to TC does not

show significant changes with respect to the unexposed material, whereas the sample exposed to 12000 h of DH test shows a decrease of all the significant peaks related to vinyl acetate moieties (1736 cm^{-1}, 1238 cm^{-1} and 1020 cm^{-1}). The sample exposed to DH showed an additional shoulder at about 1715 cm^{-1}, corresponding to formation of substances containing a ketone functional group.
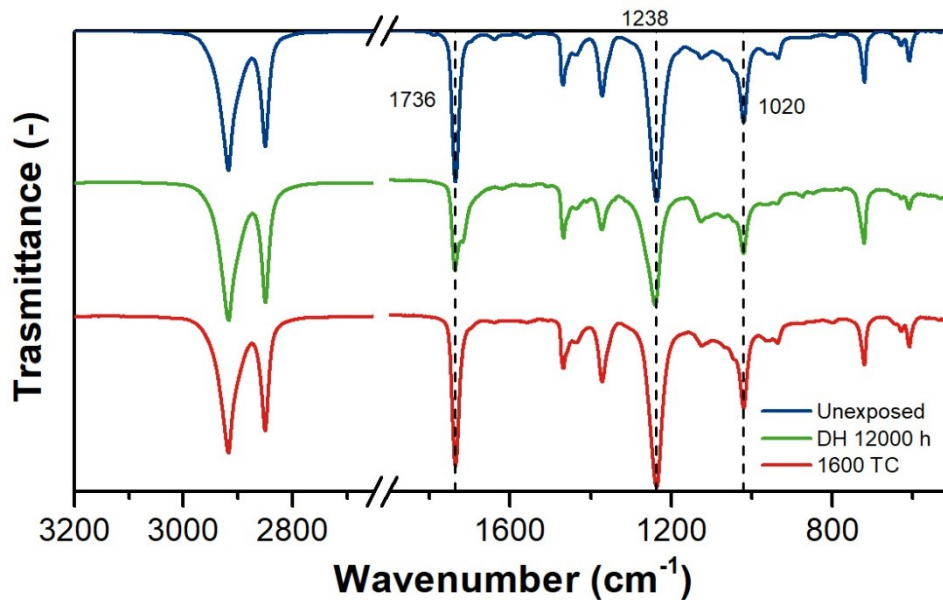
Figure 2.8: FT-IR ATR spectra of uncured EVA (upper blue curve), EVA extracted from a mini-module sample exposed to DH test for 12000 hours (85 °C / 85% R.H., middle green curve), EVA extracted from a mini-module exposed to 1600 TC (bottom red curve).

The occurrence of deacetylation reaction was studied via FT-IR spectroscopy and the trend observable in DH aged EVA [77] was observed also in EVA withdrawn from modules exposed in Japan for about 27 years [78] and in flexible PV modules [79]. However, when deacetylation and further oxidative processes take place simultaneously, the deacetylation appears less evident from FT-IR spectra. The peaks related to newly oxidized species overlap and m might prevail over the disappearance of vinyl acetate functions [79]. An example of the behavior mentioned above will be extensively described in Chapter 4.

Spinella and Bosco [80] investigated the influence of silane content and artificial ageing tests on the chemical composition and adhesion properties of the EVA to the glass. They discovered that a higher silane content well correlates with better EVA stability as well as better adhesion properties upon artificial ageing

exposure. The decrease of silane content with corresponding decrease of siloxane concentration well correlates with the decrease of debonding energy upon DH test. Upon UV exposure, the debonding energy decreases more than the decrease of the siloxane binding, thus indication that additional mechanisms contribute to the loss of adhesion.

FT-IR spectroscopy in ATR and transmission mode [81] has been also used to determine the vinyl acetate content of unexposed EVA in combination with additional characterization methods, for example based on thermal treatments. Additionally, an unsuccessful attempt to determine the EVA crosslinking degree by means of FT-IR spectroscopy was also carried out [82]. Finally, portable NIR spectrometers were proven to be very useful for material identification [83, 84] and detection of degradation [85] of field exposed PV modules.

The main advantage of using FT-IR ATR spectroscopy to analyze chemical changes that materials undergo during ageing is that it is very fast and simple to apply. Typically, only a small amount of material is needed to perform the analysis and each spectrum can measured within seconds or few minutes (depending of the settings of the device used). The downside is that it is necessary that the material measured is in direct contact with the ATR crystal, therefore it is not possible, for example, to measure the properties of the encapsulant through the glass. The encapsulant material has to be first extracted from the module sample (or test laminate) and then analyzed.

Raman Spectroscopy

Chemical changes have been often investigated by means of Raman Spectroscopy. The use of confocal microscopes enables the option to investigate non-destructively specimens in a stack configuration where different materials are present, as it can be found for a typical c-Si PV module configuration. Raman spectroscopy can be used to analyze the encapsulant material through the glass as well as the different layers constituting the backsheets [86, 87]. The characteristics bands for EVA are summarized in Table 2.2.

Table 2.2: Characteristic Raman bands and their assignment [54].

Raman characteristic bands [cm^{-1}]	Assignment
3000–2830	CH_2 and CH_3 stretching vibrations

Raman characteristic bands [cm^{-1}]	Assignment
1740	C=O stretching vibrations
1440	CH deformation vibration
1298	CH deformation vibration
1130	C−C stretching vibration
1064	C−C stretching vibration

During exposure to temperature, radiation and humidity, EVA can develop degradation products that are chromophores and that therefore exhibit fluorescence upon excitation. In Raman spectroscopy, the formation of chromophores results in an increase of the baseline of the Raman spectra due to the fluorescence of the chromophore species [51, 78, 88–90].

Kim et al. [91] used Raman spectroscopy to analyze snail trails, to identify their chemical composition and the degradation mechanisms leading to their formation. They attributed formation of sail trails to formation of silver acetate and its reaction with EVA degradation products and the same mechanism was confirmed by Fan et al. [92]. Additionally, Raman spectroscopy was proven to be a powerful tool to determine non-destructively crosslinking degree of EVA [93–97] and could be even applied to control in-line the quality of the encapsulation process [98].

Raman spectroscopy is, as well as FT-IR ATR spectroscopy, a measurement technique that is able to deliver fast results although the measurement setup might be costly. A Raman spectrometer equipped with a confocal microscope allows to measure the encapsulant and the backsheet materials through the glass. However, the major issue that researchers encounter when applying Raman spectroscopy on analysis of EVA encapsulant is the fluorescence visible in the background, as described before.

Fluorescence spectroscopy and imaging

Fluorescence spectroscopy is nowadays another quite popular spectroscopic technique applied to investigate the ageing processes taking place in encapsulant and backsheet materials [95, 99–104]. It has the advantage that is non-destructive and portable solutions, which can be used directly for field inspections [105], are reported in literature. Fluorescence spectroscopy and imaging are two complementary methods able to provide non-destructively

information regarding the degradation state of PV packaging materials. Fluorescence spectrophotometers are commercially available devices that can provide emission (and/or excitation) spectra for a given materials, as can be seen in Figure 2.9.
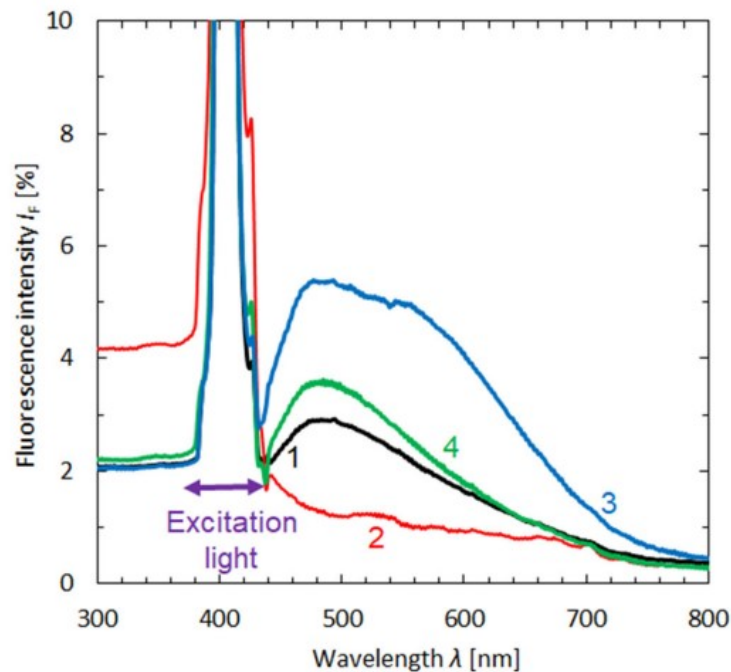
Figure 2.9: UV fluorescence spectra of the encapsulant of a PV module exposed in the field in 4 different PV module areas: (1) middle of intact cell, (2) between two cells, (3) middle of hot cell, (4) middle of moderate hot cell [104].

The main components of these devices are, briefly, a light source (typically a Xenon lamp), a monochromator and a detector. The key components of a fluorescence imaging setup are a light source and a camera. The typical output of this analysis is an image, as shown in Figure 2.10.
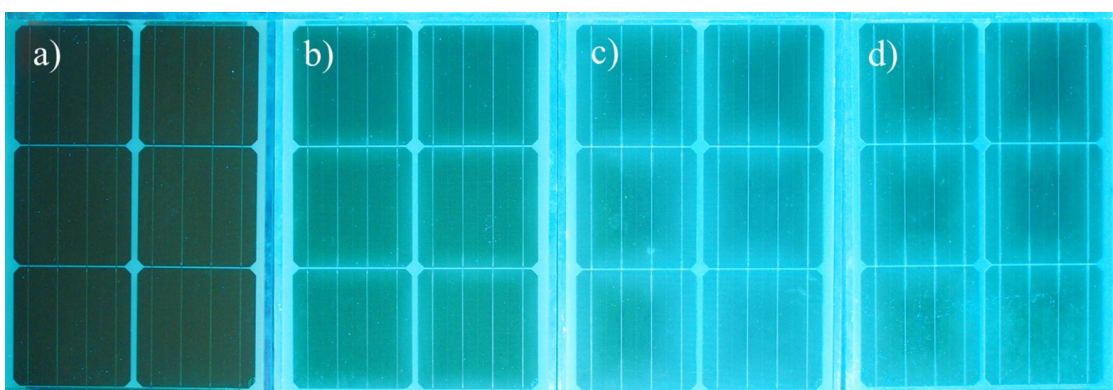
Figure 2.10: UV-fluorescence images of test modules (A) in the original state, (B) after 1000 h, (C) 2000 h, and (D) 3000 h of exposure to DH at 85°C/85% r.H. [50].

Spatially resolved investigations of EVA using fluorescence spectroscopy were reported for the first time by Schlothauer et al. [106]. The authors were able to identify different EVA fluorescence behavior according to EVA type, climate of the location where the modules were installed and specific areas within the modules. The effect of UV radiation and humidity ingress on EVA fluorescence was also demonstrated. Additionally, fluorescence spectroscopy has been also used to monitor acetic acid production by means of dual-wavelength fluorescent dyes [107, 108].

2.6.3 Thermal properties and thermal stability

Thermal properties such as glass transition temperature (T_g) and melting temperature (T_m) are fundamental in determining the right encapsulant material for PV applications. The amorphous moieties of polymers are more mobile above T_g and make the overall polymer more rubber-like. The use of PV modules with encapsulants having a T_g higher than the minimum temperature that can be reached in the surrounding environment is undesirable. The encapsulant material would be subject to embrittlement and this might cause relevant mechanical stress on the cells and interconnections. T_m is one of the parameters that have to be considered when the PV module processing conditions are defined. Characterization of thermal properties can be carried out by means of destructive methods. Little polymer amounts (typically less than 20 mg) can be investigated. Standalone polymer films can be directly analyzed, whereas encapsulant samples need to be extracted from laminated configurations (test laminates or PV modules) before being analyzed.

Differential Scanning Calorimetry (DSC) is an analytical method that is commonly used to determine several polymer characteristics such as glass transition temperature, melting temperature and enthalpy, crystallization temperature and enthalpy, crystallinity, crosslinking temperature and enthalpy [35, 36, 93]. Additionally, monitoring the evolution of the above mentioned characteristics over time can give meaningful information regarding the reversible and irreversible changes that the polymer undergo upon ageing [37, 51, 54, 103, 109, 110].

Thermogravimetric analysis (TGA) is another very common used analytical method able to detect changes in mass of a sample over temperature, time or

both [111]. Phase change that involve mass reduction due to volatiles formation as well as decomposition and chemical reactions [111] can be detected by means of TGA. This method can be additionally used to determine the amount of polymer fillers and to assess the consumption of polymer stabilizers upon ageing.

TGA is often used in photovoltaics to determine the vinyl acetate content of the EVA encapsulant [8, 81, 110], to detect and investigate signs of EVA degradation [37, 61, 89] and to indirectly evaluate the acetic acid production upon ageing [112, 113]. Additionally, TGA can be also used to compare thermal stability properties of different encapsulants [37, 77, 110, 114]. Vinyl acetate content in EVA is often determined in literature using equation 2.1. The weight loss observed in the first step is ΔW_1, $VAc(wt\%)$ corresponds to the vinyl acetate content expressed as wt%, $M_{Acetate}$ is the molar mass of the acetate ion and M_{VAc} is the molar mass of vinyl acetate.

$$\Delta W_1 = VAc(wt\%) \times \frac{M_{Acetate}}{M_{VAc}} \qquad \text{(Equation 2.1)}$$

Samples with different vinyl acetate contents show different ΔW_1, lower vinyl acetate content corresponds to lower ΔW_1. However, the determination of vinyl acetate content using this method is rather questionable for degraded EVA. It is reasonable to assume that when deacetylation is the most prominent reaction taking place upon ageing there will be a reduction of weight loss in the first step of the thermogram measured by means of TGA, as can be seen in the dashed blue curve of Figure 2.11. However, when deacetylation is accompanied by severe oxidation, the thermogram of the investigated material might look like the orange or red curve in Figure 2.11. In this case, the ΔW_1 might look higher than the value measured for the unexposed material leading to the conclusion that the vinyl acetate content increased upon exposure, which is rather unreasonable. TGA can be also combined with IR spectroscopy to better understand of degradation mechanisms taking place upon thermal stress [115].
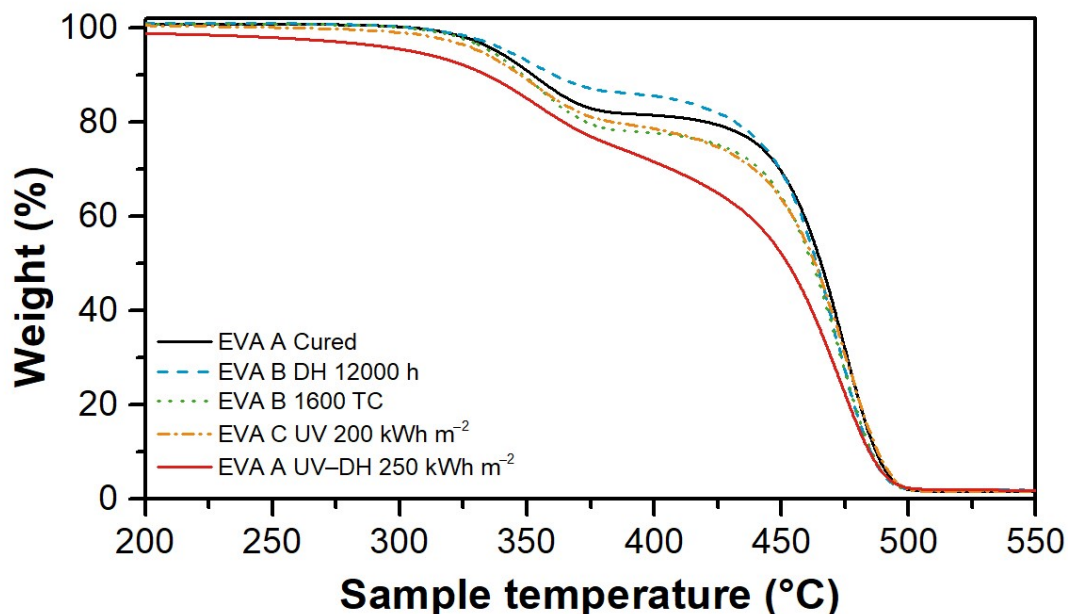
Figure 2.11: TGA measurements of EVA exposed to different artificial ageing tests. The materials analyzed are: an EVA from manufacturer A cured according to typical lamination process, not exposed to artificial ageing tests (black curve); EVA from manufacturer B extracted from a mini-module samples exposed to DH test (85% RH and 85 °C for 12000 hours) (blue dashed curve); EVA from manufacturer B extracted from a mini-module exposed to 1600 TC (green dotted curve); EVA from manufacturer A, cured and aged upon UV test (UV dose of 200 kWh m^{-2}) (orange dash-dot curve); EVA from manufacturer C, excess extracted from a mini-module exposed to UV-DH combined test, UV dose of 250 kWh m^{-2} (red curve).

2.6.4 Additives and stabilizers

Most of commercially available polymers, unless they have a very high intrinsic stability, come along with a specific stabilization recipe. Polymer stabilization plays an important role throughout the whole lifespan of the polymer because the additives help the polymers to retain their functions during processing, fabrication, storage and operation [116]. In case of EVA, a not stabilized polymer would be very susceptible to oxidation and degradation. Typically, the additives account for the 2-4 wt. % [3] and the most common additives used in EVA are summarized in Table 2.3.

Silane based coupling agents as well as peroxides react during the crosslinking reaction. Thanks to those molecules, the EVA is optimally coupled to the glass substrate and to the solar cells. The encapsulant during the crosslinking process

develops the optical and mechanical properties necessary to ensure optimal optical coupling and mechanical stability to the whole PV module. The primary antioxidants are able to transform the free radicals that are formed because of the effect of high temperatures and UV radiation and transform alkyl, alkoxy, and peroxyl radicals into hydro-peroxides [116]. The secondary antioxidants, instead, are able to decompose the hydroperoxides and prevent the formation of alkoxy and hydroxyl radicals [116]. The UV absorbers convert the harmful UV radiation and dissipate the energy without degrading the polymer, whereas the HALS protect the polymers against moderate temperatures (30 °C – 80 °C) and light [118].

Table 2.3: Additives typically present in the EVA formulation and their function [3, 117].

Additive	Function
Peroxide	Curing agent
Triallyl isocyanurate	Crosslinking accelerator
Benzotriazole, benzophenone	UV absorber
Hindered amine light stabilizers (HALS)	UV stabilizer, primary antioxidant
Primary antioxidant (phenolic based)	Antioxidant
Secondary antioxidant (phosphite)	Antioxidant
Silane	Adhesion promotor

Allen at al. [7] used FT-IR ATR spectroscopy to monitor specific functional groups to investigate different stabilizers recipes and find synergistic as well as antagonistic effects between the stabilizers. They showed that a combination of primary and secondary antioxidants is more effective with respect to the primary antioxidants alone. Additionally, the best performances were found for the combination phenol/phosphite antioxidant and HALS. In a subsequent study [119], antagonistic effects between an aromatic phosphate based antioxidant and the HALS were described. However, upon increasing of the concentration of the aromatic phosphate, the antagonistic effect was no longer observable, probably due to a shift of the reaction pathways.

Later on, Jentsch et al. [117] studied 8 EVA formulation upon UV exposure, analyzed color changes and adhesion performances between the EVA and the glass. The combination of UV absorber and HALS gave the best results regarding the occurrence of the yellowing process, especially the HALS were considered as the most promising stabilizers able to prolong the material's lifetime. Decomposition products of phosphite based antioxidant and UV absorbers were considered as the main responsible for loss of adhesion and discoloration of the encapsulant. Similar findings were described also in the work of La Mantia et al. [120] where EVA encapsulants stabilized with HALS preserved their mechanical and optical properties for longer exposure to UV radiation compared to the materials stabilized with antioxidants. Strong yellowing due to additive decomposition rather that EVA degradation was reported also by Peike at al. [121]. The UV absorber was also found to be responsible for the discoloration of PV modules exposed in Japan for 27 years [78]. The studies mentioned above, however, were carried out mainly analyzing the performances (namely, the evolution of optical, chemical and thermal properties) over the exposure to artificial ageing tests of materials developed with a known additive recipe. The material properties were often analyzed by means of FT-IR ATR spectroscopy, Raman spectroscopy, DSC, TGA, tensile test, adhesion test. However, qualitative or quantitative changes in additive composition were not directly analyzed.

Gas Chromatography coupled to Mass Spectrometry (GC/MS) as well as high performance liquid chromatography (HPLC) are analytical techniques commonly used in analytical chemistry to identify qualitatively and quantitatively the additives present in a polymeric material. The analytical methods mentioned above might give precise results but often require quite complex sample preparation procedures.

Hintersteiner et al. [122] developed protocols to extract the stabilizers from the polymer matrix of not exposed EVA, PVB and TPSE (thermoplastic silicon elastomer) and applied different analytical methods (Direct Analysis in Real Time Mass Spectrometry (DART-MS), GC/MS, HPLC/UV and HPLC/MS) to identify qualitatively and quantitatively the stabilizers. The results showed that DART-MS could be applied without any sample preparation to identify qualitatively the stabilizers only for EVA, whereas GC/MS and HPLC/MS were

proven to be powerful tools able to identify the stabilizers present in the polymer. Schlothauer et al. [101] used HPLC/UV to investigate the additive consumption in encapsulant samples exposed to UV and DH test. The samples showed the presence of an UV absorber and a HALS. The EVA exposed to UV resulted in a decrease of the UV absorber from the center of the cell towards the edge. The HALS, on the contrary, showed an inverse concentration profile. The sample exposed to DH, instead, did not show a significant difference in the concentration profile of the antioxidant, whereas the concentration of the HALS decreased from the center of the cell towards the edge.

Thermal desorption (TD)-GC/MS is an analytical method that can be applied directly to the encapsulant material with or without additional sample preparation (extraction or dissolution of the additives from the polymer matrix). It can be used, in case of EVA, to determine the presence of acetic acid, additives and stabilizers [35, 112, 123], but it can be applied to different encapsulant materials. Oreski et al. investigated [124] the DH ageing behavior of PV test modules laminated with different encapsulants and found that, when the encapsulant used was TPO, the yellowing was due to the presence of a degradation product of the antioxidant. In another study, Eder et al. [123] were able to detect by means of TD-GC/MS presence monomers of PA backsheets in the EVA encapsulant between the cell and the backsheet. The results allowed to clarify the degradation mechanism behind cracking of PA based backsheets where acetic acid reacted with the PA backsheet contributing to its cracking.

2.7 Summary and conclusions

Understanding degradation mechanisms taking place at molecular level, linking them to changes in macroscopic properties and finally determining the effect on PV power degradation is not an easy task. The environment surrounding the PV modules during operation has a major influence on polymer behavior, but the microclimate is what matters the most in determining the actual stress factors. With microclimate, it is intended the combination of environmental factors such as temperature, relative humidity and radiation, as well as, for example, peculiar transport properties due to special material coupling or additional protection to the polymer because of a particular glass composition.

To understand entirely the problems and the advantages related to use a material in PV application it is necessary to progress stepwise, testing the single materials, material combinations and finally the whole PV module configuration. The application of artificial ageing tests able to resemble the stress conditions that the modules will experience during operation is fundamental to make sure that materials will be able to withstand the climate where they will be operating. An artificial ageing test has not only to replicate the climatic stresses, but also to accelerate the degradation reactions without triggering undesired and unrealistic phenomena. Finally, a proper set of destructive and non-destructive characterization methods is necessary to achieve two fundamental goals that are easy and early identification of precursors that might lead to further degradation and to explain the observed degradation phenomena. When possible, it is preferable to make use of non-destructive methods, especially when dealing with full scale PV modules to identify precursors. The use of destructive methods can be very helpful in explaining material changes at molecular level.

2.8 References

[1]   Report IEA-PVPS T13-01:2013, "Performance and Reliability of Photovoltaic Systems: Subtask 3.2: Review on failures of PV modules," IEA PVPS Task 13, External final draft report IEA-PVPS, IEA International Energy Agency, November/2013. [Online]. Available: http://iea-pvps.org/index.php?id=95&eID=dam_frontend_push&docID=2064

[2]   A. Omazic *et al.,* "Relation between degradation of polymeric components in crystalline silicon PV module and climatic conditions: A literature review," *Solar Energy Materials and Solar Cells*, vol. 192, pp. 123–133, 2019, doi: 10.1016/j.solmat.2018.12.027.

[3]   M.C.C de Oliveira, A.S.A.C. Diniz, M. M. Viana, L.V.F. Cunha, "The causes and effects of degradation of encapsulant ethylene vinyl acetate copolymer (EVA) in crystalline silicon photovoltaic modules: A review," *Renewable and Sustainable Energy Reviews*, vol. 81, pp. 2299–2317, 2018, doi: 10.1016/j.rser.2017.06.039.

[4]   G. Zhou, X. Xiong, W. Zhou, Y. Liu, Y. Sang, and Z. Kou, "Mechanism analysis of snail trails in photovoltaic modules," in *IEEE 42nd Photovoltaic Specialists Conference (PVSC), New Orleans, 2015.,* pp. 1–4.

[5]   M. López-Escalante, L. J. Caballero, F. Martín, M. Gabás, A. Cuevas, and J. Ramos-Barrado, "Polyolefin as PID-resistant encapsulant material in 5PV6 modules," (in af), *Solar Energy Materials and Solar Cells*, vol. 144, pp. 691–699, 2016, doi: 10.1016/j.solmat.2015.10.009.

[6]   A. W. Czanderna and F. J. Pern, "Encapsulation of PV modules using ethylene vinyl acetate copolymer as a pottant: A critical review," *Solar Energy Materials and Solar Cells*, vol. 43, no. 43, pp. 101–181, 1996, doi: 10.1016/0927-0248(95)00150-6.

[7]   N. S. Allen, M. Edge, M. Rodriguez, C. M. Liauw, and E. Fontan, "Aspects of the thermal oxidation, yellowing and stabilisation of ethylene vinyl acetate copolymer," *Polymer Degradation and Stability*, no. 71, pp. 1–14, 2001.

[8]   J. Jin, S. Chen, and J. Zhang, "UV aging behaviour of ethylene-vinyl acetate copolymers (EVA) with different vinyl acetate contents," *Polymer Degradation and Stability*, vol. 95, no. 5, pp. 725–732, 2010, doi: 10.1016/j.polymdegradstab.2010.02.020.

[9]   M. Kempe, G. J. Jorgensen, K. M. Terwilliger, T. J. McMahon, C. E. Kennedy, and T. T. Borek, "Acetic acid production and glass transition concerns with ethylene-vinyl acetate used in photovoltaic devices," *Solar Energy Materials and Solar Cells*, vol. 91, no. 4, pp. 315–329, 2007, doi: 10.1016/j.solmat.2006.10.009.

[10]   A. Masuda, N. Uchiyama, and Y. Hara, "Degradation by acetic acid for crystalline Si photovoltaic modules," *Jpn. J. Appl. Phys.,* vol. 54, 4S, 04DR04, 2015, doi: 10.7567/jjap.54.04dr04.

[11]   A. Sinha, O. S. Sastry, and R. Gupta, "Nondestructive characterization of encapsulant discoloration effects in crystalline-silicon PV modules," *Solar Energy Materials and Solar Cells*, vol. 155, pp. 234–242, 2016, doi: 10.1016/j.solmat.2016.06.019.

[12]   J. Ahmad, A. Ciocia, S. Fichera, A. F. Murtaza, and F. Spertino, "Detection of Typical Defects in Silicon Photovoltaic Modules and Application for Plants with Distributed MPPT Configuration," *Energies*, vol. 12, no. 23, p. 4547, 2019, doi: 10.3390/en12234547.

[13]   J. Tracy, N. Bosco, C. Delgado, and R. Dauskardt, "Durability of ionomer encapsulants in photovoltaic modules," *Solar Energy Materials and Solar Cells*, vol. 208, p. 110397, 2020, doi: 10.1016/j.solmat.2020.110397.

[14]   N. C. Park, J. S. Jeong, B. J. Kang, and D. H. Kim, "The effect of encapsulant discoloration and delamination on the electrical characteristics of photovoltaic module," *Microelectronics Reliability*, vol. 53, 9-11, pp. 1818–1822, 2013, doi: 10.1016/j.microrel.2013.07.062.

[15]   E. Vandyk, J. Chamel, and A. Gxasheka, "Investigation of delamination in an edge-defined film-fed growth photovoltaic module," *Solar Energy Materials and Solar Cells*, vol. 88, no. 4, pp. 403–411, 2005, doi: 10.1016/j.solmat.2004.12.004.

[16]   B. M. Habersberger, P. Hacke, and L. S. Madenjian, "Evaluation of the PID-s susceptibility of modules encapsulated in materials of varying resistivity," in *IEEE 7th World Conference, 2018*.

[17]   B. M. Habersberger and P. Hacke, "Illumination and encapsulant resistivity are critical factors in polarization-type potential induced degradation on n-PERT Cells," in *37th European Photovoltaic Solar Energy Conference and Exhibition*, pp. 799–801. [Online]. Available: doi.org/10.4229/EUPVSEC20202020-4BO.12.5

[18]   E. Annigoni, A. Virtuani, M. Caccivio, G. Friesen, D. Chianese, and C. Ballif, "35 years of photovoltaics: Analysis of the TISO-10-kW solar plant, lessons learnt in safety and performance—Part 2," vol. 27, no. 9, pp. 760–778, 2019, doi: 10.1002/PIP.3146.

[19]   S. Chattopadhyay *et al.*, "Visual degradation in field-aged crystalline silicon PV modules in India and correlation with electrical degradation," *IEEE J. Photovoltaics*, vol. 4, no. 6, pp. 1470–1476, 2014, doi: 10.1109/JPHOTOV.2014.2356717.

[20]   F. Chekired, E. A. K. Boudjelthia, F. Mehareb, and A. Chahtou, "Visual Degradation of PV Modules After 30 Years of Exposure in Algeria," in *Artificial Intelligence and Renewables Towards an Energy Transition*, Cham, 2021, pp. 811–821. [Online]. Available: https://link.springer.com/chapter/10.1007%2F978-3-030-63846-7_78

[21]   D. Atsu, I. Seres, M. Aghaei, and I. Farkas, "Analysis of long-term performance and reliability of PV modules under tropical climatic conditions in sub-Saharan," *Renewable Energy*, vol. 162, pp. 285–295, 2020, doi: 10.1016/j.renene.2020.08.021.

[22]   J. A. Tanesab, A. Amheka, R. Sinaga, J. J. Mauta, and E. Hattu, "A preliminary study of common defects of photovoltaic modules in West Timor, Indonesia," *IOP Conf. Ser.: Earth Environ. Sci.*, vol. 542, p. 12041, 2020, doi: 10.1088/1755-1315/542/1/012041.

[23]   M. Kempe, "Encapsulant Materials for PV Modules," in *Photovoltaic Solar Energy: From Fundamentals to Applications*, pp. 478–490. [Online]. Available: www.wiley.com/go/reinders/photovoltaic_solar_energy

[24]   X. Cai *et al.*, "The Study On Anti-PID Performance Of High Efficiency Bifacial Cell Module," *IOP Conf. Ser.: Mater. Sci. Eng.*, vol. 556, p. 12033, 2019, doi: 10.1088/1757-899X/556/1/012033.

[25]   M. Schmela and S. K. Chunduri, "Market Survey Backsheets & Encapsulation 2020," 2020. [Online]. Available: http://taiyangnews.info/reports/market-survey-backsheets-encapsulation-2020/

[26]   M. C. López-Escalante, M. Fernández-Rodríguez, L. J. Caballero, F. Martín, M. Gabás, and J. R. Ramos-Barrado, "Novel encapsulant architecture on the road to photovoltaic module power output increase," *Applied Energy*, vol. 228, pp. 1901–1910, 2018, doi: 10.1016/j.apenergy.2018.07.073.

[27]   C. Peike, I. Häldrich, K.-A. Weiß, and I. Dürr, "Overview of PV module encapsulation materials," *Photovoltaics International*, no. 19, pp. 85–92, 2013.

[28]   I. F. Martínez, R. Merino, and B. Perez, "Lamination Cycle Optimization Using New POE Encapsulants," *Proceedings 32nd PVSEC, 2016*, 2016.

[29]   O. Hasan and A. Arif, "Performance and life prediction model for photovoltaic modules: Effect of encapsulant constitutive behavior," *Solar Energy Materials and Solar Cells*, vol. 122, pp. 75–87, 2014, doi: 10.1016/j.solmat.2013.11.016.

[30]   M. D. Kempe and P. Thapa, "Low Cost, Single Layer Replacement for the Back-sheet and Encapsulant Layers," in *Proceedings of SPIE*, 70480D-1-12.

[31]   M. Jankovec *et al.*, "In-Situ Monitoring of Moisture Ingress in PV Modules with Different Encapsulants," in *32nd European Photovoltaic Solar Energy Conference and Exhibition*, pp. 2265–2269.

[32]   A. J. Beinert, R. Leidl, P. Sommeling, U. Eitner, and J. Atkaa, "FEM-based Development of Novel-Contact PV Modules with Ultra-Thin Solar Cells," in *33rd European Photovoltaic Solar Energy Conference and Exhibition*, pp. 42–47.

[33]   VDMA, "International Technology Roadmap for Photvoltaic (ITRPV): 2019 Results," Apr. 2020.

[34]   G. Oreski, B. Ottersböck, and A. Omazic, "6 - Degradation Processes and Mechanisms of Encapsulants," in *Plastics DEsign Library*, *Durability and Reliability of Polymers and Other Materials in Photovoltaic Modules*, Hsinjin Edwin Yang, Roger H. French, and Laura S. Bruckman, Eds.: William Andrew Publishing, 2019, pp. 135–152. [Online]. Available: http://www.sciencedirect.com/science/article/pii/B9780128115459000069

[35]   G. Oreski *et al.*, "Properties and degradation behaviour of polyolefin encapsulants for PV modules," *Progress in Photovoltaics: Research and Applications*, 2020, doi: 10.1002/pip.3323.

[36]   B. Adothu, P. Bhatt, S. Zele, J. Oderkerk, F. R. Costa, and S. Mallick, "Investigation of newly developed thermoplastic polyolefin encapsulant principle properties for the c-Si PV module application," *Materials Chemistry and Physics*, vol. 243, 2020, doi: 10.1016/j.matchemphys.2020.122660.

[37]   B. Adothu *et al.*, "Newly developed thermoplastic polyolefin encapsulant–A potential candidate for crystalline silicon photovoltaic modules encapsulation," *Solar Energy*, vol. 194, pp. 581–588, 2019, doi: 10.1016/j.solener.2019.11.018.

[38]   B. Lin, C. Zheng, Q. Zhu, and F. Xie, "A polyolefin encapsulant material designed for photovoltaic modules: from perspectives of peel strength and transmittance," *Journal of Thermal Analysis and Calorimetry*, 2019, doi: 10.1007/s10973-019-09006-w.

[39]   T. Ojeda *et al.*, "Degradability of linear polyolefins under natural weathering," *Polymer Degradation and Stability*, vol. 96, no. 4, pp. 703–707, 2011, doi: 10.1016/j.polymdegradstab.2010.12.004.

[40]   H. Hanifi *et al.*, "Loss analysis and optimization of PV module components and design to achieve higher energy yield and longer service life in desert regions," *Applied Energy*, vol. 280, p. 116028, 2020, doi: 10.1016/j.apenergy.2020.116028.

[41]   *Terrestrial photovoltaic (PV) modules - Design qualification and type approval - Part 1-1: Special requirements for testing of crystalline silicon photovoltaic (PV) modules*, IEC 61215-1-1:2016., IEC, 2016. [Online]. Available: https://webstore.iec.ch/publication/24313

[42]   *Terrestrial photovoltaic (PV) modules - Design qualification and type approval - Part 2: Test procedures: Terrestrial photovoltaic (PV) modules - Design qualification and type approval - Part 2: Test procedures*, IEC 61215-2:2016, IEC, 2016. [Online]. Available: https://webstore.iec.ch/publication/24311

[43]   *Photovoltaic (PV) module safety qualification - Part 1: Requirements for construction: Photovoltaic (PV) module safety qualification - Part 1: Requirements for construction*, IEC 61730-1:2016, IEC, 2016. [Online]. Available: https://webstore.iec.ch/publication/25674

[44]   *Photovoltaic (PV) module safety qualification - Part 2: Requirements for testing: Photovoltaic (PV) module safety qualification - Part 2: Requirements for testing*, IEC 61730-2:2016, IEC, 2016. [Online]. Available: https://webstore.iec.ch/publication/25680

[45]   G. W. Ehrenstein and S. Pongratz, *Resistance and stability of polymers*. Munich: Hanser Publishers, 2013.

[46]   Y. Lyu, J. Hyun Kim, X. Gu, "Developing methodology for service life prediction of PV materials: quantitative effects of light intensity and wavelength on discoloration of a glass/EVA/PPE laminate," *Solar Energy*, vol. 174, pp. 515–526, 2018, doi: 10.1016/j.solener.2018.08.067.

[47]   A. Borne, K. R. Choudhury, W. Gambogi, and K.-A. Weiss, "Novel Accelerated Testing Methods for Faster Evaluation of PV modules and Materials," in *37th European Photovoltaic Conference and Exhibition*, pp. 900–903.

[48]   P. Hacke *et al.*, "Combined and Sequential Accelerated Stress Testing for Derisking Photovoltaic Modules," in *Advanced Micro- and Nanomaterials for Photovoltaics*, pp. 279–313.

[49]   M. Owen-Bellini *et al.*, "Advancing reliability assessments of photovoltaic modules and materials using combined-accelerated stress testing," *Prog Photovolt Res Appl*, vol. 29, no. 1, pp. 64–82, 2021, doi: 10.1002/pip.3342.

[50]   G. C. Eder *et al.*, "Climate specific accelerated ageing tests," *Conference Record of the IEEE Photovoltaic Specialists Conference*, 2019, doi: 10.1109/PVSC40753.2019.8981293.

[51]   D. E. Mansour *et al.*, "Effect of Backsheet Properties on PV Encapsulant Degradation during Combined Accelerated Aging Tests," *Sustainability*, vol. 12, no. 12, p. 5208, 2020, doi: 10.3390/su12125208.

[52]   Y. Voronko, G. C. Eder, M. Knausz, G. Oreski, T. Koch, and K. A. Berger, "Correlation of the loss in photovoltaic module performance with the ageing behaviour of the backsheets used," *Prog Photovolt Res Appl*, vol. 23, no. 11, pp. 1501–1515, 2015, doi: 10.1002/pip.2580.

[53]   C. Peike, P. Hülsmann, M. Blüml, P. Schmid, K.-A. Weiß, and M. Köhl, "Impact of Permeation Properties and Backsheet-Encapsulant Interactions on the Reliability of PV Modules," *ISRN Renewable Energy*, vol. 2012, 1–4, pp. 1–5, 2012, doi: 10.5402/2012/459731.

[54]   B. Ottersböck, G. Oreski, and G. Pinter, "Comparison of different microclimate effects on the aging behavior of encapsulation materials used in photovoltaic modules," *Polymer Degradation and Stability*, pp. 182–191, 2017, doi: 10.1016/j.polymdegradstab.2017.03.010.

[55]   Chiara Barretta, Gernot Oreski, Sonja Feldbacher, and Katharina Resch-Fauster and Roberto Pantani, "Comparison of Degradation Behavior of Newly Developed Encapsulation Materials for Photovoltaic Applications under Different Artificial Ageing Tests," *Polymers*, vol. 13, 2021, doi: 10.3390/polym13020271.

[56]   M. Knausz *et al.*, "Thermal expansion behavior of solar cell encapsulation materials," *Polymer Testing*, vol. 44, pp. 160–167, 2015, doi: 10.1016/j.polymertesting.2015.04.009.

[57]   S. Mitterhofer, C. Barretta, L. F. Castillon, G. Oreski, M. Topič, and M. Jankovec, "A Dual-Transport Model of Moisture Diffusion in PV Encapsulants for Finite-Element Simulations," *IEEE J. Photovoltaics*, vol. 10, no. 1, pp. 94–102, 2020, doi: 10.1109/JPHOTOV.2019.2955182.

[58]   P. Romer, G. Oreski, A. J. Beinert, H. Neuhaus, and M. Mittag, "More realistic considerations of backsheets coefficient of thermal expansion on thermomechanics of PV modules," in *37th European Photovoltaic Solar Energy Conference and Exhibition*, pp. 772–776.

[59]   D. C. Miller *et al.*, "Degradation in photovoltaic encapsulant transmittance: Results of the first PVQAT TG5 artificial weathering study," *Prog Photovolt Res Appl*, vol. 27, no. 5, pp. 391–409, 2019, doi: 10.1002/pip.3103.

[60]   F. Rummens, "Long Term Accelerated Weathering Tests on "Coupons" to Develop New Classes of Backsheets," *in Proc: 31st European Photovoltaic Solar Energy Conference and Exhibition*, pp. 2478–2481, 2015, doi: 10.4229/EUPVSEC20152015-5CV.2.8.

[61]   M. C. C. d. Oliveira *et al.*, "Comparison and analysis of performance and degradation differences of crystalline-Si photovoltaic modules after 15-years of field operation," *Solar Energy*, vol. 191, pp. 235–250, 2019, doi: 10.1016/j.solener.2019.08.051.

[62]   J. Y. Hartley *et al.*, "Effects of Photovoltaic Module Materials and Design on Module Deformation Under Load," *IEEE J. Photovoltaics*, vol. 10, no. 3, pp. 838–843, 2020, doi: 10.1109/JPHOTOV.2020.2971139.

[63]   *Measurement procedures for materials used in photovoltaic modules - Part 2: Polymeric materials - Frontsheets and backsheets*, IEC TS 62788-2:2017, IEC, 2017. [Online]. Available: https://webstore.iec.ch/publication/26617

[64]   K. Jäger, Olindo Isabella, A. H. Smets, R. A. van Swaaij, and M. Zemam, *Solar Energy: Fundamentals, Technology, and Systems*, 2014.

[65]   *Measurement procedures for materials used in photovoltaic modules - Part 1-4: Encapsulants - Measurement of optical transmittance and calculation of the solar-weighted photon transmittance, yellowness index, and UV cut-off wavelength*, IEC 62788-1-4:2016, IEC, 2016.

[66]   F. J. Pern, "Ethylene-Vinyl Acetate (EVA) encapsulant for photovoltaic modules: degradation and discoloration mechanisms and formulation modifications for improved photostability," *Die Angewandte Makromolekulare Chemie*, no. 252, pp. 195–216, 1997.

[67]   P. Klemchuk, E. Ezrin, G. Lavigne, W. Holley, J. Galica, and S. Agro, "Investigation of the degradation and stabilization of EVA-based encapsulant in field-aged solar energy modules," *Polymer Degradation and Stability*, no. 55, pp. 347–365, 1997, doi: 10.1016/S0141-3910(96)00162-0.

[68]   R. Meena, S. Kumar, and R. Gupta, "Comparative investigation and analysis of delaminated and discolored encapsulant degradation in crystalline silicon photovoltaic modules," *Solar Energy*, vol. 203, pp. 114–122, 2020, doi: 10.1016/j.solener.2020.04.041.

[69]   B. Adothu, S. Chattopadhyay, P. Bhatt, P. Hui, F. R. Costa, and S. Mallick, "Early-stage identification of encapsulants photobleaching and discoloration in crystalline silicon photovoltaic module laminates," *Prog Photovolt Res Appl*, vol. 28, no. 8, pp. 767–778, 2020, doi: 10.1002/pip.3269.

[70]   H. Han *et al.*, "Degradation analysis of crystalline silicon photovoltaic modules exposed over 30 years in hot-humid climate in China," *Solar Energy*, vol. 170, pp. 510–519, 2018, doi: 10.1016/j.solener.2018.05.027.

[71]   A. Bouraiou *et al.*, "Experimental evaluation of the performance and degradation of single crystalline silicon photovoltaic modules in the Saharan environment," *Energy*, vol. 132, pp. 22–30, 2017, doi: 10.1016/j.energy.2017.05.056.

[72]   J. Huang, Y. Liu, Y. Cao, Q. Liu, J. Shen, and X. Wang, "Durable silica antireflective coating prepared by combined treatment of ammonia and KH570 vapor," *J Coat Technol Res*, vol. 16, no. 2, pp. 615–622, 2019, doi: 10.1007/s11998-018-0142-8.

[73]   I. Arabatzis *et al.*, "Photocatalytic, self-cleaning, antireflective coating for photovoltaic panels: Characterization and monitoring in real conditions," *Solar Energy*, vol. 159, pp. 251–259, 2018, doi: 10.1016/j.solener.2017.10.088.

[74]   X. Sun *et al.*, "Preparation of hydrophobic SiO2/PTFE sol and antireflective coatings for solar glass cover," *Optik*, vol. 212, p. 164704, 2020, doi: 10.1016/j.ijleo.2020.164704.

[75]   G. Socrates, *Infrared and Raman Characteristic Group Frequencies: Tables and Charts,* 3rd ed. Chichester, West Sussex, England: John Wiley & Sons, Ltd, 2001.

[76]   F.J. Pern, "Factors that affect the EVA encapsulant discoloration rate upon accelerated exposure," *Solar Energy Materials and Solar Cells*, 41/42, pp. 587–615, 1996.

[77]   U. Desai, B. K. Sharma, A. Singh, and A. Singh, "Enhancement of resistance against damp heat aging through compositional change in PV encapsulant poly (ethylene-co-vinyl acetate)," *Solar Energy*, vol. 211, pp. 674–682, 2020, doi: 10.1016/j.solener.2020.09.083.

[78]   K. Hara and Y. Chiba, "Spectroscopic investigation of long-term outdoor-exposed crystalline silicon photovoltaic modules," *Journal of Photochemistry and Photobiology A: Chemistry*, vol. 404, p. 112891, 2021, doi: 10.1016/j.jphotochem.2020.112891.

[79]   E. Planes, B. Yrieix, C. Bas, and L. Flandin, "Chemical degradation of the encapsulation system in flexible PV panel as revealed by infrared and Raman microscopies," *Solar Energy Materials and Solar Cells*, vol. 122, pp. 15–23, 2014, doi: 10.1016/j.solmat.2013.10.033.

[80]   L. Spinella and N. Bosco, "FTIR Investigation of EVA Chemical Bonding Environment and Its Impact on Debond Energy," *IEEE J. Photovoltaics*, vol. 9, no. 3, pp. 790–795, 2019, doi: 10.1109/JPHOTOV.2019.2904219.

[81]   S.-S. Choi and C. E. Son, "Novel analytical method for determination of contents of backbone and terminal/branch vinyl acetate groups of poly(ethylene-co-vinyl acetate) using deacetylation   reaction," *Polymer   Testing*,   vol.   56,   pp.   214–219,   2016,   doi: 10.1016/j.polymertesting.2016.10.012.

[82]   M. Jaunich, M. Böhning, U. Braun, G. Teteris, and W. Stark, "Investigation of the curing state of ethylene/vinyl acetate copolymer (EVA) for photovoltaic applications by gel content determination, rheology, DSC and FTIR," *Polymer Testing*, vol. 52, pp. 133–140, 2016, doi: 10.1016/j.polymertesting.2016.03.013.

[83]   O. Stroyuk, C. Buerhop-Lutz, A. Vetter, J. Hauch, and C. J. Brabec, "Nondestructive characterization of polymeric components of silicon solar modules by near-infrared absorption spectroscopy (NIRA)," *Solar Energy Materials and Solar Cells*, vol. 216, p. 110702, 2020, doi: 10.1016/j.solmat.2020.110702.

[84]   G. C. Eder, Y. Lin, Y. Voronko, and L. Spoljaric-Lukacic, "On-site identification of the material composition of PV modules with mobile spectroscopic devices," *Energies*, vol. 13, no. 8, 2020, doi: 10.3390/en13081903.

[85]   H. Li *et al.*, "Nondestructive estimation of strength deterioration in photovoltaic backsheets using a portable near infrared spectrometer," *Solar Energy Materials and Solar Cells*, vol. 101, no. 0, pp. 166–169, 2012, doi: 10.1016/j.solmat.2012.01.017.

[86]   Chiao-Chi Lin, Peter J. Krommenhoek, Stephanie S. Watson, and Xiaohong Gu, "Depth profiling of degradation of multilayer photovoltaic backsheets after accelerated laboratory weathering: Cross-sectional Raman imaging," *Solar Energy Materials and Solar Cells*, vol. 144, pp. 289–299, 2016, doi: 10.1016/j.solmat.2015.09.021.

[87]   Y. Voronko, B. S. Chernev, and G. C. Eder, "Spectroscopic investigations on thin adhesive layers in multi-material laminates," *Applied Spectroscopy*, vol. 68, no. 5, pp. 584–592, 2014, doi: 10.1366/13-07291.

[88]   C. Peike, T. Kaltenbach, K.-A. Weiß, and M. Koehl, "Non-destructive degradation analysis of encapsulants in PV modules by Raman Spectroscopy," (in af), *Solar Energy Materials and Solar Cells*, vol. 95, no. 7, pp. 1686–1693, 2011, doi: 10.1016/j.solmat.2011.01.030.

[89]   H. Han *et al.*, "Analysis of the degradation of encapsulant materials used in photovoltaic modules exposed to different climates in China," *Solar Energy*, vol. 194, pp. 177–188, 2019, doi: 10.1016/j.solener.2019.10.014.

[90]   C. Peike, S. Hoffmann, M. Heck, T. Kaltenbach, K.-A. Weiß, and M. Köhl, "Nondestructive Determination of Climate-Specific Degradation Patterns for Photovoltaic-Module Encapsulation," *Energy Technology*, vol. 2, no. 1, pp. 121–129, 2014, doi: 10.1002/ente.201300075.

[91]   N. Kim, K.-J. Hwang, D. Kim, J. H. Lee, S. Jeong, and D. H. Jeong, "Analysis and reproduction of snail trails on silver grid lines in crystalline silicon photovoltaic modules," *Solar Energy*, vol. 124, pp. 153–162, 2016, doi: 10.1016/j.solener.2015.11.040.

[92]   J. Fan *et al.*, "Study on snail trail formation in PV module through modeling and accelerated aging tests," *Solar Energy Materials and Solar Cells*, vol. 164, pp. 80–86, 2017, doi: 10.1016/j.solmat.2017.02.013.

[93]   C. Hirschl *et al.*, "Determining the degree of crosslinking of ethylene vinyl acetate photovoltaic module encapsulants—A comparative study," *Solar Energy Materials and Solar Cells*, vol. 116, pp. 203–218, 2013, doi: 10.1016/j.solmat.2013.04.022.

[94]   J. C. Schlothauer, R. M. Ralaiarisoa, A. Morlier, M. Koentges, and B. Röder, "Determination of the cross-linking degree of commercial ethylene-vinyl-acetate polymer by luminescence spectroscopy," *J Polym Res*, vol. 21, no. 5, pp. 457–462, 2014, doi: 10.1007/s10965-014-0457-9.

[95]   J. C. Schlothauer, C. Peter, C. Hirschl, G. Oreski, and B. Röder, "Non-destructive monitoring of ethylene vinyl acetate crosslinking in PV-modules by luminescence spectroscopy," *J Polym Res*, vol. 24, no. 12, p. 203, 2017, doi: 10.1007/s10965-017-1409-y.

[96]   G. Oreski, A. Rauschenbach, C. Hirschl, M. Kraft, G. C. Eder, and G. Pinter, "Crosslinking and post-crosslinking of ethylene vinyl acetate in photovoltaic modules," *J. Appl. Polym. Sci.*, vol. 134, no. 23, p. 101, 2017, doi: 10.1002/app.44912.

[97]   A. Sanoria, D. Ulbricht, T. Schuster, and R. Brüll, "Monitoring crosslinking inhomogeneities in ethylene vinyl acetate photovoltaic encapsulants using Raman microscopy," *RSC Adv.*, vol. 5, no. 113, pp. 93522–93529, 2015, doi: 10.1039/C5RA18988H.

[98]   Ch. Hirschl *et al.*, "In-line determination of the degree of crosslinking of ethylene vinyl acetate in PV modules by Raman spectroscopy," *Solar Energy Materials and Solar Cells*, vol. 152, pp. 10–20, 2016, doi: 10.1016/j.solmat.2016.03.019.

[99]   G. C. Eder *et al.*, "Climate specific accelerated ageing tests and evaluation of ageing induced electrical, physical, and chemical changes," *Prog Photovolt Res Appl*, vol. 27, no. 11, pp. 934–949, 2019, doi: 10.1002/pip.3090.

[100]   G. Eder, Y. Voronko, C. Hirschl, R. Ebner, G. Újvári, and W. Mühleisen, "Non-Destructive Failure Detection and Visualization of Artificially and Naturally Aged PV Modules," *Energies*, vol. 11, no. 5, p. 1053, 2018, doi: 10.3390/en11051053.

[101]   J. C. Schlothauer, K. Grabmayer, I. Hintersteiner, G. M. Wallner, and B. Röder, "Non-destructive 2D-luminescence detection of EVA in aged PV modules: Correlation to calorimetric properties, additive distribution and a clue to aging parameters," *Solar Energy Materials and Solar Cells*, vol. 159, pp. 307–317, 2017, doi: 10.1016/j.solmat.2016.09.011.

[102]   J. C. Schlothauer, K. Grabmayer, G. M. Wallner, and B. Röder, "Correlation of spatially resolved photoluminescence and viscoelastic mechanical properties of encapsulating EVA in

differently aged PV modules," *Prog. Photovolt: Res. Appl.*, vol. 24, no. 6, pp. 855–870, 2016, doi: 10.1002/pip.2734.

[103]   Y. Lyu *et al.*, "Fluorescence imaging analysis of depth-dependent degradation in photovoltaic laminates: insights to the failure," *Prog Photovolt Res Appl*, vol. 28, no. 2, pp. 122–134, 2020, doi: 10.1002/pip.3212.

[104]   M. Köntges, A. Morlier, G. Eder, E. Fleis, B. Kubicek, and J. Lin, "Review: Ultraviolet Fluorescence as Assessment Tool for Photovoltaic Modules," *IEEE J. Photovoltaics*, vol. 10, no. 2, pp. 616–633, 2020, doi: 10.1109/JPHOTOV.2019.2961781.

[105]   A. Morlier, M. Siebert, I. Kunze, G. Mathiak, and M. Kontges, "Detecting Photovoltaic Module Failures in the Field During Daytime With Ultraviolet Fluorescence Module Inspection," *IEEE J. Photovoltaics*, vol. 7, no. 6, pp. 1710–1716, 2017, doi: 10.1109/JPHOTOV.2017.2756452.

[106]   J. Schlothauer, S. Jungwirth, M. Köhl, and B. Röder, "Degradation of the encapsulant polymer in outdoor weathered photovoltaic modules: Spatially resolved inspection of EVA ageing by fluorescence and correlation to electroluminescence," *Solar Energy Materials and Solar Cells*, vol. 102, pp. 75–85, 2012, doi: 10.1016/j.solmat.2012.03.022.

[107]   T. Asaka *et al.*, "Development of a pH sensor based on a nanostructured filter adding pH-sensitive fluorescent dye for detecting acetic acid in photovoltaic modules," *Jpn. J. Appl. Phys.*, vol. 54, 8S1, 08KG07, 2015, doi: 10.7567/JJAP.54.08KG07.

[108]   T. Asaka, K. Iwami, A. Taguchi, N. Umeda, and A. Masuda, "Detection of acid moisture in photovoltaic modules using a dual wavelength pH-sensitive fluorescent dye," *Jpn. J. Appl. Phys.*, vol. 53, 4S, 04ER18, 2014, doi: 10.7567/JJAP.53.04ER18.

[109]   A. P. Patel, A. Sinha, and G. TamizhMani, "Field-Aged Glass/Backsheet and Glass/Glass PV Modules: Encapsulant Degradation Comparison," *IEEE J. Photovoltaics*, vol. 10, no. 2, pp. 607–615, 2020, doi: 10.1109/JPHOTOV.2019.2958516.

[110]   B. K. Sharma, U. Desai, A. Singh, and A. Singh, "Effect of vinyl acetate content on the photovoltaic-encapsulation performance of ethylene vinyl acetate under accelerated ultra-violet aging," *J. Appl. Polym. Sci.*, vol. 137, no. 2, p. 48268, 2020, doi: 10.1002/app.48268.

[111]   G. W. Ehrenstein, G. Riedel, and P. Trawiel, *Thermal analysis of plastics: Theory and practice*. Munich: Carl Hanser Verlag, 2004.

[112]   E. Wang, H. E. Yang, J. Yen, S. Chi, and C. Wang, "Failure Modes Evaluation of PV Module via Materials Degradation Approach," *Energy Procedia*, vol. 33, pp. 256–264, 2013, doi: 10.1016/j.egypro.2013.05.066.

[113]   J. Zhu, D. Montiel-Chicharro, T. R. Betts, and R. Gottschalg, "Correlation of Degree of EVA Crosslinking with Formation and Discharge of Acetic Acid in PV Modules," in *33rd European Photovoltaic Solar Energy Conference and Exhibition; 1795-1798 / 33rd European Photovoltaic Solar Energy Conference and Exhibition*, pp. 1795–1798. [Online]. Available: doi.org/10.4229/EUPVSEC20172017-5DV.3.21

[114]   D. C. Miller, M. Kempe, M. T. Muller, M. H. Gray, K. Araki, and S. R. Kurtz, "Durability of polymeric encapsulation materials in a PMMA/glass concentrator photovoltaic system," *Prog. Photovolt: Res. Appl.*, vol. 24, no. 11, pp. 1385–1409, 2016, doi: 10.1002/pip.2796.

[115]   A. Marcilla, A. Gómez, and S. Menargues, "TG/FTIR study of the thermal pyrolysis of EVA copolymers," *Journal of Analytical and Applied Pyrolysis*, vol. 74, 1-2, pp. 224–230, 2005, doi: 10.1016/j.jaap.2004.09.009.

[116]   N. S. Allen and M. Edge, "Perspectives on additives for polymers. 1. Aspects of stabilization," *J Vinyl Addit Technol*, pp. 1–23, 2020, doi: 10.1002/vnl.21807.

[117]   A. Jentsch, K.-J. Eichhorn, and B. Voit, "Influence of typical stabilizers on the aging behavior of EVA foils for photovoltaic applications during artificial UV-weathering," *Polymer Testing*, vol. 44, pp. 242–247, 2015, doi: 10.1016/j.polymertesting.2015.03.022.

[118]   N. S. Allen and M. Edge, "Perspectives on additives for polymers. Part 2. Aspects of photostabilization and role of fillers and pigments," *J Vinyl Addit Technol*, 2020, doi: 10.1002/vnl.21810.

[119]   S. Isarankura Na Ayutthaya and J. Wootthikanokkhan, "Investigation of the photodegradation behaviors of an ethylene/vinyl acetate copolymer solar cell encapsulant and effects of antioxidants on the photostability of the material," *J. Appl. Polym. Sci.*, vol. 107, no. 6, pp. 3853–3863, 2008, doi: 10.1002/app.27428.

[120]   F. P. La Mantia, V. Malatesta, M. Ceraulo, M. C. Mistretta, and P. Koci, "Photooxidation and photostabilization of EVA and cross-linked EVA," *Polymer Testing*, vol. 51, pp. 6–12, 2016, doi: 10.1016/j.polymertesting.2016.01.018.

[121]   C. Peike, L. Purschke, K.-A. Weiß, M. Köhl, and M. Kempe, "Towards the origin of photochemical EVA discoloration," in *39th Photovoltaic Specialists Conference IEEE, Tampa Bay, USA, 2013*.

[122]   I. Hintersteiner, L. Sternbauer, S. Beissmann, W. W. Buchberger, and G. M. Wallner, "Determination of stabilisers in polymeric materials used as encapsulants in photovoltaic modules," (in af), *Polymer Testing*, vol. 33, pp. 172–178, 2014, doi: 10.1016/j.polymertesting.2013.12.004.

[123]   G. C. Eder *et al.*, "Error analysis of aged modules with cracked polyamide backsheets," *Solar Energy Materials and Solar Cells*, vol. 203, p. 110194, 2019, doi: 10.1016/j.solmat.2019.110194.

[124]   G. Oreski *et al.*, "Performance of PV modules using co-extruded backsheets based on polypropylene," *Solar Energy Materials and Solar Cells*, vol. 223, p. 110976, 2021, doi: 10.1016/j.solmat.2021.110976.

3 Experimental methods and analytical techniques used to describe polymer degradation

The following paragraphs describe the characterization techniques and analytical methods used to analyze polymers degradation and consequent changes of their properties/characteristics. The methods described were used to characterize polymers in Chapter 4, Chapter 5 and Chapter 6. When additional methods were used, they are described in the corresponding chapters.

3.1 Thermal Desorption Gas Chromatography coupled to Mass Spectrometry (TD-GC/MS)

The TD-GC/MS measurements were carried out to qualitatively analyze the additive composition of the encapsulants. Thermal desorption phase takes place in an Evolved Gas Analysis (EGA)/Pyrolyzer-3030D from Frontier Laboratories Ltd. The sample, around 0.5 mg of material, is heated from 60 °C to 320 °C, with a heating rate of 20 °C min^{-1}, and kept at 320 °C for 3 minutes, the maximum interface temperature is set at 300 °C. During this phase, the gaseous substances desorbed from the sample are collected and, when the process is completed, they are sent to the GC/MS (GC–MS QM2010 Ultra from Shimadzu) system and then analyzed. The column used is an Optima-5-Accent (length of 30 m, internal diameter of 0.25 mm, film thickness of 0.25 μm) and the carrier gas is helium. The separation in the column is carried out using the following parameters: heating from 50 °C to 90 °C, hold for 2 minutes, heat to 300 °C and hold for 10 minutes, the heating rate is set to 10 °C/min. Ion source temperature and interface temperature are set at 300 °C and splitless mode is selected. The Mass Spectrometer is set in Scan Mode in the range from 50 m/z to 800 m/z, with ionization energy of 0.70 eV. The identification of the detected substances is performed by means of alignment with the NIST (National Institute of Standard and Technology) database.

3.2 UV-Visible-Near Infrared Spectroscopy (UV-Vis-NIR)

Hemispherical transmittance of the encapsulants before and over the exposure was recorded over the wavelength range between 250 nm and 2500 nm with a Lambda 950 UV-Vis-NIR Spectrophotometer from PerkinElmer Inc.

The Yellowness Index is determined according to the standard ASTM E313 [1] in Chapter 5.

3.3 Fourier Transform Infrared Spectroscopy (FT-IR) in Attenuated Total Reflectance (ATR) mode

FT-IR measurements were performed using a Spectrum Two FT-IR Spectrometer from PerkinElmer Inc. in Attenuated Total Reflectance (ATR) mode using a MIRacle unit, equipped with a Zn/Se crystal with diamond tip. The spectra were measured in the interval 4000 cm^{-1} to 650 cm^{-1}, averaging 16 scans with a resolution of 4 cm^{-1}. The displayed spectra are normalized with respect to the intensity of the peak at 2850 cm^{-1}, which is referred to methyl and methylene groups of polyethylene chains [2]. Oxidation Indices (OI) were evaluated to compare the overall oxidation state of the materials. The values were calculated as the ratio between the integral of the spectra from 1680 cm^{-1} to 1800 cm^{-1} (carbonyl region, related to oxidation products) and the reference band from 2760 cm^{-1} to 2875 cm^{-1} [3, 4].

3.4 Differential Scanning Calorimetry (DSC)

DSC 6000 from PerkinElmer Inc. was used to measure thermograms of encapsulant materials before and after exposure. For each material, around 10 mg were placed in an aluminum pan and subjected to heating and cooling steps. During each step, heating (and cooling) rates were set to 10 K min^{-1} and a nitrogen flow of 50 mL min^{-1} was imposed. Two heating steps are necessary to distinguish reversible changes due to physical processes, such as post crystallization, from irreversible chemical processes with effect on molecular structure. Melting enthalpies and temperatures were calculated by evaluating the area between the melting/crystallization peaks and the baseline. At least three measurement were performed for each sample at each ageing step. Generally, a first heating run from −70 °C to 150 °C was followed by a cooling

run from 150 °C to −70 °C and a second heating run from −70 °C to 150 °C. Crystallinity was calculated as the ratio between measured heat of fusion and the literature value for the 100% crystalline polyethylene ($\Delta H_m^0 = 293$ J g^{-1}) [5, 6].

3.5 Thermogravimetric Analysis (TGA)

Thermogravimetric analysis was performed by using a Thermogravimetric Analysis TGA/DSC 1 from Mettler Toledo GmbH. The weight loss of around 10 mg of encapsulant material was monitored while heating the sample in nitrogen atmosphere (50 mL min^{-1}) from 25 °C to 600 °C, with a heating rate of 10 °C min^{-1}. Temperature values at which the weight loss is equal to 5% with respect to the initial value (T_5) is considered as an indicator for the beginning of the material's decomposition process. Additionally T_{40} values (temperature corresponding at 40% weight loss) are also considered as further indicators for material degradation [7–9] in Chapters 5 an in Chapter 6.

3.6 References

[1]   *Standard Practice for Calculating Yellowness and Whiteness Indices from Instrumentally Measured Color Coordinates*, ASTM E313 - 05, ASTM International. [Online]. Available: http://www.astm.org/cgi-bin/resolver.cgi?E313-05

[2]   M. Rodríguez-Vázquez, C. M. Liauw, N. S. Allen, M. Edge, and E. Fontan, "Degradation and stabilisation of poly(ethylene-stat-vinyl acetate): 1 – Spectroscopic and rheological examination of thermal and thermo-oxidative degradation mechanisms," *Polymer Degradation and Stability*, vol. 91, no. 1, pp. 154–164, 2006, doi: 10.1016/j.polymdegradstab.2005.04.034.

[3]   B. Ottersböck, G. Oreski, and G. Pinter, "Comparison of different microclimate effects on the aging behavior of encapsulation materials used in photovoltaic modules," *Polymer Degradation and Stability*, pp. 182–191, 2017, doi: 10.1016/j.polymdegradstab.2017.03.010.

[4]   W. Yagoubi, A. Abdelhafidi, M. Sebaa, and S. F. Chabira, "Identification of carbonyl species of weathered LDPE films by curve fitting and derivative analysis of IR spectra," *Polymer Testing*, vol. 44, pp. 37–48, 2015, doi: 10.1016/j.polymertesting.2015.03.008.

[5]   G. W. Ehrenstein, G. Riedel, and P. Trawiel, *Thermal analysis of plastics: Theory and practice*. Munich: Carl Hanser Verlag, 2004.

[6]   C. Hirschl *et al.,* "Determining the degree of crosslinking of ethylene vinyl acetate photovoltaic module encapsulants—A comparative study," *Solar Energy Materials and Solar Cells*, vol. 116, pp. 203–218, 2013, doi: 10.1016/j.solmat.2013.04.022.

[7]   J. Jin, S. Chen, and J. Zhang, "UV aging behaviour of ethylene-vinyl acetate copolymers (EVA) with different vinyl acetate contents," *Polymer Degradation and Stability*, vol. 95, no. 5, pp. 725–732, 2010, doi: 10.1016/j.polymdegradstab.2010.02.020.

[8]   B. K. Sharma, U. Desai, A. Singh, and A. Singh, "Effect of vinyl acetate content on the photovoltaic-encapsulation performance of ethylene vinyl acetate under accelerated ultra-violet aging," *J. Appl. Polym. Sci.*, vol. 137, no. 2, p. 48268, 2020, doi: 10.1002/app.48268.

[9]   Z. Liu, J. Jin, S. Chen, and J. Zhang, "Effect of crystal form and particle size of titanium dioxide on the photodegradation behaviour of ethylene-vinyl acetate copolymer/low density polyethylene composite," *Polymer Degradation and Stability*, vol. 96, no. 1, pp. 43–50, 2011, doi: 10.1016/j.polymdegradstab.2010.11.010.

4 Comparison performances of newly developed encapsulants exposed to artificial ageing tests

The research work described in this chapter is based on the publication *"Comparison of degradation behavior of newly developed encapsulation materials for photovoltaic applications under different artificial ageing tests"*, published in the journal "Polymers" (DOI: 10.3390/polym13020271).

4.1 Motivation

Despite relevant effort has been made over the years to develop material properties and improve EVA encapsulant reliability, several degradation modes of PV modules can still be attributed to EVA degradation. Acetic acid, in particular, is a major cause of corrosion effects for metallization and cell connectors as well as delamination and potential induced degradation (PID) [1–3]. Negative material interaction between encapsulant, additives and electrical components of PV modules have been reported in literature as well [4–8].

Recently, an interest in new encapsulant materials has increased to overcome the issues due to the use of EVA and new formulations have been tested. In particular, TPO and POE have been introduced as alternatives to EVA as encapsulants for PV applications [1, 9–14]. TPO and POE are polyethylene-based materials, as well as EVA, but do not have vinyl acetate moieties. TPO and POE present in their structure, as additional functional groups, acrylates, acrylic acids and n-alkanes [1].

The main advantage of TPO and POE is that they cannot produce acetic acid during degradation because they do not have vinyl acetate moieties. POEs undergo chemical crosslinking, as well as EVA, therefore their formulation includes typically peroxides as crosslinking agents that react forming covalent bonds between the polymer chains. TPOs, instead, being thermoplastic materials, do not require peroxides or additional crosslinking agents to crosslink because they physically form hydrogen bonds upon the application of high temperatures. The materials mentioned above do not have particular drawbacks because they are similar to EVA in terms of costs and processing

conditions. Additionally, the lack of vinyl acetate units limits the occurrence of corrosion and PID [1]. In a work published recently, Oreski et al. proved that module laminated with POE and TPO materials did not show signs of corrosion upon exposure to high temperature and high humidity values [14].

Even though degradation of polyethylene based polymers has been largely studied and reported in literature [15–17], more in detail studies regarding formulations for PV applications are still in progress. Moreover, the influence of the materials formulation in terms of additives and their effects on encapsulants degradation over long term exposure is still an open question.

In this study, two newly developed PV encapsulant materials (a TPO and a POE) were subject to artificial ageing tests and their performances were compared to the most widely used encapsulant (EVA). The influence of the exposure to UV radiation, temperature and humidity was studied and the effects on additive composition, chemical degradation and thermal stability are discussed. Bare polymer films, thermally pre-treated but not encapsulated within the typical PV module stack configuration were the object of this study. The choice of using films was made to better understand how environmental factors influence the degradation behavior of the polymer itself directly exposed and to have an insight of what could happen to the materials in case that additional degradation modes, such as backsheet cracks and extensive delamination, might occur [18, 19]. The work aims to make a step forward in understanding and comparing performances of newly developed material with respect to the state-of-the-art EVA by means of a comprehensive analysis that has not been performed before. Additionally, a new methodology that correlates oxidation indices measured via infrared spectroscopy and thermal stability indicators is presented.

4.2 Experimental

Three types of polymer materials commercially available were chosen in this study: an ultra-fast cure EVA, a thermoplastic polyolefin (TPO) and a polyolefin elastomer (POE). The materials mentioned above are all polyethylene based and used as encapsulants in photovoltaic applications. The samples were pre-treated in a vacuum laminator between two non-adhesive sheets at maximum temperature of 150 °C for a total duration of 20 minutes and were cut into

stripes before being subject to artificial ageing tests. Main encapsulants characteristics are summarized in Table 4.1.

Table 4.1 Encapsulants characteristics

Encapsulant	Thickness (μm)	Chemical crosslinking	Acetic acid
EVA	450	Yes, with peroxides	Yes
TPO	500	No	No
POE	550	Yes, with peroxides	No

The samples were aged under damp heat (DH) test up to 3300 hours in a climate chamber WLK 64-40 from Weiss Umwelttechnik GmbH. The temperature was set to 85 °C and relative humidity to 85%. Samples were withdrawn from the climate chamber after 1000 hours, 1800 hours, 2300 hours, and 3300 hours of exposure and were characterized according to the methods described in Chapter 3

To evaluate the effect of UV radiation, samples were aged in an UVTest™ Fluorescent UV/Condensation Weathering instrument from Atlas Material Testing Technology LLC. The test cycles were programmed according to the standard ISO 4892-3 Cycle 1 [20] (Table 4.2), using fluorescent lamps with an irradiation peak at 340 nm and the maximum dose applied is 200 kW h m^{-2}. Samples were withdrawn from the UV test after being exposed to a dose of 23 kW h m^{-2}, 85 kW h m^{-2}, 127 kW h m^{-2} and 200 kW h m^{-2} and were characterized as described in Chapter 3.

Table 4.2 UV test cycles parameters

Function	Irradiation (W m^{-2} nm^{-1})	Black Panel Temperature (°C)	Time (hours : minutes)
UV light	0.76	60	8:00
Condensation	n/a	50	4:00

4.3 Results and discussion

4.3.1 TD-GC/MS for qualitative additive analysis

TD-GC/MS measurements were performed to detect qualitatively the stabilizers present in the encapsulants selected throughout their exposure to artificial ageing tests [21]. In general, the area below the peaks in the chromatogram can be related to concentration values, but the strong dependency of the peaks' height on the amount of the material itself as well as on inhomogeneity of polymers do not allow, in this case, quantitative interpretations of results. Additionally, it is possible that not all the additives and stabilizers present in the encapsulants are detected. Nevertheless, the method is very useful to get insights regarding the main stabilization recipe for each material.

A butylated hydroxytoluene (BHT) was identified as antioxidant for the EVA material as well as an UV absorber belonging to the benzophenone class (2-Hydroxy-4-(octyloxy)phenyl(phenyl)methanone. It was possible to detect both stabilizers after 3300 hours of exposure in DH test, as shown in Figure 4.1. Additionally, a benzotriazole-type UV absorber (2-(2H-benzotriazol-2-yl)-4,6-bis(1,1-dimethylpropyl)phenol) was detected after 1000 hours of DH exposure and until the end of the artificial ageing test [8, 22]. Benzotriazole-type UV absorbers are soluble in water and it is possible that due to the high humidity values, a relevant fraction of the stabilizers migrated from the bulk to the surface of the material, hence facilitating thermal desorption processes and detection via TD-GC/MS. The combination of benzophenone and benzotriazole based stabilizers was proven to give a positive effect on the ageing behavior of polyolefin based materials [23]. After the exposure to UV test, the BHT antioxidant was detected up to 85 kW h m^{-2}, whereas the benzophenone-based UV absorber was detected up to 200 kW h m^{-2}. No additional benzotriazole-type UV absorber could be identified.
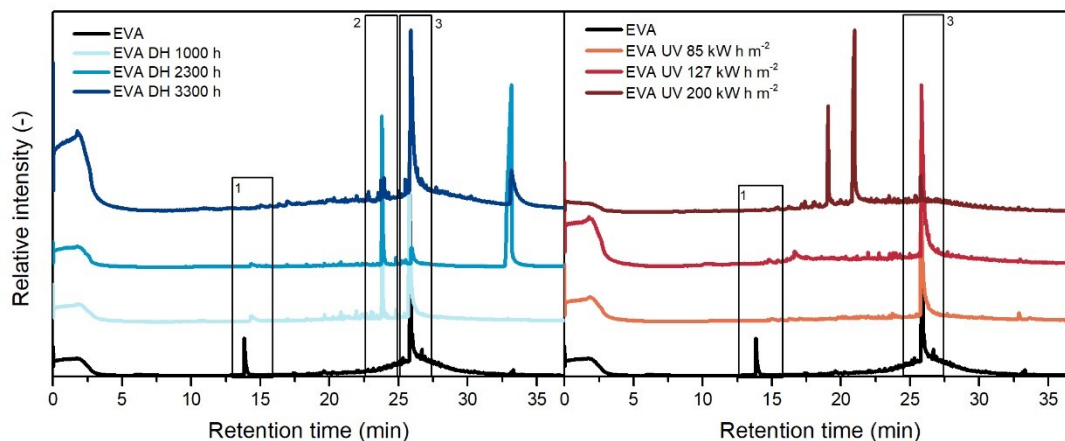
Figure 4.1: Chromatograms of EVA samples exposed to DH test (left) and UV test (right).

A fragment of BHT antioxidant [24] as well as an additional sterically hindered phenolic antioxidant (Octadecyl 3-(3,5-di-tert-butyl-4-hydroxyphenyl)propionate, also known as Antioxidant 1076) were detected in unexposed TPO encapsulant, Figure 4.2. At the end of the DH test it was still possible to detect the BHT antioxidant, but it was no longer possible to detect the hindered phenolic antioxidant. As for EVA, it was possible to detect after 1000 hours of the DH test and up to 3300 hours, a benzotriazole-type UV absorber. Extensive degradation of this encapsulant could be assessed after the exposure to UV radiation. A dose of 85 kW h m^{-2} was sufficient to deplete all the stabilizers present in the bare material, as it was no longer possible to detect any stabilizer. Details of resulting degradation processes will be given in the next sections. Additionally, at the end of the UV exposure test (applied dose of 200 kW h m^{-2}), only degradation products of the encapsulant itself were detectable.

The analysis carried out on the POE sample before the exposure to artificial ageing tests showed the presence of a BHT antioxidant, which was no longer detected after 1000 hours of DH test, Figure 4.3. A benzotriazole-type UV absorber was, instead, detected after 1000 hours of DH exposure. During UV test, the BHT was no longer detected, while traces of the hindered phenolic antioxidant were detected up to a dose of 200 kW h m^{-2}.
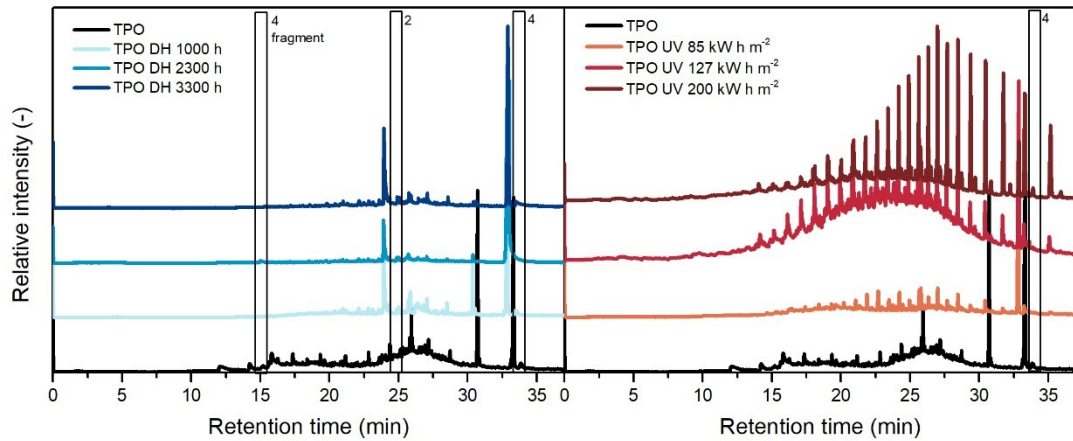
Figure 4.2: Chromatograms of TPO samples exposed to DH test (left) and UV test (right)
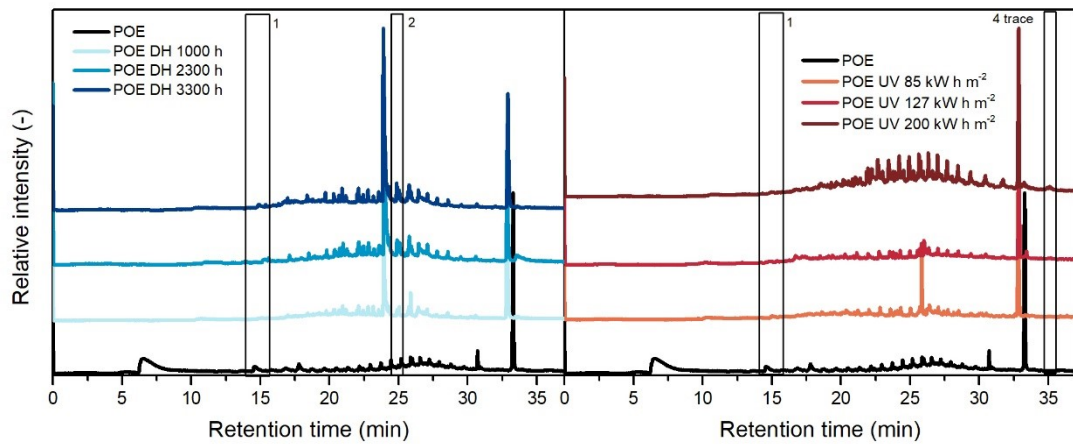

Figure 4.3: Chromatograms of POE samples exposed to DH test (left) and UV test (right).

The mass spectra of the detected stabilizers are showed in Figure 4.4. The identification of the substances based on their mass spectra, as described in Figure 4.4. A summary of the detected stabilizers over the exposure to the artificial ageing tests is shown Table 4.3
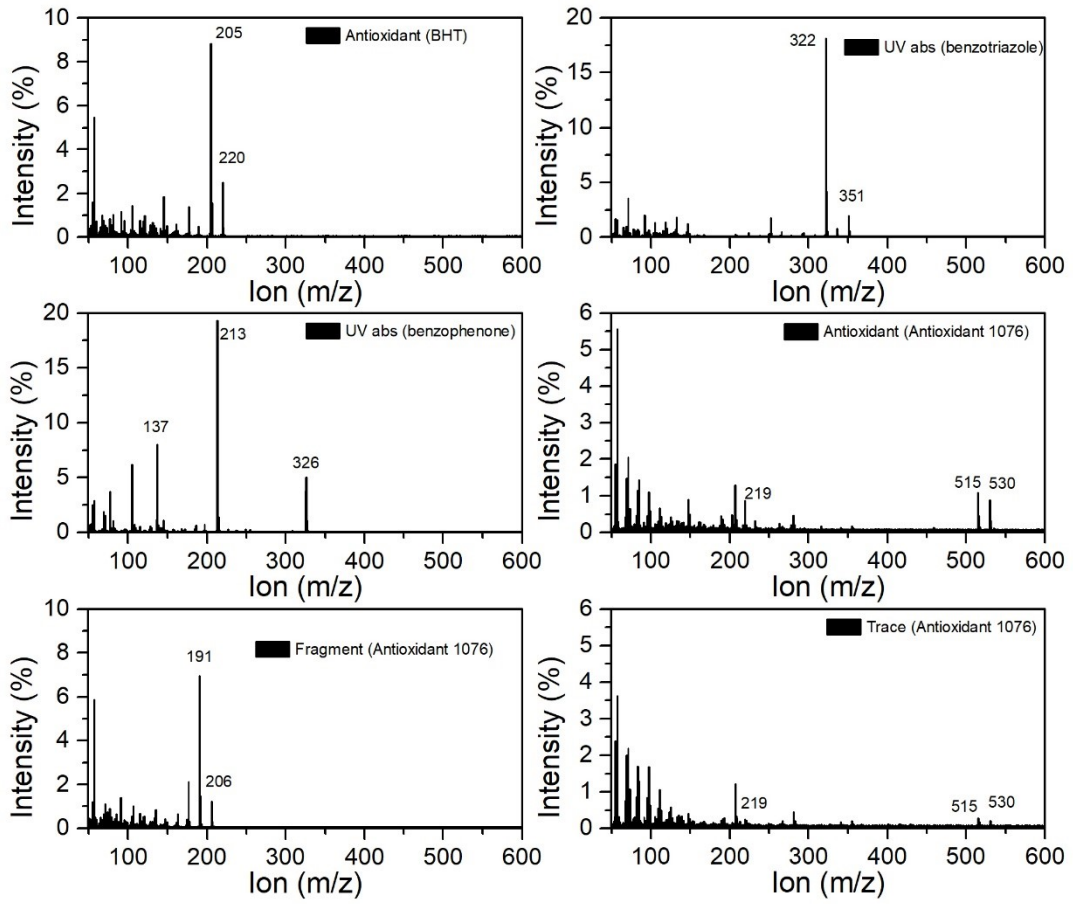
Figure 4.4: Mass spectra of the additives detected by means of TD-GC/MS.

.

Table 4.3 Summary of TD-GCMS measurements on the encapsulants exposed to DH and UV tests

EVA					
	Unexposed	**DH ageing time** **3300 hours**	**UV dose** **85 kW h m^{-2}**	**UV dose** **127 kW h m^{-2}**	**UV dose** **200 kW h m^{-2}**
Antioxidant (BHT)	✓	✓	✓	✓	n.d.
UV absorber (benzophenone)	✓	✓	✓	✓	✓
UV absorber (benzotriazole)	n.d.	✓	n.d.	n.d.	n.d.
TPO					
	Unexposed	**DH ageing time** **3300 hours**	**UV dose** **85 kW h m^{-2}**	**UV dose** **127 kW h m^{-2}**	**UV dose** **200 kW h m^{-2}**
Antioxidant (Antioxidant 1076)	✓	fragment	n.d.	n.d.	n.d.
UV absorber (benzotriazole)	n.d.	✓	n.d.	n.d.	n.d.
POE					
	Unexposed	**DH ageing time** **3300 hours**	**UV dose** **85 kW h m^{-2}**	**UV dose** **127 kW h m^{-2}**	**UV dose** **200 kW h m^{-2}**
Antioxidant (BHT)	✓	fragment	n.d.	n.d.	n.d.
UV absorber (benzotriazole)		✓	n.d.	n.d.	n.d.
Antioxidant (Antioxidant 1076)	n.d.	n.d.	traces	traces	traces

n.d. = not detected

4.3.2 UV-Vis-NIR Spectroscopy

Maximum transmittance values of EVA, Figure 4.5, decreased over the exposure in both DH and UV test from (91% to 88%). After the exposure to a dose of 200 kW h m^{-2} a decrease in transmittance values in the blue range of the spectra (380 nm – 500 nm) could be connected to a yellowing of the material. A slight decrease of the UV cut-off values was observable as well as an increase of the transmittance value in the region between 250 nm and 350 nm, which might be correlated to the consumption of the UV absorbers. Additionally, the peak present at around 260 nm, possibly associated to presence of the BHT antioxidant, disappeared after a dose of 200 kW h m^{-2} and this result is in good accordance with the results from qualitative additive analysis.
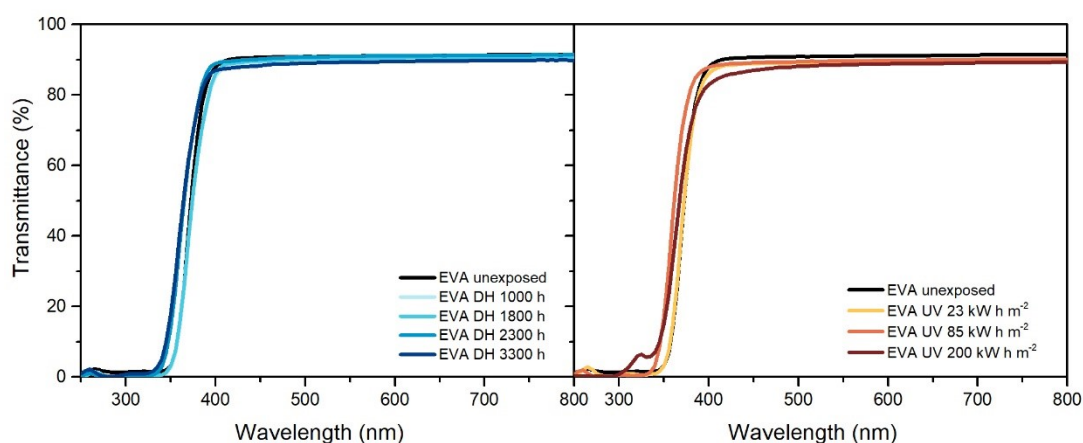
Figure 4.5: UV-Vis spectra of EVA unexposed, exposed to DH (left) and UV test (right).

In the case of TPO, Figure 4.6, results showed transmittance values higher than 90% below 390 nm. After the exposure to DH test, it was possible to observe a decrease of transmittance value below 390 nm, but the maximum value of transmittance in the visible range remained the same. The samples exposed to 127 kW h m^{-2} and to 200 kW h m^{-2} showed very strong signs of embrittlement and it was not possible to perform further measurements on these materials. Nevertheless, already after a dose of 85 kW h m^{-2} the material showed a decrease of transmittance below 390 nm as well as above. The decrease between 380 nm and 580 nm can be attributed to chromophore formation that results in material discoloration [25] and increase of crosslinking due to photo-oxidation reactions.
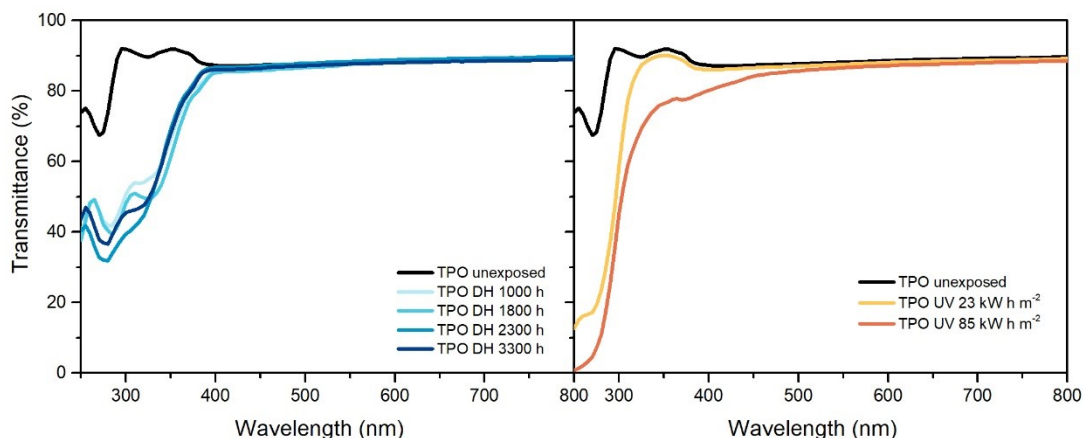
Figure 4.6: UV-Vis spectra of TPO unexposed, exposed to DH (left) and UV test (right).

POE, similarly to TPO, showed a transmittance value higher than 90% below 390 nm, which decreased upon UV exposure (Figure 4.7). The maximum transmittance in the visible range decreases from 92% to 90% and finally to 88%. During DH exposure, instead, transmittance values decreased in the UV ranges as well as in the visible range below 500 nm, indicating material's yellowing due to chromophore formation [25]. Formation of chromophores as well as migration of additives might have caused also the changes in transmittance below 390 nm, observable for POE and TPO [14, 25].
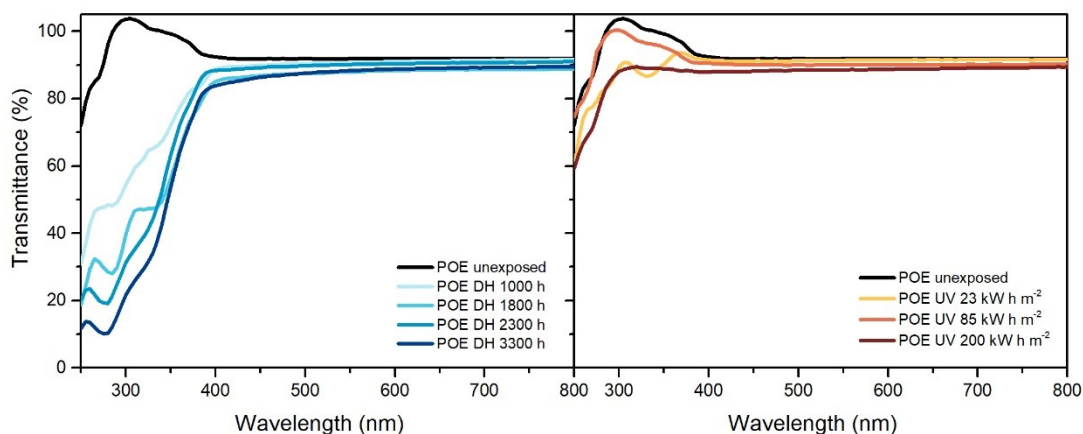
Figure 4.7: UV-Vis spectra of POE unexposed, exposed to DH (left) and UV test (right).

4.3.3 FT-IR ATR Spectroscopy

Analysis of degradation behavior of EVA can be performed by means of FT-IR ATR Spectroscopy measurements, Figure 4.8 The bands that can be seen at

2920 cm^{-1}, 2850 cm^{-1}, 1465 cm^{-1} and 1370 cm^{-1} can be assigned to stretching and deformation vibrations of methylene and ethylene groups, whereas the band at 720 cm^{-1} can be assigned to rocking vibrations of ethylene groups. The bands mentioned above are all characteristics of polyethylene [26].
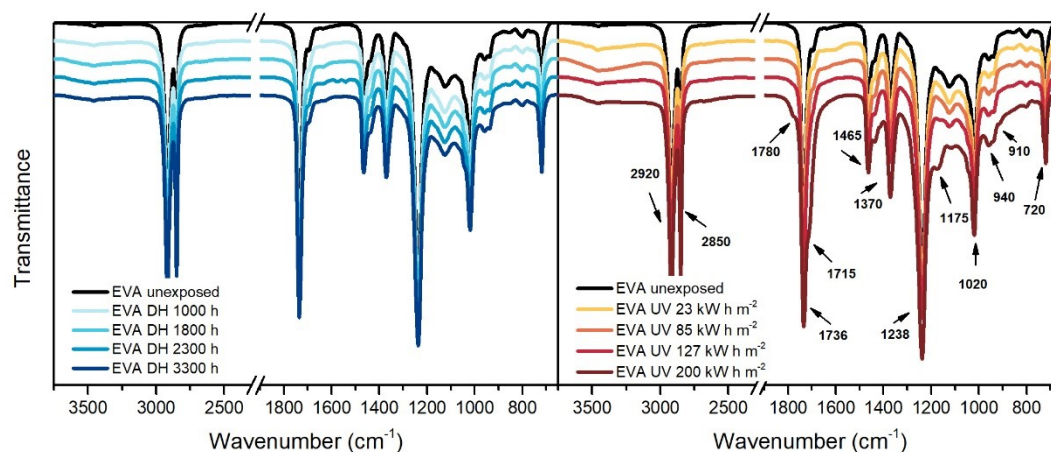

Figure 4.8: FT-IR ATR Spectroscopy measurements of EVA samples before and after exposure to DH (left) and UV test (right).

Vinyl acetate moieties can be identified from the bands at 1736 cm^{-1} (corresponding to C=O stretching vibrations), 1238 cm^{-1} and 1020 cm^{-1}, which can be assigned to C−O−C stretching vibrations [27].

The EVA spectra after 3300 hours of exposure in the climate chamber does not show presence of new peaks. Photo-thermal degradation processes, instead, take place during UV exposure and it is possible to observe the presence of new peaks due to formation of new functional groups. The typical thermal degradation pathway for EVA involves the production of acetic acid followed by main chain decomposition processes. Polyethylene chains, as result of thermal degradation, form hydroperoxide groups that can further react and form various carbonyl groups. The formation of the shoulder at 1780 cm^{-1} can be attributed to the formation of γ-lactone due to back-biting process of vinyl acetate moieties [27]. The broadening of the shoulder at 1715 cm^{-1} as well as the band at 1175 cm^{-1} are associated to ketones. Those species might be produced by means of acetaldehyde evolution or breakdown of hydroperoxides. The characteristic bands of EVA as well as appearance of new bands with their assignment are summarized in Table 4.4.

Table 4.4: Assignment of FT-IR bands in EVA spectra.

Wavenumber [cm^{-1}]	Assignment
2920	Asymmetric stretching vibration of CH_2
2850	Symmetric deformation vibration of CH_2
1780	C=O stretching vibration of γ-lactones
1715/1175	C=O stretching vibration of ketones
1736	C=O stretching vibration
1465	Asymmetric deformation vibration of CH_3
1370	Symmetric deformation of CH_3
1238	C–O–C stretching vibration
1020	C–O–C stretching vibration
960-940	CH out-of-plane deformation vibration of vinyl ether
910	CH out-of-plane deformation vibration of vinyl
720	CH_2 skeleton rocking vibration

TPO, Figure 4.9, is a polyethylene based encapsulant and, therefore, it shows in the IR spectra the typical peaks of polyethylene at 2920 cm^{-1}, 2850 cm^{-1}, 1465 cm^{-1}, 1370 cm^{-1} and 720 cm^{-1}. Additionally, the unexposed material shows the presence of a band around 1600 cm^{-1} that might be attributed to the C=C aromatic bonds of the hindered phenolic antioxidant [28], detected by means of TD-GCMS as well.

After the exposure in DH test, the spectrum does not show relevant changes. The dose of 85 kW h m^{-2} during the UV test is, instead, already sufficient to cause damages to the material. The main differences with the unexposed material are noticeable in the ranges 800 cm^{-1} – 1400 cm^{-1}, 1680 cm^{-1} – 1800 cm^{-1} and 3100 cm^{-1} – 3700 cm^{-1} corresponding to unsaturation, carbonyl and hydroxyl regions, respectively. The material exposed to 200 kW h m^{-2} of UV dose shows a progression of the damage and extensive effects. According to the work published by Yagoubi et al. [29], macro-radicals are formed when macromolecules absorb energy from UV light. Subsequently, macro-radicals can react with the surrounding oxygen molecules and light can catalyze the formation of substances that eventually react with the polymer chain giving hydroperoxides. These latter can further decompose and produce ketones, aldehydes, carboxylic acids and esters through different routes.
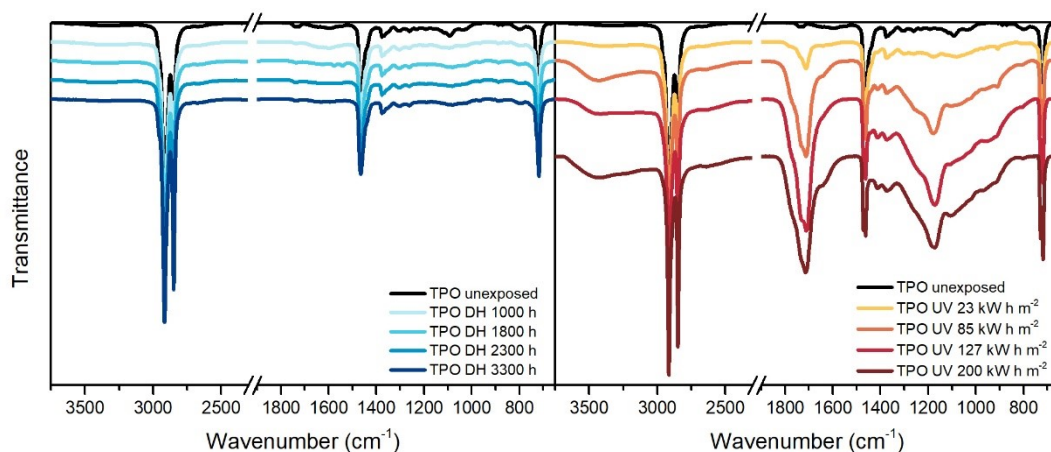
Figure 4.9: FT-IR ATR Spectroscopy measurements of TPO samples before and after exposure to DH (left) and UV test (right).

Peaks similar to TPO can be identified in the unexposed POE sample. Typical peaks of polyethylene-based materials can be identified and they are summarized in Table 4.5.

Table 4.5: Assignment of FT-IR bands in POE spectra.

Wavenumber [cm^{-1}]	Assignment
2920	Asymmetric stretching vibration of CH_2
2850	Symmetric stretching vibration of CH_2
1800-1600	C=O stretching vibration
1715/1175	C=O stretching vibration of ketones
1465	Asymmetric deformation vibration of CH_3
1370	Symmetric deformation of CH_3
909	CH out of plane deformation-vibration of vinyl
720 (doublet)	CH_2 skeleton rocking vibration

During DH exposure no relevant changes can be detected, see Figure 4.10, and slight differences can be seen after UV exposure. In particular, it is possible to notice the formation of a new peak at 909 cm^{-1} corresponding to vinyl group, as well as in the carbonyl region, between 1670 cm^{-1} and 1800 cm^{-1}, and in the hydroperoxide region, between 3100 cm^{-1} and 3700 cm^{-1}. The presence of a peak around 1715 cm^{-1} and 1175 cm^{-1} indicates the formation of ketones. The ageing mechanism seems to be similar to the one taking place in the TPO encapsulant

(but less pronounced), as expected since the two materials are similar from the chemical point of view.
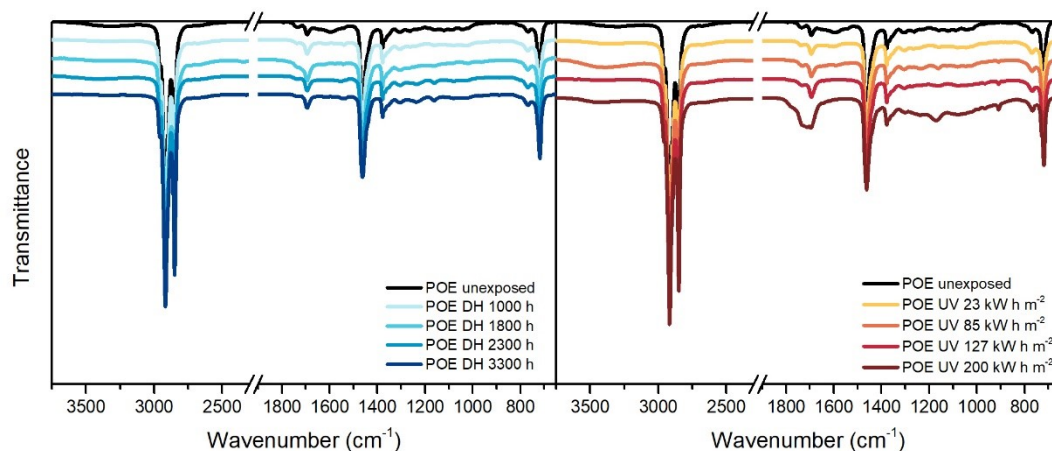

Figure 4.10: FT-IR ATR Spectroscopy measurements of POE samples before and after exposure to DH (left) and UV test (right).

Oxidation Indices (OI) have been evaluated to compare the overall oxidation state of the materials. The values were calculated as the ratio between the integral of the spectra from 1680 cm^{-1} to 1800 cm^{-1} (carbonyl region, related to oxidation products) and the reference band from 2760 cm^{-1} to 2875 cm^{-1}. Results were normalized with respect to the initial value and are shown in Figure 4.11.

The samples exposed to DH test do not show any substantial change, whereas each encapsulant shows signs of oxidation after UV exposure. An increase of almost 1.5 times compared to the initial values can be observed for the EVA material when the UV dose applied is 200 kW h m^{-2}. By applying a linear piecewise fitting function to the data, the dose from which the material begins to show oxidation is extrapolated. To evaluate the accordance of the fitting function to the data, R^2 values were considered. In the case of EVA, the fitting function shows an R^2 value of 0.997 and a dose of about 113 kW h m^{-2} is sufficient to initiate oxidation. The final value of OI is about 3.4 times higher than the initial one for POE encapsulant and a dose of about 131 kW h m^{-2} (R^2=0.984) is necessary to initiate degradation.
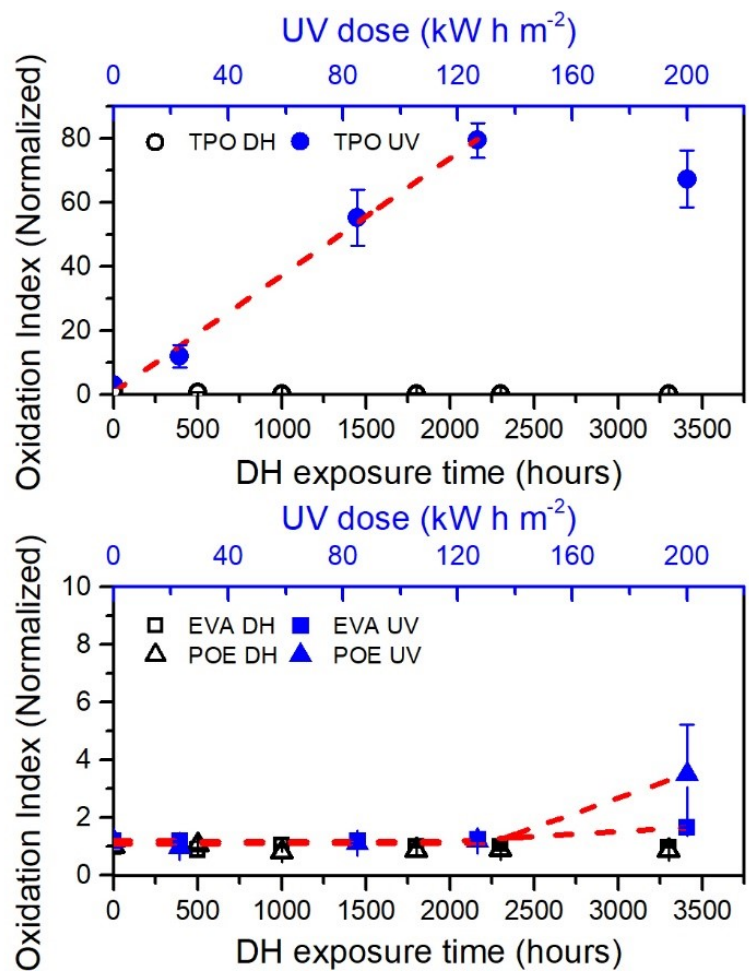
Figure 4.11: Oxidation Index versus exposure time (DH test, open symbols in black color) and dose (UV test, full symbols in blue color). Red dashed lines are fitting functions applied to the data to extrapolate the oxidation induction time/dose. TPO (top chart), EVA and POE (bottom chart).

TPO is the material that shows the most severe degradation. Considering only the first four steps of the artificial ageing tests, a liner fit can be applied to the data and an OI increasing rate of 0.0293 m^2 kW^{-1} h^{-1} is obtained, with an R^2 value of 0.994. The OI value calculated at 127 kW h m^{-2} is almost 80 times higher than the initial value. The OI value at the final stage of the UV test is considered as outlier in this analysis because of the very strong physical degradation, associated to chemical processes. The occurrence of the oxidation processes well correlates with consumption of antioxidants, for all the materials, as detected by means of TD-GCMS.

4.3.4 DSC

Samples aged under different accelerated ageing procedures showed significant changes in thermal behavior. In general, thermal properties can be influenced by both physical and chemical ageing processes. Chemical processes such as chain scission that might occur during UV ageing due to photo-oxidation are responsible for chemo-crystallization, namely secondary crystallization. The effects of chemical ageing are irreversible and can be detected by observing changes in crystallinity and melting temperature in the second heating curve. The first heating curve might show the same signs of degradation, but they are the results of a combination of chemical and physical ageing. Physical processes have similar effects to the ones due to annealing at high temperatures, changes in melting temperature and enthalpy might occur and are visible in the first heating curve. No reversible effects of physical ageing can be seen in the second heating curve [30–33].

For EVA, Figure 4.12 (a), it is possible to notice that there is a change in its thermal behavior in the first heating cycle. The main melting peak of EVA, with maximum at 66 °C, does not change its position, even after 3300 hours of DH test. The secondary melting peak, instead, shifts towards lower temperature values from 45 °C to 37 °C indicating a physical change in the crystal population of the material, not associated with chemical degradation. The presence of vinyl acetate moieties in EVA induces a different ability of the material to crystallize. Ethylene segments in vinyl acetate moieties have the tendency to form smaller and less perfect crystals, which melt at lower temperature compared to the polyethylene units [13, 34].

During the UV test, Figure 4.12 (c), a combination of effects from physical and chemical ageing can be observed. On one side, the first heating run reveals the presence of a shoulder below the main melting temperature and a shift of this latter towards higher values (from 66 °C to 83 °C). This is a typical effect that can occur when the annealing (ageing) temperature lies within the melting region. During the exposure in the test chamber at 60 °C, smaller crystals with thinner lamellae can melt and crystallize again to form more perfect crystals with thicker lamellae, which melt at higher temperatures [30, 31, 33]. Additionally, in the last two steps of the UV test, it is possible to notice a shift of the melting temperature visible in the second heating run of the DSC

measurement from 66 °C to 68 °C and finally to 86 °C, which is an indicator for the occurrence of deacetylation reaction [13, 34]. Signs of chemo-crystallization are noticeable also when looking at the cooling curve of the thermogram (Figure 4.12(d)) because the crystallization peak is shifted to much higher temperatures and the temperature range in which the crystallization process takes place is enlarged.
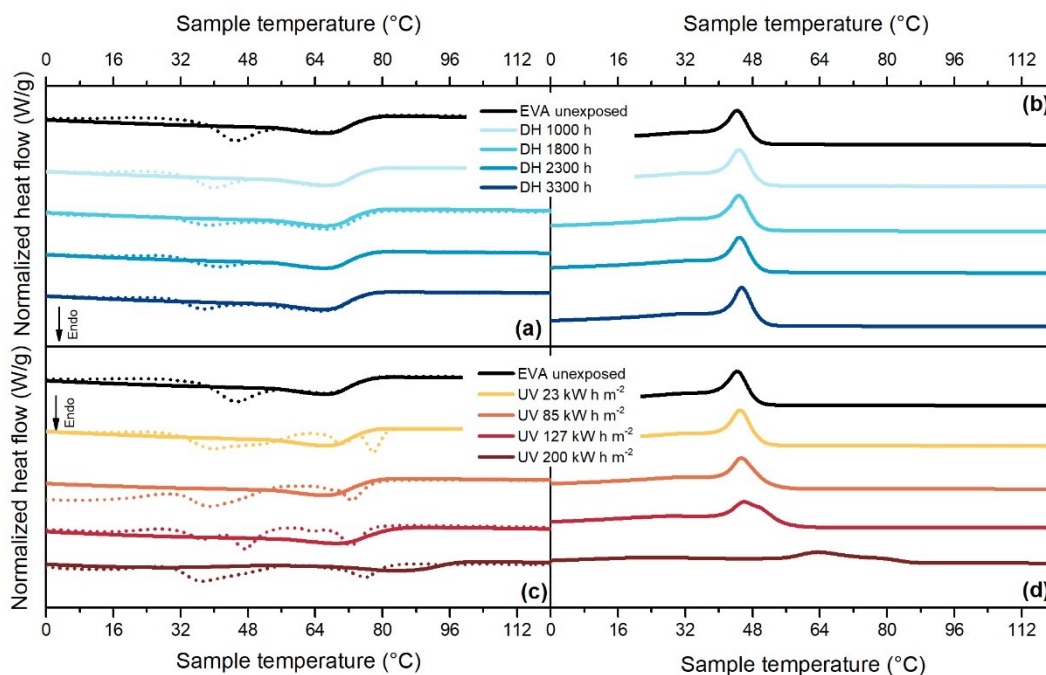

Figure 4.12: DSC thermograms for EVA. First heating curves (dashed lines) and second heating curves (full lines) from samples exposed to DH test (a). Cooling curves for samples exposed to DH test (b). First heating curves (dashed lines) and second heating curves (full lines) from samples exposed to UV test (c). Cooling curves for samples exposed to UV test (d).

TPO material, Figure 4.13 (a), shows a main melting peak at around 109 °C as well as a shoulder at about 94 °C, which is no longer visible during the second heating run. During DH test exposure, no significant changes in crystallinity and melting temperature can be observed. Only a rearrangement of the crystal population can be seen in the first heat run, similarly to EVA. During UV exposure, instead, the crystallinity significantly increases from 30% (unexposed sample) to 50% (sample exposed to 200 kW h m^{-2}). Additionally, the shoulder's temperature increases from 94 °C to 105 °C, whereas the main melting peak's temperature shifts from 109 °C to almost 115 °C, as can be seen in Figure 4.13 (c). The shift of the main melting peak is not visible when looking at the

thermogram of the second heating run. During the cooling cycle, Figure 4.13 (d), there is an increase of the crystallization peak's temperature from 95 °C (unexposed material) up to 98 °C (sample exposed to 85 kW h m⁻²) followed to a decrease down to 94 °C for the sample exposed to the maximum dose (200 kW h m⁻²). Additionally, the peak visible at around 76 °C is shifted to about 86 °C.
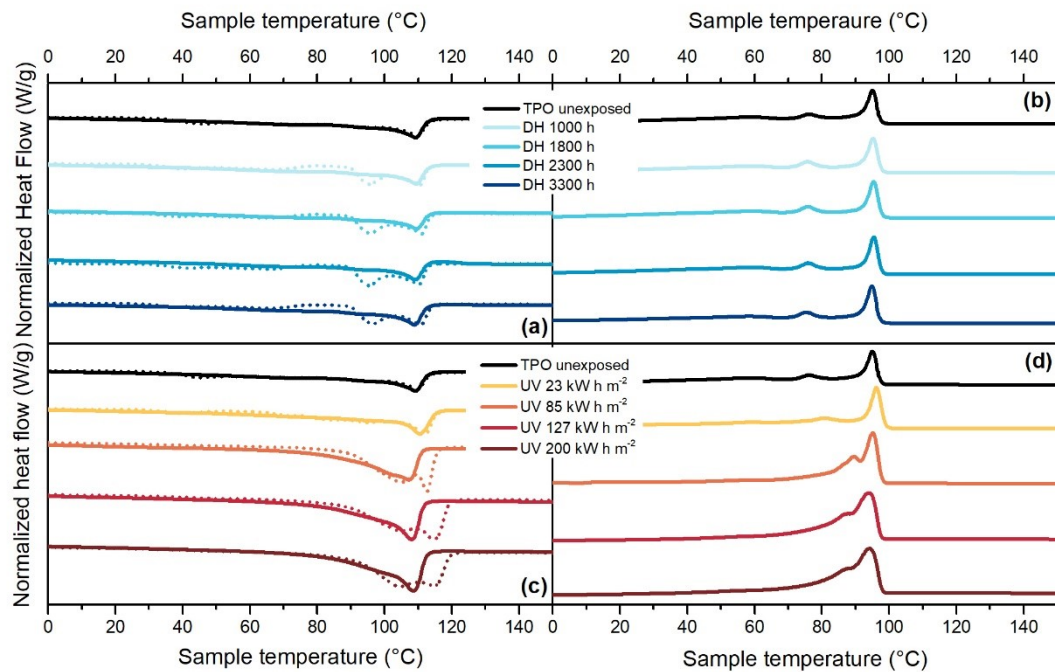

Figure 4.13: DSC thermograms for TPO. First heating curves (dashed lines) and second heating curves (full lines) from samples exposed to DH test (a). Cooling curves for samples exposed to DH test (b). First heating curves (dashed lines) and second heating curves (full lines) from samples exposed to UV test (a). Cooling curves for samples aged under UV test (b).

In this case, there is a competitive effect between changes in thermal behavior due to chain scission processes and crosslinking phenomena. These phenomena take place simultaneously when photo-oxidation reaction take place, as in the case of UV exposure, and both are responsible for severe embrittlement of the material [35–37]. Due to chain scission there is a formation of smaller chains that work as nucleating agents. A larger number of nuclei is present, and this leads to an increase in crystallinity, Figure 4.14, as well as an increase in crystallization temperature. Additionally, the presence of these smaller nuclei is shown by the tail of the crystallization peak that is shifted towards lower temperature [30].

The thermogram of POE, Figure 4.15 (a), shows a main melting peak at about 55 °C for the unexposed material and a secondary melting peak at about 41 °C. In the second heating run, the secondary melting peak disappears, thus showing a difference in the crystals' population.
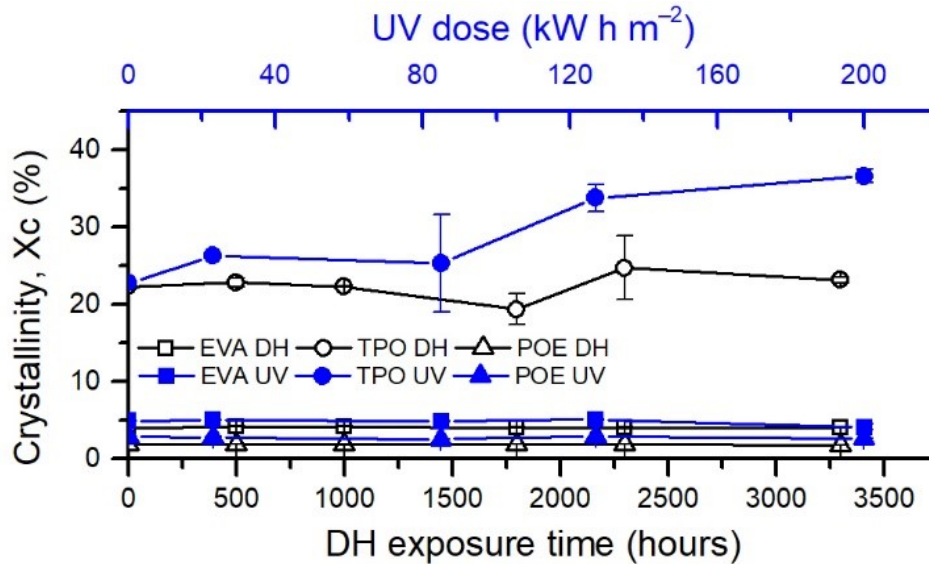

Figure 4.14: Evolution of crystallinity over UV and DH exposure of the encapsulants (EVA, TPO, and POE).
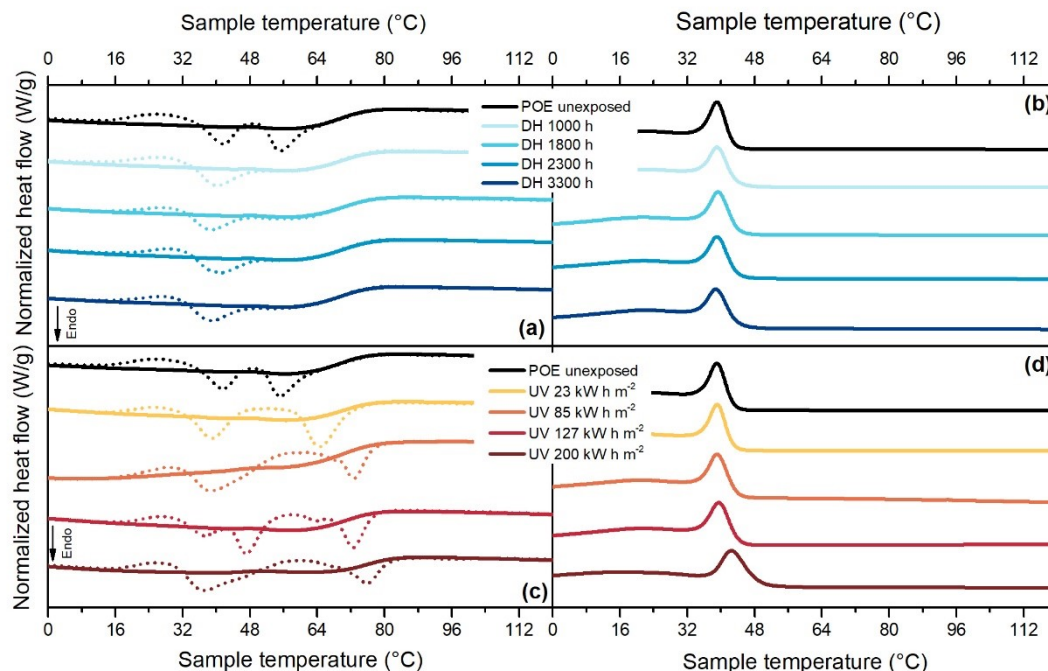

Figure 4.15: DSC thermograms for POE. First heating curves (dashed lines) and second heating curves (full lines) from samples exposed to DH test (a). Cooling curves for samples exposed to DH test (b). First heating curves (dashed lines) and

After DH exposure, it is possible to notice that the secondary melting peak slightly shifts to lower temperatures, from 41 °C to 39 °C, whereas the main melting peak appears more similar to a shoulder at around 56 °C. After the exposure to UV radiation significant effects of physical ageing can be observed, Figure 4.15 (c). For POE encapsulant, as well as for EVA, the temperature of the ageing test (65 °C during the light cycle and 50 °C during the dark cycle) plays an important role influencing the crystal population present in the material because it is within the melting interval. Two melting peaks are detected at 39 °C and at 76 °C (after a dose of 200 kW h m^{-2}). The second heating run shows signs of chemical degradation due possibly to chain scission because the melting temperature increases from 55 °C to 62 °C. The occurrence of chain scission is supported by the increase of crystallization temperature from 39 °C to almost 43 °C and by the shift of the tail of the crystallization process towards lower temperatures, Figure 4.15 (d).

4.3.5 TGA

TGA measurements on the encapsulants before and after the exposure to the artificial ageing tests have been carried out to monitor the evolution of the thermal stability of the materials.

For the EVA material, Figure 4.16, the decomposition process takes place in two steps: the first step is typical of the cleavage of vinyl acetate moieties, whereas the second step corresponds to the decomposition of the main polyethylene chains. As can be seen from the first derivative of the thermogram, the maximum weight loss rate during the deacetylation and polyethylene decomposition reaction is detectable at around 350 °C and 474 °C, respectively.
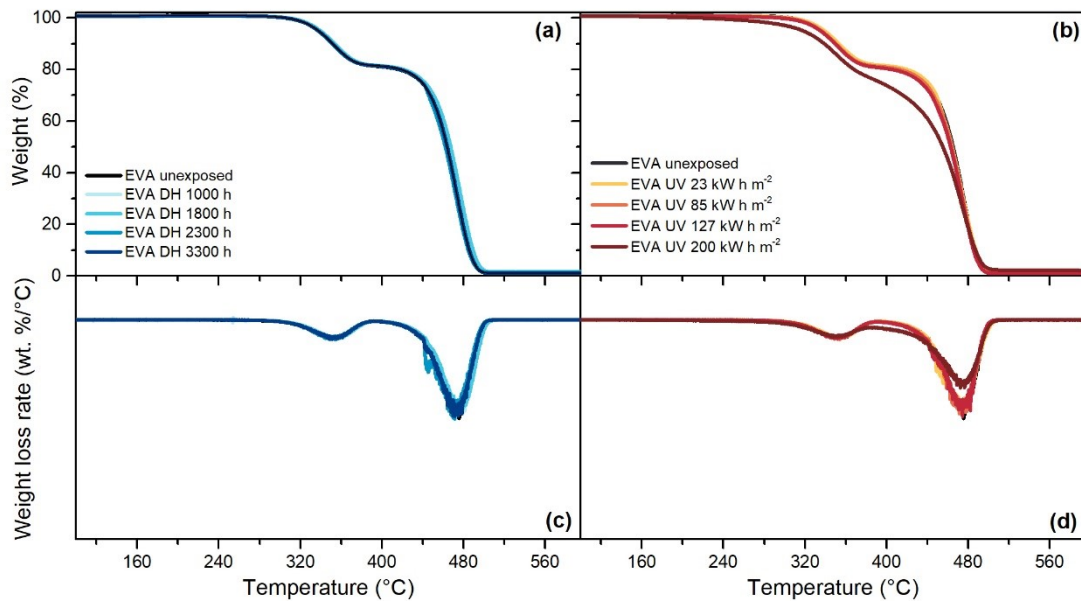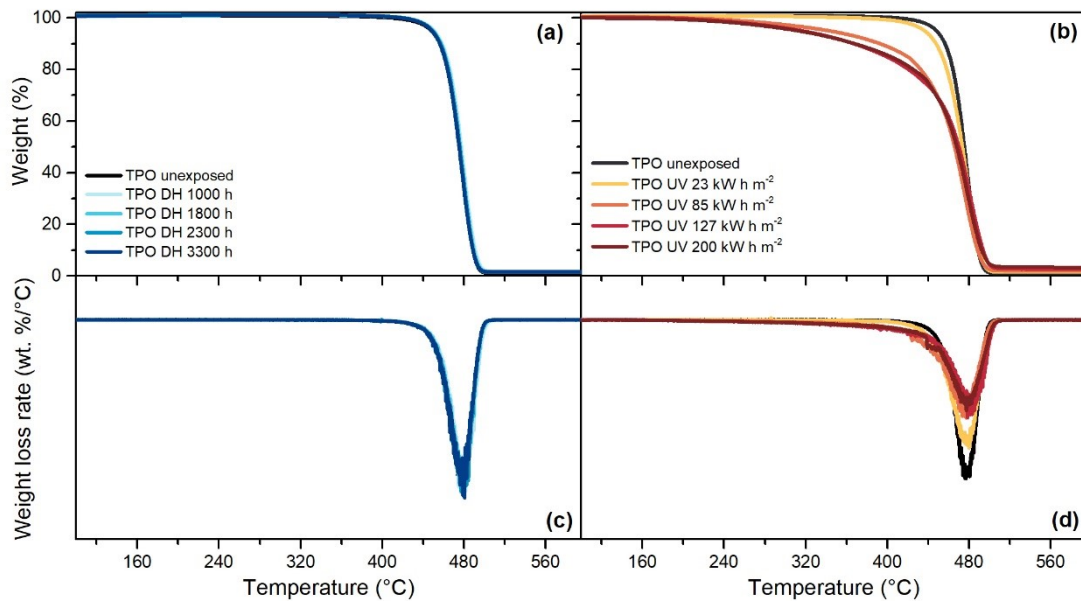
Figure 4.16: Residual weight over temperature during TGA measurements of EVA after the exposure to DH test (a). Residual weight over temperature during TGA measurements of EVA after the exposure to UV test (b). Weight loss rate over temperature of EVA samples exposed to DH test (c). Weight loss rate over temperature of EVA samples exposed to DH test (d).

TPO, Figure 4.17, and POE, Figure 4.18, are characterized by a one-step decomposition process, with a maximum weight loss rate at around 478 °C and 474 °C, respectively. The exposure to DH test does not show significant differences for any of the encapsulants, as can be seen from the good overlapping of the thermograms of the unexposed and the materials exposed to DH test after 3300 hours. Signs of degradation are detectable after UV test. For TPO, the thermogram of the material exposed to a dose of 85 kW h m^{-2} shows already a deviation from the unexposed material and the deviation is visible also for materials exposed to higher doses, the same trend can be seen when looking at the weight loss rate curve, the intensity of the peak, indeed, is halved after 85 kW h m^{-2} with respect to the unexposed encapsulant. For POE, the thermograms overlap to the unexposed material except that for the materials exposed to 200 kW h m^{-2}, evident also from the weight loss rate curve that shows a lower intensity of the peak.

Figure 4.17: Residual weight over temperature during TGA measurements of TPO after the exposure to DH test (a). Residual weight over temperature during TGA measurements of TPO after the exposure to UV test (b). Weight loss rate over temperature of TPO samples exposed to DH test (c). Weight loss rate over temperature of TPO samples exposed to DH test (d).
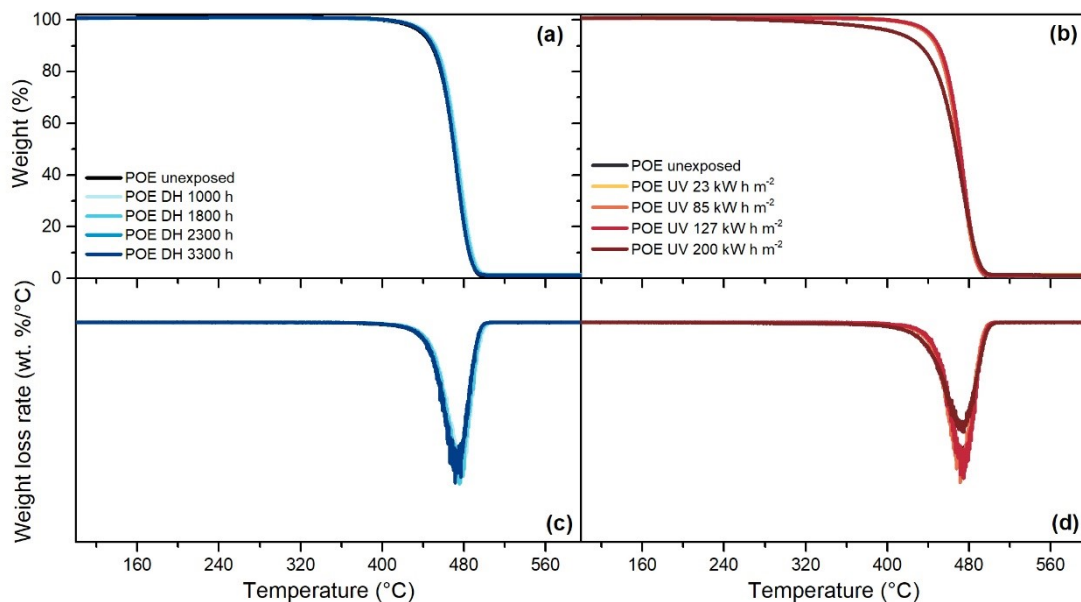

Figure 4.18: Residual weight over temperature during TGA measurements of POE after the exposure to DH test (a). Residual weight over temperature during TGA measurements of POE after the exposure to UV test (b). Weight loss rate over temperature of POE samples exposed to DH test (c). Weight loss rate over temperature of POE samples exposed to DH test (d).

Figure 4.19 summarizes the temperature at which each material reaches a residual weight of 95%, defined as T_5. Photo-degradation processes that took place during UV test significantly lowered the thermal stability of TPO. In fact, the decomposition process begins at much lower temperatures compared to the unexposed material. A dose of 85 kW h m^{-2} is sufficient to cause a 5% weight drop at around 343 °C instead of 448 °C (106 °C of difference). Considering the first four steps of the UV test and applying a linear fit to the data a value of $R^2 = 0.96$ is obtained, thus indicating a linear decrease of the thermal stability upon the UV dose up to 127 kW h m^{-2}. The value measured for TPO exposed to 200 kW h m^{-2}, also in this analysis, results as an outlier compared to the other data. The results mentioned above are in good accordance to what has been shown with the analysis of the OI and with the evolution of the thermal properties measured with DSC. It can be derived that UV doses lower that 130 kW h m^{-2} are sufficient to severely degrade a bare TPO encapsulant.

The dose of 200 kW h m^{-2} is sufficient to decrease the thermal stability of EVA and POE because the aged material reaches T_5 at lower temperatures compared to the unexposed materials of about 21 °C and 29 °C, respectively. A linear piecewise fitting can be applied to the data of EVA and POE to extrapolate the UV dose necessary to cause significant decrease of the thermal stability. Doses of 127 kW h m^{-2} ($R^2 = 0.994$) and of 148 kW h m^{-2} ($R^2 = 0.982$) for EVA and POE, respectively, can be extrapolated.
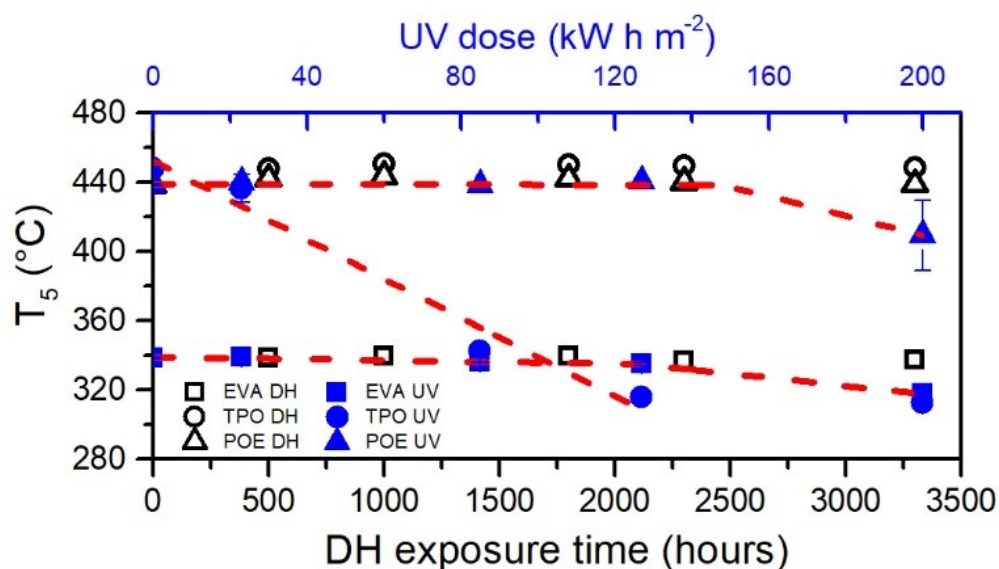

Figure 4.19: Temperature corresponding at 95% residual weight (T_5) versus exposure time (DH test, open symbols in black color) and dose (UV test, full symbols in blue

color). **Red dashed lines are linear fittings applied to the data to extrapolate the oxidation induction time/dose.**

4.4 Comparison of performances

Comparing the evolution of oxidation indices and T_5 values over the UV dose, the results show a very good agreement (Figure 4.20). A linear fitting has been applied to each dataset and R^2 values of 0.968, 0.980 and 0.983 have been determined for EVA, TPO and POE, respectively. In the case of TPO, the linear fitting is applied neglecting the value corresponding to an OI equal to 67, because it corresponds to the severely degraded material. If the whole dataset is considered the R^2 value obtained for the fitting is equal to 0.967.
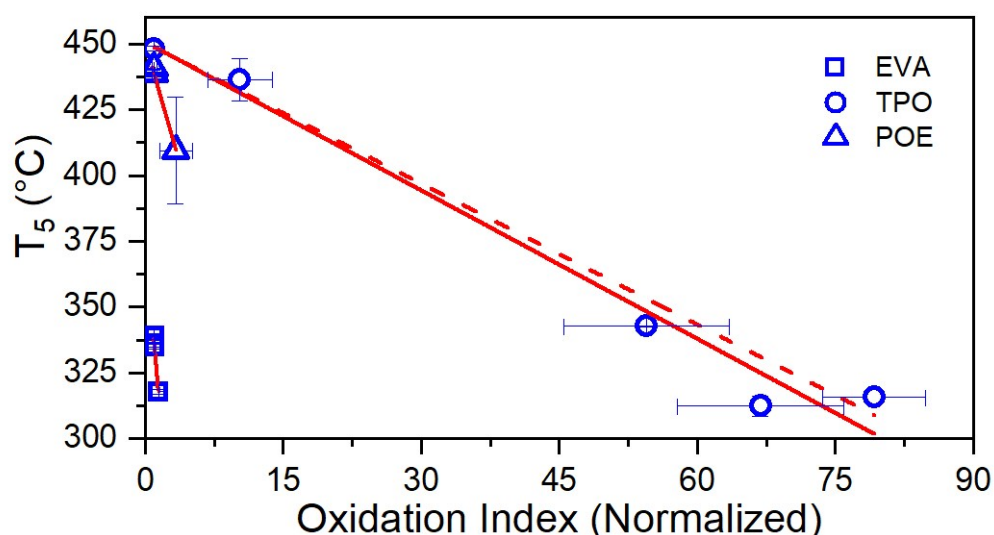

Figure 4.20: T_5 values vs. Normalized Oxidation Index. Solid lines correspond to the linear fitting applied to the datasets for EVA and POE. For TPO, the solid line corresponds to the fitting applied to the whole dataset, whereas the dashed line corresponds to the fitting applied to four points over five.

T_5 values might be used as indicators to detect oxidation processes taking place in materials subject to ageing. In fact, the dose at which the temperature values of the exposed materials deviate from the unexposed ones, well correlate with the increase of oxidation index evaluated using FT-IR spectroscopy measurements and with depletion of the antioxidants, qualitatively detected by means of TD-GCMS.

To summarize, as can be seen in Table 6, all the encapsulants showed a good behavior upon DH test and no significant material changes could be detected. The direct exposure to UV radiation, instead, provoked significant damages especially to TPO. Material stabilizers have been rapidly consumed and the chemical structure, thermal stability and morphology experienced severe changes. POE is the material that showed most similarities to EVA with the important advantage that this material does not present the formation of acetic acid upon ageing. Therefore, it seems to be a very promising material for PV applications.

Table 4.6: Summary of encapsulants characteristics and observed performances.

	EVA	POE	TPO
Chemical crosslinking	Yes	Yes	No
Acetic acid	Yes	No	No
General DH stability after 3300 hours	Very good	Very good, transmittance decreases in UV range	Very good, transmittance decreases in UV range
Presence of stabilizers upon UV exposure	Yes	Partial	No
Optical properties upon UV exposure	Slight transmittance decrease	Slight transmittance decrease	Not measurable
Chemical oxidation upon UV exposure	Initial stage	Initial stage	Severe
Crystallinity changes upon UV exposure	Not relevant	Not relevant	Yes
Thermal stability upon UV exposure	Decreased	Decreased	Very much decreased

4.5 Conclusions

The aim of the work was to compare the stability and degradation behavior characteristic of two different types of emerging encapsulant materials for PV modules, a TPO and a POE, to the most widely used EVA encapsulant under the influence of two different artificial ageing tests. The choice of testing bare films allows to better understand what happens to the materials when it is directly exposed, circumstance that might occur or partially occur in concomitance of degradation modes such as backsheet cracks and extensive delamination. Additionally, testing bare materials highlights even more the importance of PV module components, such as glazing and insulating adhesives that prevent polymers from degradation.

Results showed that the additives and stabilizers are qualitatively detectable by means of TD-GCMS for both exposed and unexposed samples. In particular, additives detected in the unexposed materials are generally present at the end of the exposure to the DH test. UV test, instead, is much more severe and causes depletion of stabilizers and subsequent polymer degradation. Analysis of surface chemistry by means of FT-IR Spectroscopy confirmed that photo-oxidation reactions take place during the exposure to UV radiation and that the effect are particularly pronounced for TPO, which seems to be the less stabilized polymer compared to the others. The results regarding the evolution of thermal properties with exposure are in good agreement with the typical behavior of polyethylene-based polymers experiencing photo-oxidative degradation. Summarizing, EVA and POE encapsulants showed very good stability upon DH exposure, whereas they showed initial signs of photo-oxidation properties upon a dose of 200 kW h m^{-2}. TPO, instead, showed good behavior upon DH exposure, but poor performances upon exposure to UV.

UV test reproduces in a more reliable way what actually happens in the field during outdoor exposure, although the damages that the polymers have faced are over estimated and more severe than the damages that the materials might have experienced in the usual PV module stack configuration. Nevertheless, findings from this experimental setup might be transferred to encapsulated samples with a different microclimate. Especially the oxidation induction time analysis carried out using the evolution of Carbonyl Index as well as evaluation

of T_5 values from TGA thermograms might be extended to different field of polymer degradation studies.

Further work might be focused on correlating degradation mechanisms of the bare materials to the encapsulated ones, simulating moisture and oxygen ingress as well as backsheet cracks and delamination. Additionally, a better stabilization might be considered to improve weather resistance of materials that showed stronger degradation.

4.6 References

[1]   G. Oreski, B. Ottersböck, and A. Omazic, "6 - Degradation Processes and Mechanisms of Encapsulants," in *Plastics DEsign Library, Durability and Reliability of Polymers and Other Materials in Photovoltaic Modules*, Hsinjin Edwin Yang, Roger H. French, and Laura S. Bruckman, Eds.: William Andrew Publishing, 2019, pp. 135–152. [Online]. Available: http://www.sciencedirect.com/science/article/pii/B9780128115459000069

[2]   U. Weber *et al.*, "Acetic Acid Production, Migration and Corrosion Effects in Ethylene-Vinyl-Acetate- (EVA-) Based PV Modules," in *27th European Photovoltaic Solar Energy Conference and Exhibition, September 24-28, 2012 Frankfurt, Germany*, pp. 2992–2995.

[3]   K. Matsuda, T. Watanabe, K. Sakaguchi, M. Yoshikawa, T. Doi, and A. Masuda, "Microscopic Degradation Mechanisms in Silicon Photovoltaic Module under Long-Term Environmental Exposure," *Jpn. J. Appl. Phys.*, vol. 51, 10NF07, 2012, doi: 10.1143/JJAP.51.10NF07.

[4]   S. Jonai, K. Hara, Y. Tsutsui, H. Nakahama, and A. Masuda, "Relationship between cross-linking conditions of ethylene vinyl acetate and potential induced degradation for crystalline silicon photovoltaic modules," *Japanese Journal of Applied Physics*, vol. 54, 8S1, 08KG01, 2015, doi: 10.7567/JJAP.54.08KG01.

[5]   K. Brecl, C. Barretta, G. Oreski, B. Malic, and M. Topic, "The Influence of the EVA Film Aging on the Degradation Behavior of PV Modules Under High Voltage Bias in Wet Conditions Followed by Electroluminescence," *IEEE J. Photovoltaics*, vol. 9, no. 1, pp. 259–265, 2019, doi: 10.1109/JPHOTOV.2018.2875196.

[6]   C. Peike, L. Purschke, K.-A. Weiß, M. Köhl, and M. Kempe, "Towards the origin of photochemical EVA discoloration," in *39th Photovoltaic Specialists Conference IEEE, Tampa Bay, USA, 2013*.

[7]   J. Chang, H. Yang, H. Wang, and D. Cao, "The investigation of snail trails in photovoltaic modules," in *2015 IEEE 42nd Photovoltaic Specialist Conference*, pp. 1–5.

[8]   A. Jentsch, K.-J. Eichhorn, and B. Voit, "Influence of typical stabilizers on the aging behavior of EVA foils for photovoltaic applications during artificial UV-weathering," *Polymer Testing*, vol. 44, pp. 242–247, 2015, doi: 10.1016/j.polymertesting.2015.03.022.

[9]   M. López-Escalante, L. J. Caballero, F. Martín, M. Gabás, A. Cuevas, and J. Ramos-Barrado, "Polyolefin as PID-resistant encapsulant material in 5PV6 modules," (in af), *Solar Energy Materials and Solar Cells*, vol. 144, pp. 691–699, 2016, doi: 10.1016/j.solmat.2015.10.009.

[10]   S. Mitterhofer, C. Barretta, L. F. Castillon, G. Oreski, M. Topič, and M. Jankovec, "A Dual-Transport Model of Moisture Diffusion in PV Encapsulants for Finite-Element Simulations," *IEEE J. Photovoltaics*, vol. 10, no. 1, pp. 94–102, 2020, doi: 10.1109/JPHOTOV.2019.2955182.

[11]   B. Adothu *et al.*, "Newly developed thermoplastic polyolefin encapsulant–A potential candidate for crystalline silicon photovoltaic modules encapsulation," *Solar Energy*, vol. 194, pp. 581–588, 2019, doi: 10.1016/j.solener.2019.11.018.

[12]   B. Adothu, P. Bhatt, S. Zele, J. Oderkerk, F. R. Costa, and S. Mallick, "Investigation of newly developed thermoplastic polyolefin encapsulant principle properties for the c-Si PV

module application," *Materials Chemistry and Physics*, vol. 243, 2020, doi: 10.1016/j.matchemphys.2020.122660.

[13]   B. Ottersböck, G. Oreski, and G. Pinter, "Comparison of different microclimate effects on the aging behavior of encapsulation materials used in photovoltaic modules," *Polymer Degradation and Stability*, pp. 182–191, 2017, doi: 10.1016/j.polymdegradstab.2017.03.010.

[14]   G. Oreski *et al.*, "Properties and degradation behaviour of polyolefin encapsulants for PV modules," *Progress in Photovoltaics: Research and Applications*, 2020, doi: 10.1002/pip.3323.

[15]   M. Salvalaggio, R. Bagatin, M. Fornaroli, S. Fanutti, S. Palmery, and E. Battistel, "Multi-component analysis of low-density polyethylene oxidative degradation," *Polymer Degradation and Stability*, vol. 91, no. 11, pp. 2775–2785, 2006, doi: 10.1016/j.polymdegradstab.2006.03.024.

[16]   R. Yang, P. A. Christensen, T. A. Egerton, and J. R. White, "Degradation products formed during UV exposure of polyethylene–ZnO nano-composites," *Polymer Degradation and Stability*, vol. 95, no. 9, pp. 1533–1541, 2010, doi: 10.1016/j.polymdegradstab.2010.06.010.

[17]   A. Abdelhafidi *et al.*, "Sun radiation and temperature impact at different periods of the year on the photooxidation of polyethylene films," *IJHT*, vol. 35, no. 2, pp. 255–261, 2017, doi: 10.18280/ijht.350204.

[18]   G. C. Eder *et al.*, "Error analysis of aged modules with cracked polyamide backsheets," *Solar Energy Materials and Solar Cells*, vol. 203, p. 110194, 2019, doi: 10.1016/j.solmat.2019.110194.

[19]   E. Annigoni, A. Virtuani, M. Caccivio, G. Friesen, D. Chianese, and C. Ballif, "35 years of photovoltaics: Analysis of the TISO-10-kW solar plant, lessons learnt in safety and performance—Part 2," vol. 27, no. 9, pp. 760–778, 2019, doi: 10.1002/PIP.3146.

[20]   *Kunststoffe - Künstliches Bestrahlen oder Bewittern in Geräten Teil 3 Fluoreszenzlampen: Part 3: Fluorescent UV lamps*, 4892-3, International Organisation for Standardisation, ISO 4892-3, 2006.

[21]   P. Klemchuk, E. Ezrin, G. Lavigne, W. Holley, J. Galica, and S. Agro, "Investigation of the degradation and stabilization of EVA-based encapsulant in field-aged solar energy modules," *Polymer Degradation and Stability*, no. 55, pp. 347–365, 1997, doi: 10.1016/S0141-3910(96)00162-0.

[22]   I. Hintersteiner, L. Sternbauer, S. Beissmann, W. W. Buchberger, and G. M. Wallner, "Determination of stabilisers in polymeric materials used as encapsulants in photovoltaic modules," (in af), *Polymer Testing*, vol. 33, pp. 172–178, 2014, doi: 10.1016/j.polymertesting.2013.12.004.

[23]   F. Gugumus, "Possibilities and limits of synergism with light stabilizers in polyolefins 2. UV absorbers in polyolefins," *Polymer Degradation and Stability*, vol. 75, no. 2, pp. 309–320, 2002.

[24]   B. Nieva-Echevarría, M. J. Manzanos, E. Goicoechea, and M. D. Guillén, "2,6-Di-Tert-Butyl-Hydroxytoluene and Its Metabolites in Foods," *Comprehensive Reviews in Food Science and Food Safety*, vol. 14, no. 1, pp. 67–80, 2015, doi: 10.1111/1541-4337.12121.

[25]   D. C. Miller *et al.*, "Degradation in photovoltaic encapsulant transmittance: Results of the first PVQAT TG5 artificial weathering study," *Prog Photovolt Res Appl*, vol. 27, no. 5, pp. 391–409, 2019, doi: 10.1002/pip.3103.

[26]   G. Socrates, *Infrared and Raman Characteristic Group Frequencies: Tables and Charts*, 3rd ed. Chichester, West Sussex, England: John Wiley & Sons, Ltd, 2001.

[27]   N. S. Allen, M. Edge, M. Rodriguez, C. M. Liauw, and E. Fontan, "Aspects of the thermal oxidation, yellowing and stabilisation of ethylene vinyl acetate copolymer," *Polymer Degradation and Stability*, no. 71, pp. 1–14, 2001.

[28]   J. V. Gulmine, P. Janissek, H. Heise, and L. Akcelrud, "Degradation profile of polyethylene after artificial accelerated weathering," *Polymer Degradation and Stability*, no. 79, pp. 385–397, 2003.

[29]   W. Yagoubi, A. Abdelhafidi, M. Sebaa, and S. F. Chabira, "Identification of carbonyl species of weathered LDPE films by curve fitting and derivative analysis of IR spectra," *Polymer Testing*, vol. 44, pp. 37–48, 2015, doi: 10.1016/j.polymertesting.2015.03.008.

[30]   G. W. Ehrenstein, G. Riedel, and P. Trawiel, *Thermal analysis of plastics: Theory and practice*. Munich: Carl Hanser Verlag, 2004.

[31]   J. C. Schlothauer, K. Grabmayer, I. Hintersteiner, G. M. Wallner, and B. Röder, "Non-destructive 2D-luminescence detection of EVA in aged PV modules: Correlation to calorimetric properties, additive distribution and a clue to aging parameters," *Solar Energy Materials and Solar Cells*, vol. 159, pp. 307–317, 2017, doi: 10.1016/j.solmat.2016.09.011.

[32]   G. W. Ehrenstein and S. Pongratz, *Resistance and stability of polymers*. Munich: Hanser Publishers, 2013.

[33]   G. Oreski and G. M. Wallner, "Damp Heat induced physical ageing of PV encapsulation materials," in *12th Intersociety Conference on Thermal and Thermomechanical Phenomena in Electronic Systems, Las Vegas, USA, 2010*.

[34]   B. K. Sharma, U. Desai, A. Singh, and A. Singh, "Effect of vinyl acetate content on the photovoltaic-encapsulation performance of ethylene vinyl acetate under accelerated ultra-violet aging," *J. Appl. Polym. Sci.*, vol. 137, no. 2, p. 48268, 2020, doi: 10.1002/app.48268.

[35]   J. R. White, "Polymer ageing: physics, chemistry or engineering? Time to reflect," *Comptes Rendus Chimie*, vol. 9, 11-12, pp. 1396–1408, 2006, doi: 10.1016/j.crci.2006.07.008.

[36]   A. Fairbrother *et al.*, "Temperature and light intensity effects on photodegradation of high-density polyethylene," *Polymer Degradation and Stability*, vol. 165, pp. 153–160, 2019, doi: 10.1016/j.polymdegradstab.2019.05.002.

[37]   B. Fayolle, X. Colin, L. Audouin, and J. Verdu, "Mechanism of degradation induced embrittlement in polyethylene," *Polymer Degradation and Stability*, vol. 92, no. 2, pp. 231–238, 2007, doi: 10.1016/j.polymdegradstab.2006.11.012.

5 Influence of sample configuration on EVA degradation modes

Parts of this work were presented as conference contributions:

- *"Investigating the influence of sample configuration on EVA degradation modes"*, poster presentation, 37th European PV Solar Energy Conference and Exhibition (EU PVSEC), 7th-11th of September 2020, virtual event;

- *"Effects of artificial ageing tests on EVA degradation: influence of microclimate and methodology approach"*, poster presentation, 48th IEEE Photovoltaic Specialists Conference (PVSC), 20th -25th of June, online event. The work presented received the "Best Poster Award" in Area 9: PV Module and System Reliability. A brief paper was published in the conference proceedings, doi: 10.1109/PVSC43889.2021.9518725.

5.1 Motivation

Even though extensive research has been carried out, EVA degradation mechanisms and interactions with other PV module components are not yet fully understood. EVA is the state of the art encapsulant material used in c-Si PV technologies since the 1960s-1970s and it has been largely studied over the years [1–7].

The ageing behavior of materials in photovoltaic (PV) modules is strongly affected by the climatic conditions that influence the microclimate that the polymer actually experiences [8–12]. The microclimate also depends on the materials used because e.g. backsheet with different transport properties might lead to different behavior [13]. Understanding how materials degrade upon the application of different external stress factors (temperature, humidity and UV

radiation) is fundamental to better understand PV degradation modes and to determine whether those processes result in a PV module power decrease. The simulation of the stress factors that are typical of the operational environment can be reproduced in indoor weathering devices where one or multiple stresses can be applied [14–17]. Obviously, a chamber where all the stresses can be reproduced simultaneously gives conditions very similar to the ones that a polymeric material in a PV module would experience in the field. However, the technological complexity of such devices makes the fixed and running cost substantial. Additionally, to able to reproduce in a multi-stress chamber what actually happens during operation to PV materials, it is necessary to have a deep understanding of the degradation mechanisms taking place. The degradation mechanisms are influenced not only by the single stresses, but especially by their combination. Needless to say, this kind of approach requires relevant effort. Additionally, not all the characterization methods are able to effectively describe the changes taking place within the polymers encapsulated in a module. By means of different techniques, it is possible to learn different information, but not all the changes that the polymer experience during degradation can be related to changes in power output.

The work presented in this chapter aims to give a thorough explanation of degradation behavior of the EVA encapsulant used in PV mini-modules. Additionally, it is discussed how the microclimate due to different environmental conditions (realized within artificial ageing test equipment) has an influence on polymer degradation. A comprehensive study including additives analysis, chemical structure, thermal stability, morphology is carried out to describe phenomena taking place during EVA degradation. Compatibility and interactions between EVA and other PV modules components, such as backsheet and glass, are discussed and several destructive and non-destructive characterization techniques are applied and discussed. Finally, the effect of polymer degradation on the PV mini-modules power output is discussed.

5.2 Experimental

5.2.1 Sample preparation and conditioning

PV mini-modules were produced using a standard glass, a fast cure EVA, commercially available c-Si solar cells, and a multilayer polymer backsheet with composition PET/PET/Primer (air side/core layer/encapsulant side). Solar cells were soldered using Pb-Sn-Cu ribbons manually. The mini-modules were produced with a size of 20 cm x 20 cm. Encapsulants and backsheets were cut in a size slightly larger with respect to the glass, to prevent delamination processes from the edges. Additionally, the exceeding encapsulant, directly exposed to the environment, was object of further characterization. Lamination of the samples was carried out in a 2BG flat-bed type laminator L176A, Figure 5.1, according to a standard procedure and the details of the parameters used are listed in Table 5.1. The lamination process begins with step 1.

Table 5.1: Parameters used for lamination of mini-modules.

Steps	Time (s)	Temperature (°C)	Pressure Up (kPa)	Pressure Down (kPa)
Prestart	120	140	0	-
1	240	145	0	0
2	600	155	1000	0
3	20	155	1000	1000
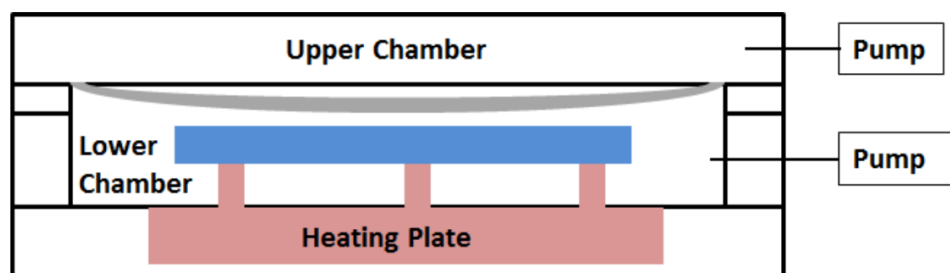
Figure 5.1: Schematic of the 2BG laminator L176A [18].

After lamination, the quality of the produced mini-modules were checked with electroluminescence, thanks to which goodness of soldering and absence of cell cracks were ensured. After production, the mini-modules were subjected to different artificial ageing regimes, summarized in Table 5.2.

The produced mini-modules were characterized by means of current vs. voltage (I-V) curve measurements before the exposure to artificial ageing tests, in an intermediate step of the ageing tests and at the end of the exposure. One of the mini-modules was kept in the dark as a reference. The mini-modules were characterized non-destructively by means of UV-Vis-NIR spectroscopy to determine changes in optical properties of the encapsulants in contact with cell and backsheet. The equipment used to carry out the measurements is described in Chapter 3. Additionally, Fluorescence spectroscopy and imaging were carried out and described in the following section 5.2.3. The encapsulant were destructively withdrawn in three different positions to investigate the interaction with the other module components (cell and backsheet), as shown in Figure 5.2. The exceeding encapsulant was also withdrawn and further characterized.

Table 5.2: Artificial ageing tests.

Artificial ageing tests	Main parameters	Maximum Time / Dose
Damp Heat (IEC 61215- 2:2016 MQT 13)	85 °C, 85% RH	2000 h
Dry UV IEC 61215- 2:2016 MQT 11	250 W m^{-2} (280 nm – 400 nm), 60 °C	500 kWh m^{-2}
UV-DH combined	180 W m^{-2} , 60 °C, 85% RH	250 kWh m^{-2}

The characterization methods applied to the withdrawn encapsulants were:

- TD-GC/MS for additive analysis,
- FT-IR ATR spectroscopy to highlight the changes in chemical structure
- DSC to evaluate the changes of thermal behavior and
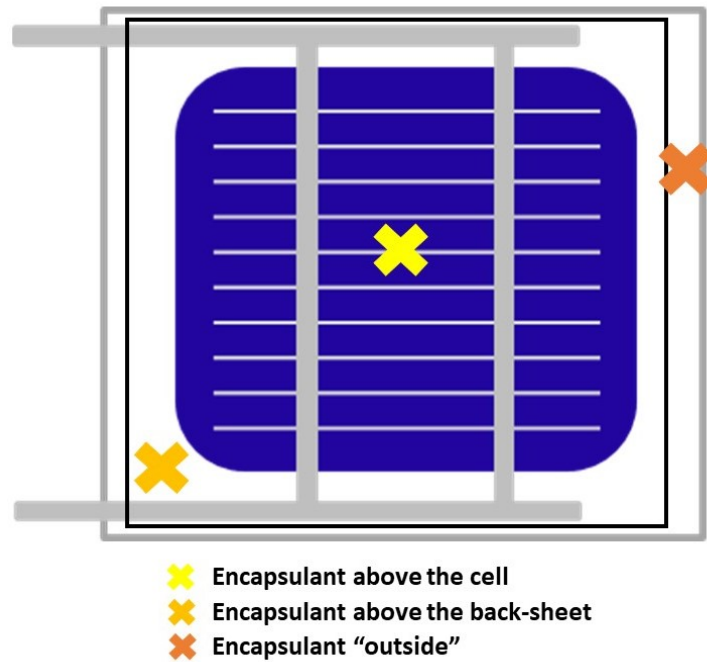- TGA to assess the changes in thermal stability.

Figure 5.2: Scheme of sample configuration and encapsulant extraction points.

5.2.2 Characterization of electrical performances

Measurements of I-V curves were carried out using a solar simulator Pasan IIIb solar (flash) simulator, Figure 5.3, equipped with Xenon long-arc lamps, which receive energy from 600 V capacitor. Different irradiance levels and wavelengths are achieved by using filters, irradiance measurements are performed with the use of a reference cell. Different levels of voltage are applied and the current produced by the sample is measured with a 4-wire connection. Standard temperature conditions are maintained by means of A/C in the laboratory room and the system is controlled via a LabVIEW interface.
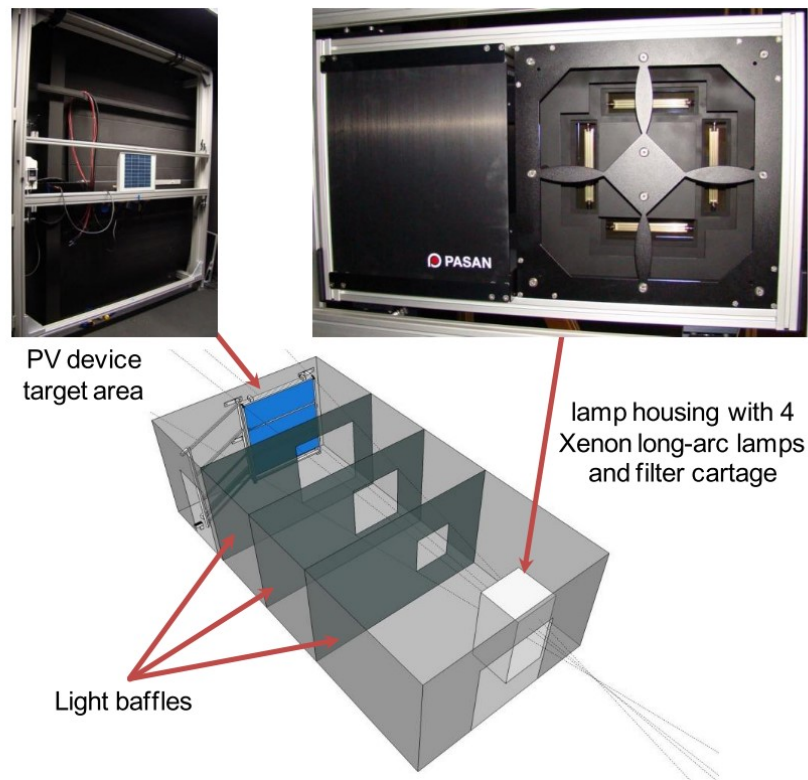
Figure 5.3: I-V curves measurement setup [19].

5.2.3 Fluorescence spectroscopy and imaging

A Cary Eclipse Fluorescence Spectrophotometer was used to carry out fluorescence spectroscopy measurements on the PV mini-module samples. The device is equipped with a Xenon lamp as a light source and a monochromator that is able to deliver the light at a specific wavelength. Fluorescence emission spectra were obtained using an excitation wavelength of 365 nm and were recorded between 375 nm and 700 nm. The measurements were performed in triplicates. Fluorescence images were obtained using an Enigma365 UV LED (light-emitting diode) light source manufactured by UV Light Technology Limited with an excitation peak at 365 nm, Figure 5.4. The pictures were recorded using a Porosilica GC camera produced by Allied Vision Technologies GmbH equipped with a Fujinon TV Lens HF50SA-1 1:1.8/50mm optic and a LP415-49 UV Block filter from Polytec GmbH to remove possible UV light going through the camera and to make sure that only visible light was detected. The camera is controlled via the Vimba viewer interface and an aperture of 30000 μs was set for all the pictures. The focus was set manually on the optic unit.
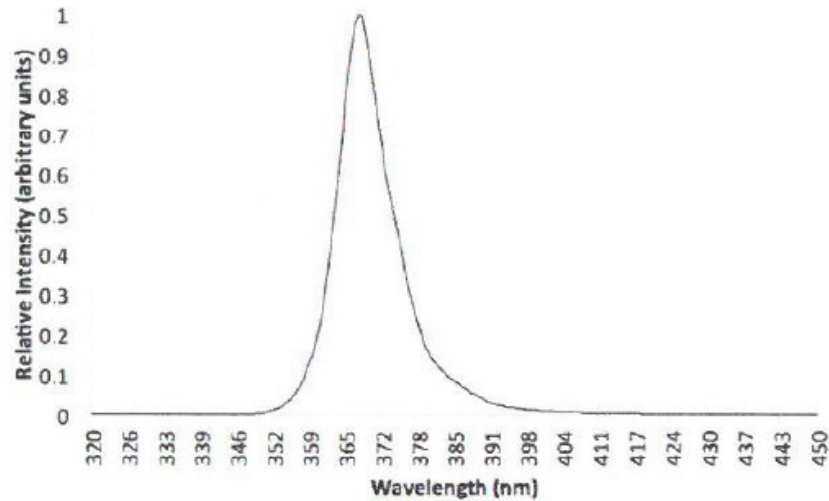
Figure 5.4: UV spectral output of the Enigma365 LED UV light source, according to the manufacturer's datasheet.

5.3 Results and discussion

5.3.1 Electrical performances

The electrical performances of the mini-modules were monitored by means of current versus voltage (I-V) measurements. The most important parameters extrapolated from the I-V curves are short circuit current (I_{SC}), open-circuit voltage (V_{OC}), series resistance (R_S) and maximum power point (P_{MAX}), described in Figure 5.5. Additionall, the Fill Factor (FF) is typically associated to the quality of the cell and it might decrese upon exposure. The FF is calculated according to Equation 1:

$$FF = \frac{P_{MAX}}{I_{SC} \cdot V_{OC}} \qquad \text{(Equation 1)}$$

The next charts (from Figure 5.6 to Figure 5.9) show the evolution of the above-mentioned parameters of the mini-module samples before the exposure to artificial ageing tests, at an intermediate point and at the end of the tests. The electrical performances of the reference sample were measured as well, at beginning of the artificial tests as well as at the end. The reference was stored in the dark at room temperature and humidity conditions, while the other mini-modules were stored in the climate chambers and subjected to the different artificial ageing tests.
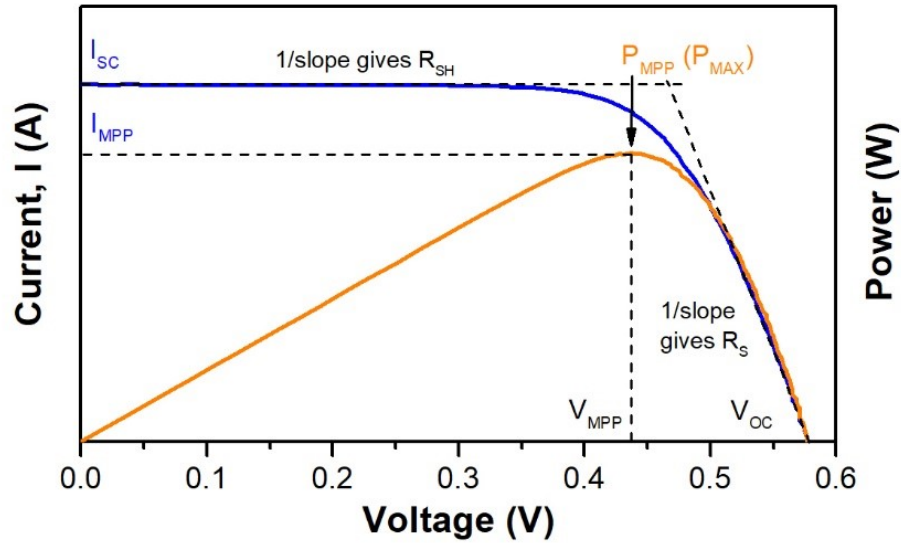
Figure 5.5: Illustration of an I-V curve and description of relevant parameters.

Each mini-module was flashed three times and three I-V curves were recorded. The values shown in the charts, from Figure 5.6 to Figure 5.9, were extracted from the I-V curves and averaged. Results show that the power at maximum point, Figure 5.6, did not change substancially for the reference sample as well as for the sample exposed to DH test up to 2000 hours (reduction of ~0.5%). The sample exposed to the dry UV test, instead, showed a different behaviour because it showed a reduction of about 1% after the exposure to 500 kWh m^{-2}. The sample exposed to UV-DH combined test experienced the most relevant power reduction, namely 5.5% after the exposure to 250 kWh m^{-2} at 60 °C and 85% RH. The reduction of the power can be attributed especially to a reduction of the current produced by the solar cell. The same trend observed for the power at the maximum point can be, indeed, detected for the short circuit current (I_{SC}), Figure 5.7.
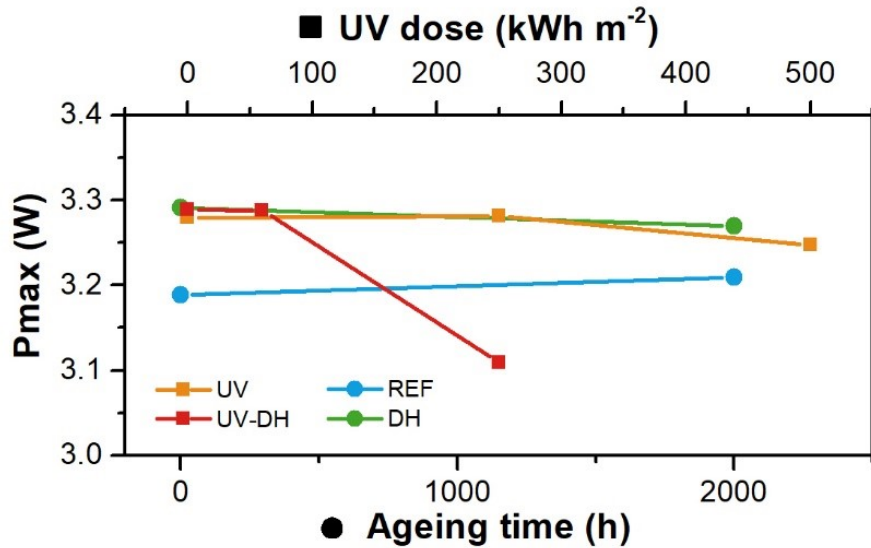
Figure 5.6: Maximum power point of mini-modules exposed to artificial ageing tests.
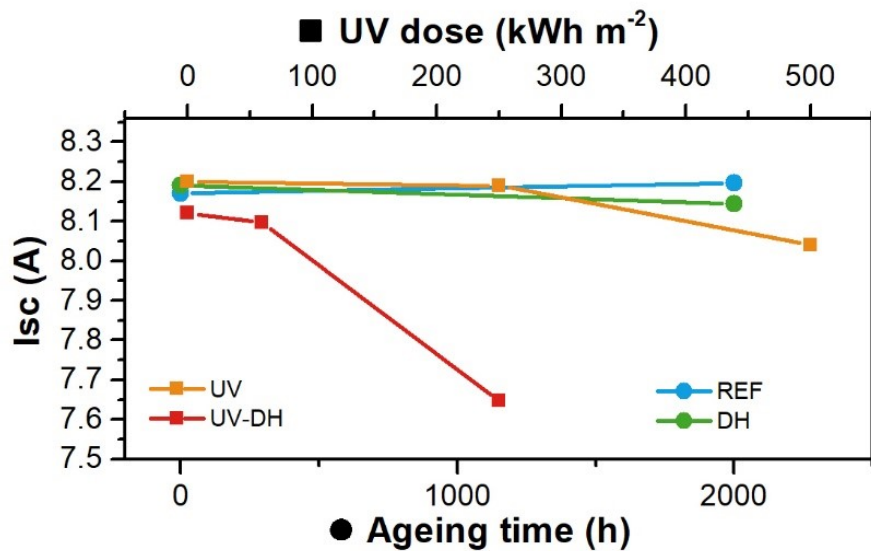

Figure 5.7: Short circuit current of mini-modules exposed to artificial ageing tests.

The sample exposed to DH test showed a slight reduction of the current produced with respect to the initial value (~0.5%). The sample exposed to UV test showed both a reduction of about 2% with respect to the initial value and the sample exposed to the UV-DH combined test showed the most relevant current reduction (5.5%). The evolution of R_s and V_{OC}, Figure 5.9 and Figure 5.8, respectively, did not show significant differences. Changes in R_s might have been related to loss of transparency, glass corrosion, and delamination, whereas changes in V_{OC} might have been connected to cracked cells [20]. The reduction of power with associated reduction of I_{SC} might be attributed to several factors,

among which loss of transparency, glass corrosion, delamination, corrosion of the anti-reflective coating of the cells, and cracked cells [20]. Power degradation associated to a significant acetic acid production might be excluded because a decrease in Fill Factor (not shown here) could not be detected for any of the exposed samples.
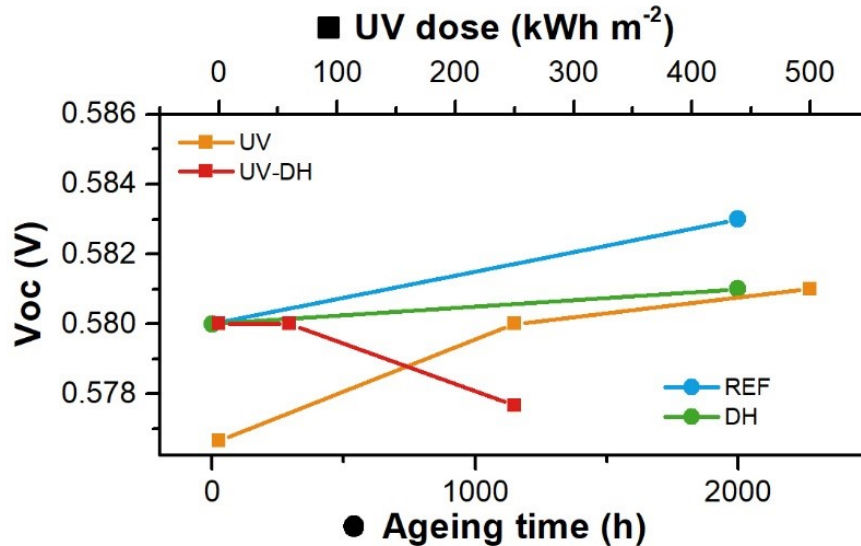

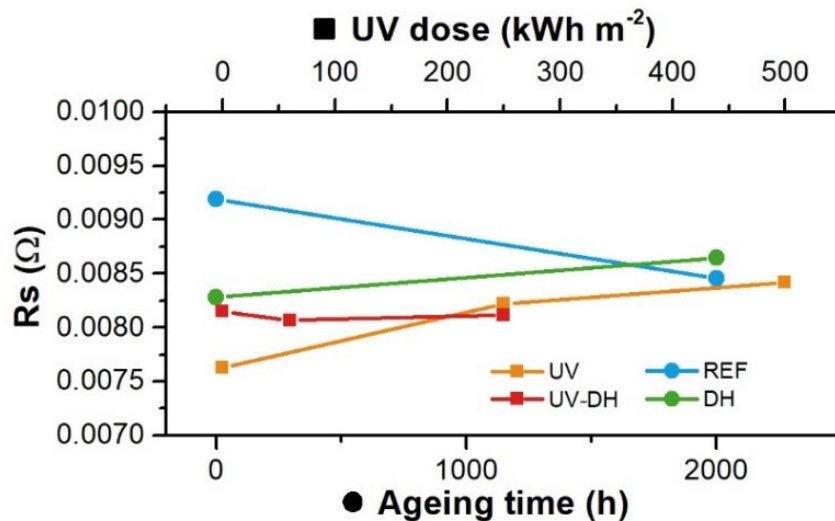**Figure 5.8: Open-circuit voltage of mini-modules exposed to artificial ageing tests.**

Figure 5.9: Series resistance of mini-modules exposed to artificial ageing tests.

5.3.2 TD-GC/MS for qualitative additive analysis

TD-GC/MS measurements were performed to determine qualitatively the additives present in the encapsulant and to monitor the consumption of the stabilizers during the exposure to the artificial ageing tests. Additionally, the encapsulants were withdrawn from different locations within the mini-

modules to determine whether there was an influence of interaction between the different materials. TD-GC/MS can help not only to monitor the additive consumption but also to investigate material degradation itself [21].

Chromatograms of the EVA withdrawn from above the backsheet are displayed in Figure 5.10 and they are normalized with respect to the highest peak. The displayed peaks correspond to a substance eluting from the separation column at particular retention time (corresponding to a temperature). Mass spectra are continuously scanned throughout the whole duration of the measurements and the mass spectra recorded at the same time in which a peak is visible in the chromatogram allows substance identification.
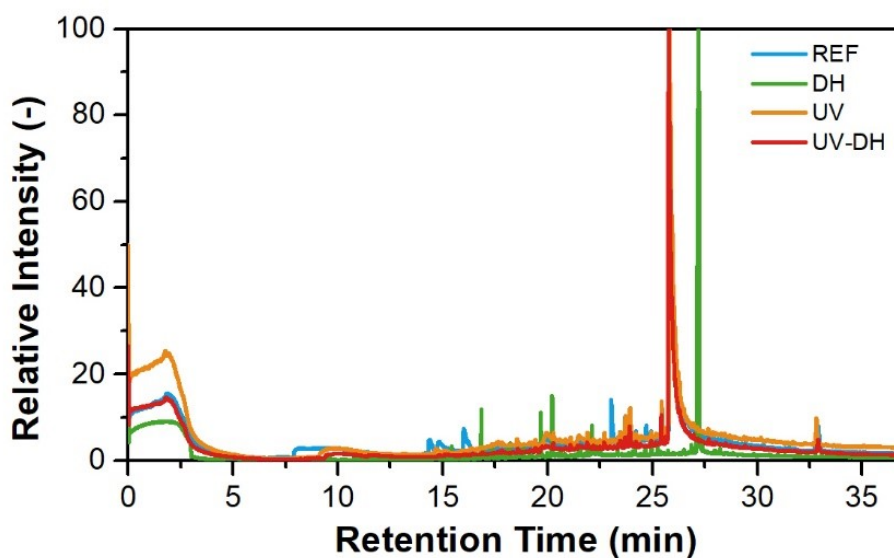

Figure 5.10: Chromatograms of encapsulant samples withdrawn from above the backsheet.

The NIST database is used to match the measured mass spectrum to a specific substance. The main stabilizers detected were 2,6-bis(1,1-dimethylethyl)-4-methylphenol, also known as butylated hydrohytoluene, which is used as antioxidant, and 2-hydroxy-4-(octyloxy)benzophenone with the function of UV absorber. The two stabilizers eluted from the column at a retention time of about 16-17 min and 26-27 min, respectively, as shown in Figure 5.11. The shift of the position (retention time) of the peaks observable to the samples exposed to DH test might be due to the fact that a new separation column has been used. The "new" column is exactly the same column type as the "old" one, therefore with the same properties and characteristics.

The antioxidant was detected in the encapsulant of the reference sample as well as in the sample exposed to DH test for 2000 h. The samples exposed to UV and UV-DH combined tests did not show the presence of the antioxidant, possibly because it reacted to prevent polymer degradation and it was consumed. The area beneath the peaks is correlated to the concentration of the stabilizer present in the material, however the performed measurements did not allow quantification because of lack of calibration curves for the additives detected. Nevertheless, it is reasonable to assume that the antioxidant was present in a lower concentration with respect to the UV absorber, although quantitative values could not be given.
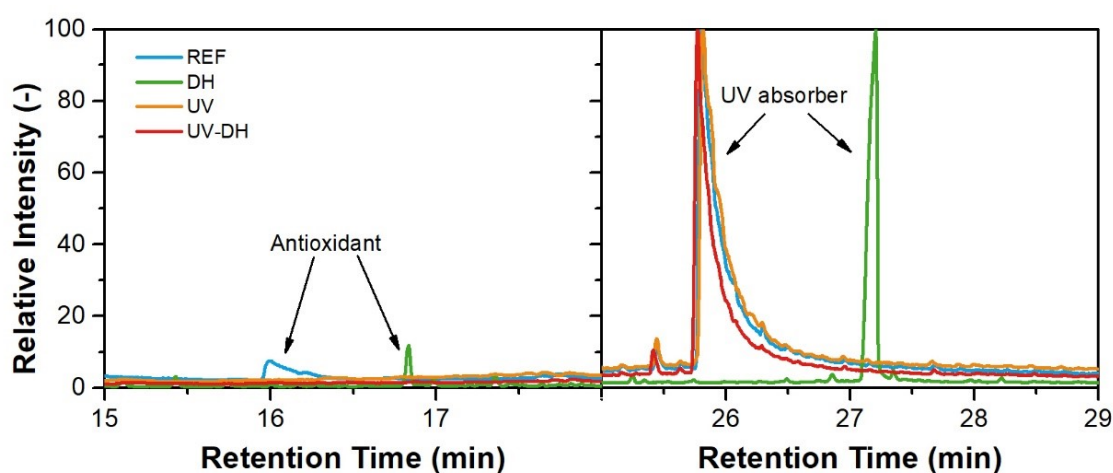

Figure 5.11: Details of chromatograms of encapsulant samples withdrawn from above the backsheet.

In Figure 5.12, the chromatograms of the EVA withdrawn from above the cell are shown. The benzophenone-based UV absorber was detected in all the samples, whereas the phenolic antioxidant (BHT) was not detected for the sample exposed to UV-DH test, as can be seen in details in Figure 5.13.

Additionally, a 1,3,5-Triazine-2,4,6(1H,3H,5H)-trione, 1,3,5-tri-2-propenyl-(crosslinking accelerator) was detected for the sample exposed to DH test. The crosslinking accelerator should have normally reacted completely during the crosslinking process in the lamination step. From results of DSC mesurements, that will be described in the following chapters, an exhotermic peak could be detected between 100 °C and 115 °C. The presence of the exhotermic peak, if connected to a crosslinking reaction, might justify the presence of the crosslinking accelerator, which did not react completely during the lamination process.
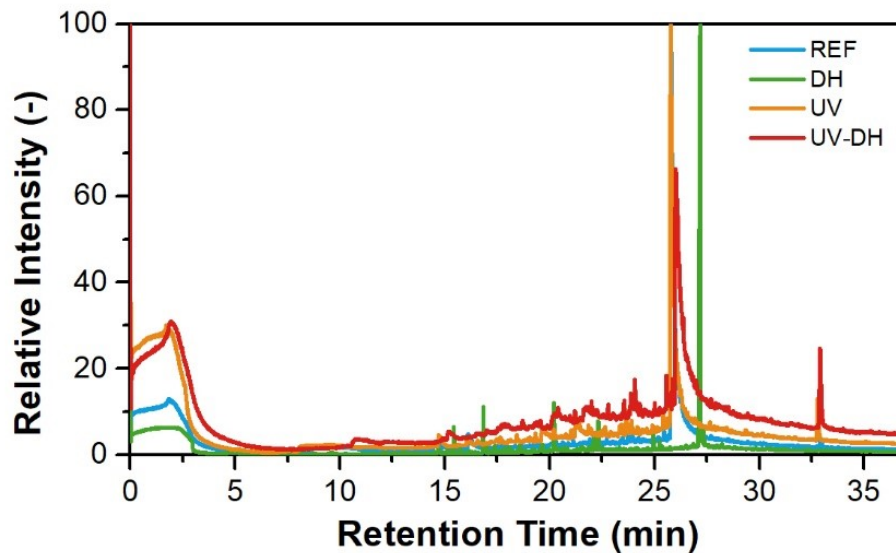
Figure 5.12: Chromatograms of encapsulant samples withdrawn from above the cell.
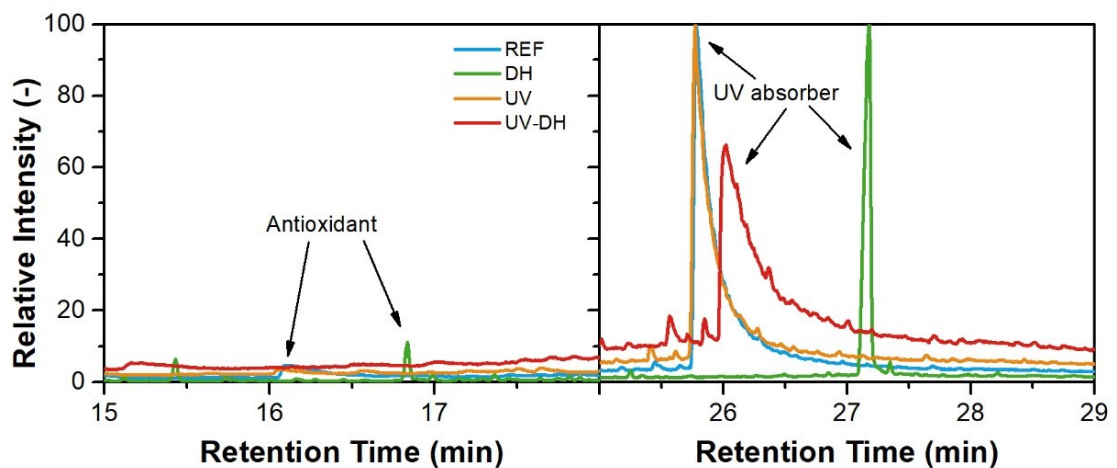

Figure 5.13: Details of chromatograms of encapsulant samples withdrawn from above the cell.

The EVA material in excess and directly exposed to the environment was measured as well and the results are shown in Figure 5.14 and Figure 5.15. It is possible to notice how the samples exposed to dry UV and UV-DH combined tests showed an increase of the baseline with respect to the reference sample and the sample exposed to DH test. Moreover, many additional peaks were visible. Results of TGA measurements, described in the following chapters, will show how the thermal stability of the material withdrawn from the "outside" position for the samples exposed to dry UV and UV-DH combined tests is worsened with respect to the reference sample. The temperature at which there is a 5% weight loss is below 320 °C, which is the maximum temperature reached

during the TD process. At this temperature, the material was no longer stable and it began to decompose. Typical pyrolysis products of Polyethylene (PE) based materials were detectable (sequences of alkane, alkenes, α-ω alkadiene with increasing molecular weight as the retention time increases [22, 23]) in the samples exposed to UV and UV-DH combined test. Benzophenone-based UV absorber was no longer detectable for the sample exposed to UV test, but it was still detectable for all the other samples.
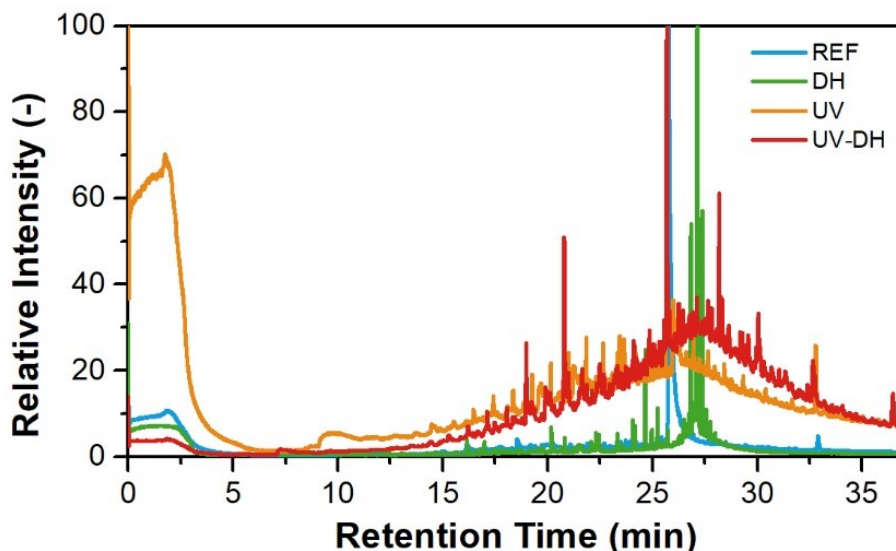

Figure 5.14: Chromatograms of excess "outside" encapsulant samples directly exposed to different artificial ageing tests.
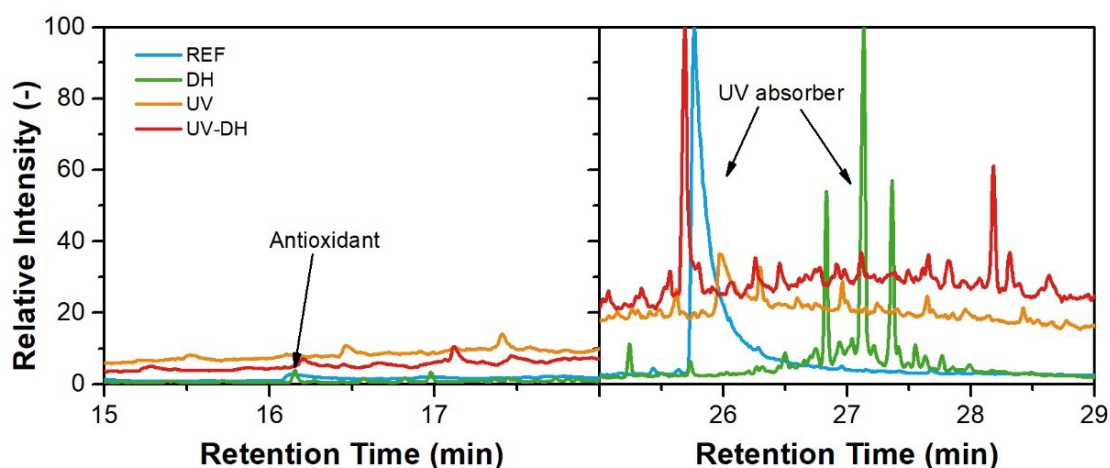

Figure 5.15: Details of chromatograms of encapsulant samples withdrawn from the excess "outside" directly exposed to different artificial ageing tests.

The BHT antioxidant was detectble only for the reference sample and for the sample exposed to DH test. Additionally, a residue of the crosslinking

accelerator was detectable for the sample exposed to DH. A summary of the results described above can be seen in Table 5.3.

Table 5.3: TD-GC/MS additive analysis on encapsulants withdrawn from different locations within the mini-modules.

EVA above the backsheet	REF	DH	UV	UVDH
Antioxidant - BHT	✓	✓	n.d.	n.d.
Crosslinking accelerator – Triallyl isocyanurate	n.d.	n.d.	n.d.	n.d.
UV absorber - Benzophenone	✓	✓	✓	✓.
EVA above the cell	**REF**	**DH**	**UV**	**UVDH**
Antioxidant - BHT	✓	✓	✓	n.d.
Crosslinking accelerator - Triallyl isocyanurate	n.d.	✓	n.d.	n.d.
UV absorber - Benzophenone	✓	✓	✓	✓
EVA "Outside"	**REF**	**DH**	**UV**	**UVDH**
Antioxidant - BHT	✓	✓	n.d.	n.d.
Crosslinking accelerator - Triallyl isocyanurate	n.d.	✓	n.d.	n.d.
UV absorber - Benzophenone	✓	✓	n.d.	✓

5.3.3 UV-Vis-NIR Spectroscopy

The reflectance of the EVA samples was measured in two different positions, through the glass above the backsheet and through the glass above the cell. Obviously, the effect of the material above and below the encapsulant has an influence on the measured spectra.

The spectra of the EVA encapsulant measured above the cell can be seen in Figure 5.16. The spectra of the materials above the backsheet in the NIR region, above 780 nm, did not show any relevant differences and are omitted in the chart. No differences could be detected in the visible range, between 380 nm and 780 nm. The reflectance of the samples increased in the region between 280 nm and 380 nm, region of interest for the benzophenone based UV absorber [24], for the material exposed to UV and even more for the material exposed to UV-DH combined test. Additionally, a decrease of reflectance could be seen for the samples exposed to UV irradiation in the region below 300 nm, the region of interest of the BHT antioxidant [25].
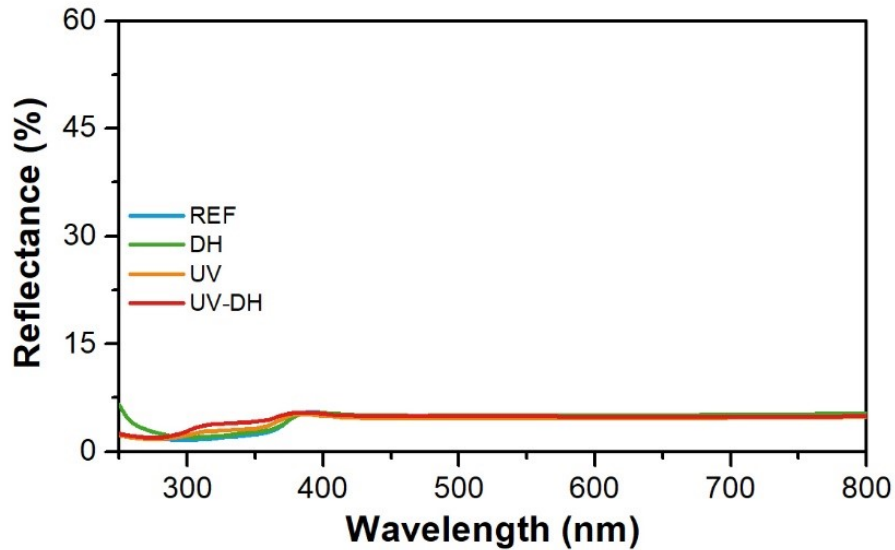
Figure 5.16: UV-Vis-NIR spectra of encapsulant above the cell measured through the glass.

The results shown in Figure 5.17 show the spectra of the EVA samples measured above the backsheet. In this case, as well as for the encapsulant above the cell, no significant differences were detected in the NIR region. All the exposed samples showed a decrease of reflectance in the blue region of the visible spectra, hence indicating yellowing.
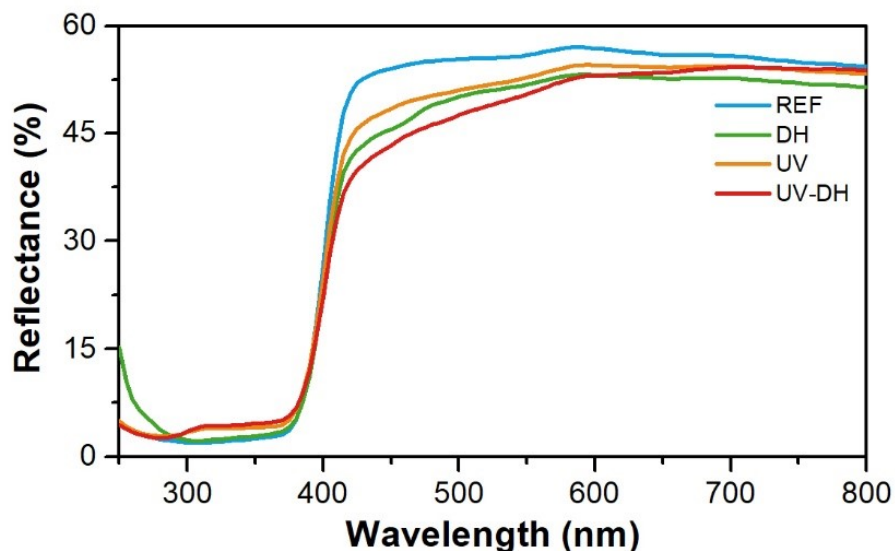

Figure 5.17: UV-Vis-NIR spectra of encapsulant above the backsheet measured through the glass.

This result well correlates with the consumption of the benzophenone-based UV absorber detected by means of TD-GC/MS. This stabilizer, indeed, absorbs UV radiation between 260 nm and 370 nm [24]. Even though no clear statement

can be given regarding the actual concentration of the UV absorber in the sample exposed to UV-DH combined test, it is observable that the peak had a smaller area compared to the material in the reference mini-module. The decrease was more severe for the sample exposed to UV-DH test, less severe for the sample exposed to DH test, and even less pronounced for the sample exposed to dry UV. Additionally, a decrease of the reflectance could be seen in the region below 300 nm, related to the BHT antioxidant [25].

The Yellowness Index was calculated according to the standard ASTM E313 [26]. The value of the YI of the EVA above the backsheet for the sample exposed to UV-DH is about 3.4 times higher than the value measured for the reference sample, Figure 5.18. The ratio between the YI of the sample exposed to DH is 2.6 and for the sample exposed to UV is about 2.1.
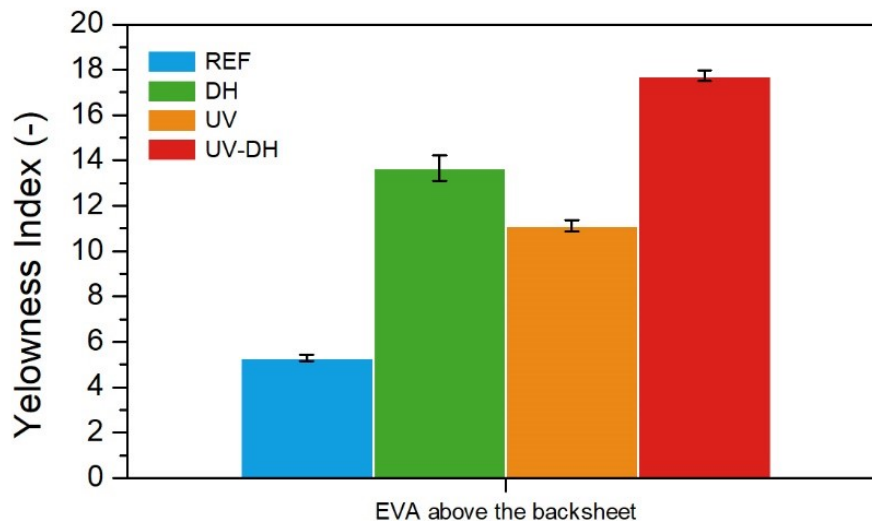

Figure 5.18: Yellowness index of encapsulants measured above the cell and above the backsheet upon artificial ageing tests.

The increase of YI for the exposed samples might be a reason of the power reduction associated to reduction of I_{SC}. It seems like two different mechanism are behind the formation of chromophores between the illuminate and not illuminated samples. On one side, for the illuminated samples it is possible to observe a consumption of the antioxidant, even if not homogeneous. The illuminated samples, indeed, did not show presence of the antioxidant for the encapsulant withdrawn from above the backsheet, whereas the sample exposed to UV test showed still present of antioxidant above the cell. However, the consumption of antioxidant is connected with formation of chromophores

because of quinoid products, deriving from oxidative transformation products of BHT [27]. On the other hand, for the sample exposed to DH test, the presence of leftovers of unreacted species during the crosslinking reaction would well correlate to the discoloration of the material [7].

5.3.4 FT-IR ATR Spectroscopy

The extracted encapsulant were analyzed by means of FT-IR ATR spectroscopy. Peaks identification has been described in depth in Chapter 3. The objective of this paragraph is to better highlight the differences resulting from different microclimates, therefore some relevant information is recalled from the previous chapter and further discussed. All the samples were measured from the encapsulant side in contact with the glass. Results are summarized in Table 5.4 [28, 29]. The charts displayed in Figure 5.19 to Figure 5.21, show the results of the FT-IR ATR spectroscopy analysis. The results are displayed according to the position in the module from which they have been extracted.

Table 5.4: FT-IR ATR spectroscopy bands of EVA and their assignments.

Wavenumber [cm^{-1}]	Assignment	Remark
2920	Asymmetric stretching vibration of CH_2	Ethylene moieties
2850	Symmetric deformation vibration of CH_2	Ethylene moieties
1780	C=O stretching vibration of γ-lactones	Degradation product
1715/1175	C=O stretching vibration of ketones	Degradation product
1736	C=O stretching vibration	Vinyl acetate moieties
1465	Asymmetric deformation vibration of CH_2	Ethylene moieties
1370	Symmetric deformation of CH_3	Ethylene moieties
1238	C−O−C stretching vibration	Vinyl acetate moieties
1020	C−O−C stretching vibration	Vinyl acetate moieties

Wavenumber [cm^{-1}]	Assignment	Remark
960-940	CH out-of-plane deformation vibration of vinyl ether	Degradation product
910	CH out-of-plane deformation vibration of vinyl	Degradation product
720	CH$_2$ skeleton rocking vibration	Ethylene moieties

In Figure 5.19, the spectra of the EVA extracted from the location of the mini-module above the backsheet are shown. The reference sample shows the typical EVA peaks (ethylene and vinyl acetate moieties) and no additional peaks can be detected. The sample stored in the climate chamber for the DH test for 2000 h additionally shows the presence of a peak at about 1560 cm^{-1}. The presence of this peak has been mentioned in several studies, although the assignment of this band is not unanimous. Possible explanations might be the presence and migration of stabilizers (such as hindered amine light stabilizers, HALS) [30], formation of carboxylic acids due to oxidation reactions [31], formation of carboxylate salt (COO$^-$) due to material interactions of glass and encapsulant [32]. The presence of HALS might be excluded because additives belonging to this category have not been detected by means of TD-GC/MS. Alternatively, the band at 1560 cm^{-1} might be attributed to the crosslinking accelerator, characterized by a Triazine ring that has a strong band at the wavenumber mentioned above [28]. However, additional bands should be visible to assign certainly the band to the Triazine based (Triallyl isocyanurate) crosslinking accelerator. A band of variable intensity due to in-plane stretching vibrations between 1450 cm^{-1} and 1350 cm^{-1} should be present [28] in this case possibly overlapping with the deformation in the plane of CH$_2$ present in ethylene moieties. One weak band at 860–775 cm^{-1} due to out-of-plane deformation of the ring [28] is not visible in the measured spectrum. Extensive materials oxidation might be neglected as well because of the absence of shoulders/peaks at 1780 cm^{-1} and 1715/1175 cm^{-1}, related to formation of lactones and ketones, as well as absence of peaks between 3700 cm^{-1} and 3100 cm^{-1}, related to formation of hydroxyl groups.
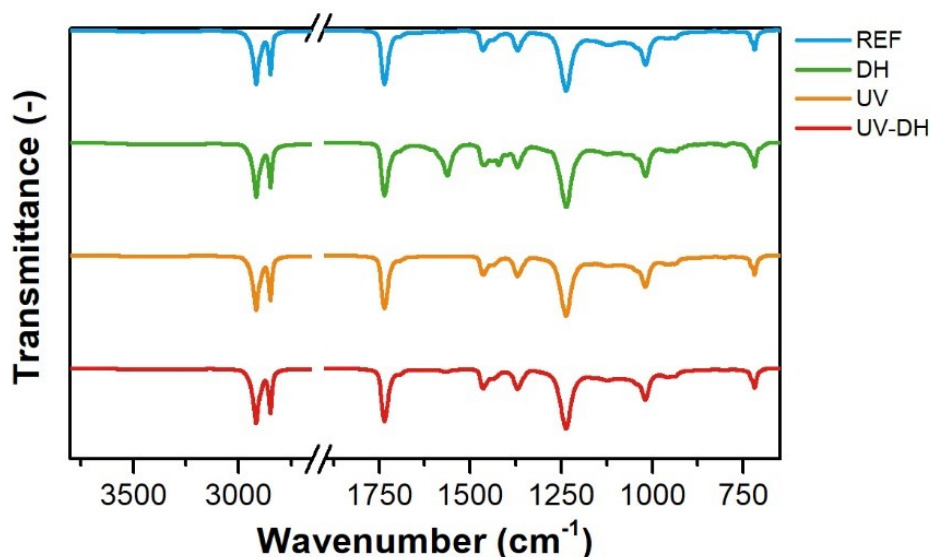
Figure 5.19: FT-IR ATR spectra of encapsulant samples withdrawn from above the backsheet.

Hara et al. [32] showed that under DH conditions sodium ions (Na⁺) can react with acetyl group promoting deacetylation and forming carboxylate salt (COO⁻). An additional peak is present at about 1420 cm⁻¹ (that might be associated to the formation of acetate [28]), which is also present in the EVA described in this study. Mansour et al. [13] also reported that the glass acts as a catalyst for EVA degradation in DH conditions. In the work from Hara et al. [33], the formation of acetic acid provokes corrosion of the silver grids with consequent increase of series resistance after 4000 h of DH exposure. In this study, a very slight decrease of power at the maximum point could be detected, as well as a very slight increase of the series resistance. However, no signs of corrosion could be seen by visual inspection of the mini-module, although it might be not excluded a further worsening of the performances with longer exposure time.

The samples extracted from mini-modules aged under UV and UV-DH combined tests did not show significant differences with respect to the EVA extracted from the reference mini-module. The EVA samples extracted from above the cell, Figure 5.20, did not show relevant differences with respect to the reference sample, regardless the artificial ageing test applied. The excess EVA withdrawn from the outside of the glass and above the backsheet has been tested and the surface in contact with the air is shown in Figure 5.21. Typical products of photo-oxidation reactions can be detected. The peak at 1736 cm⁻¹

shifts towards about 1720 cm^{-1} for the samples exposed to dry UV and to about 1709 cm^{-1} for the sample exposed to UV-DH combined test. The increase of this peak is related to formation of ketones upon oxidation [31]. Additional changes can be seen in the regions between 3500 cm^{-1} and 3000 cm^{-1}, between 1500 cm^{-1} and 1300 cm^{-1}, and between 1300 cm^{-1} and 825 cm^{-1} corresponding to hydroxyl groups, aldehydes, vinylene, vinyl and vinyl dienes, respectively [34, 35]. The Oxidation Indices calculated as the ratio of the integral of the spectra within the "carbonyl region" between 1800 cm^{-1} and 1680 cm^{-1} and the "reference band" between 2875 cm^{-1} and 2760 cm^{-1} are displayed in Figure 5.22.
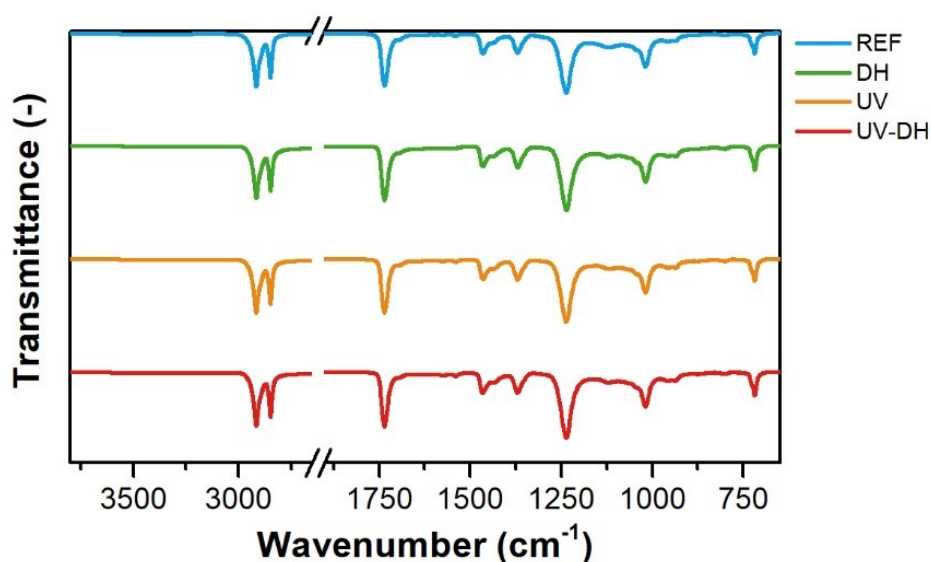

Figure 5.20: FT-IR ATR of encapsulant samples withdrawn from above the cell.
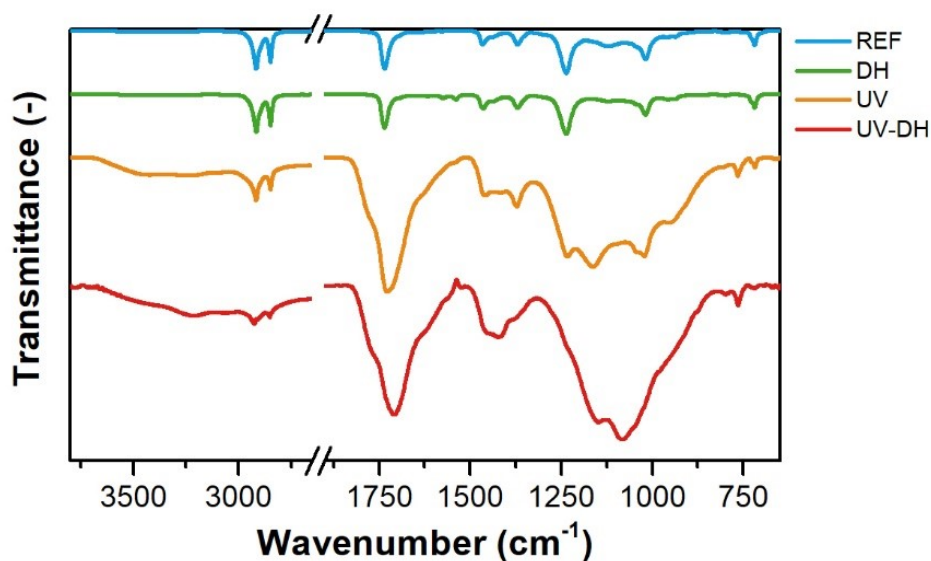

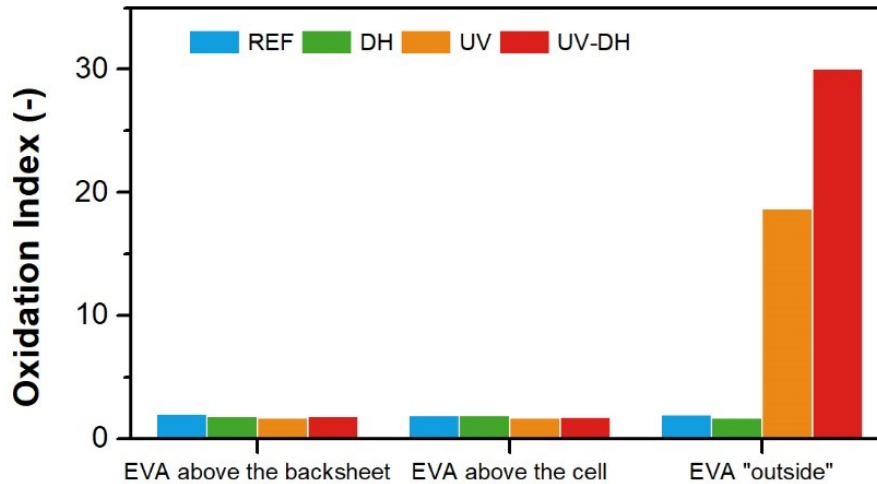**Figure 5.21: FT-IR ATR spectra of excess "outside" encapsulant samples.**

Figure 5.22: Oxidation Indices calculated using FT-IR ATR spectra of EVA samples withdrawn from mini-modules exposed to different artificial ageing tests in different positions.

The EVA samples withdrawn from above the backsheet and above the cell show similar values to the reference sample, regardless the artificial ageing tests applied. The material taken from the "outside" of the mini-module exposed to DH test showed a similar OI compared to the reference. The samples exposed to dry UV test have an OI 10 times higher than the reference, whereas the samples exposed to UV-DH combined tests have an OI about 15 times higher than the reference. The results highlight how the direct exposure of the bare encapsulant to the environment highly influences the ageing behavior.

5.3.5 Fluorescence spectroscopy and imaging

The results of fluorescence spectroscopy measurements are displayed in Figure 5.23 (a) to (d). Fluorescence emission spectra were recorded focusing on an area above the cell (full lines) and above the backsheet (dotted lines) using an excitation wavelength of 365 nm. The reference module did not show any significant fluorescence, as well as the module exposed to DH test. The latter showed little fluorescence only during one measurement (DH_above cell_1), probably due to an inhomogeneity of material's ageing behavior. The modules exposed to UV and UV-DH combined test showed, instead, significant fluorescence with two main emission peaks at about 410 -450 nm and 535 nm. The results are in good agreement with previous studies reported in literature [4]. The modules exposed to UV test showed fluorescence with a slightly lower

intensity compared to the modules exposed to UV-DH test. However, it was possible to observe for both modules a higher fluorescence intensity when the measurements took place above the cell rather than above the backsheet. This behavior might be explained with the higher temperature reached by the encapsulant material above the cell due to the heat released by the solar cell upon illumination. Additionally, the presence of humidity might have accelerated the formation of chromophores and further stressed the stability of the EVA encapsulant.
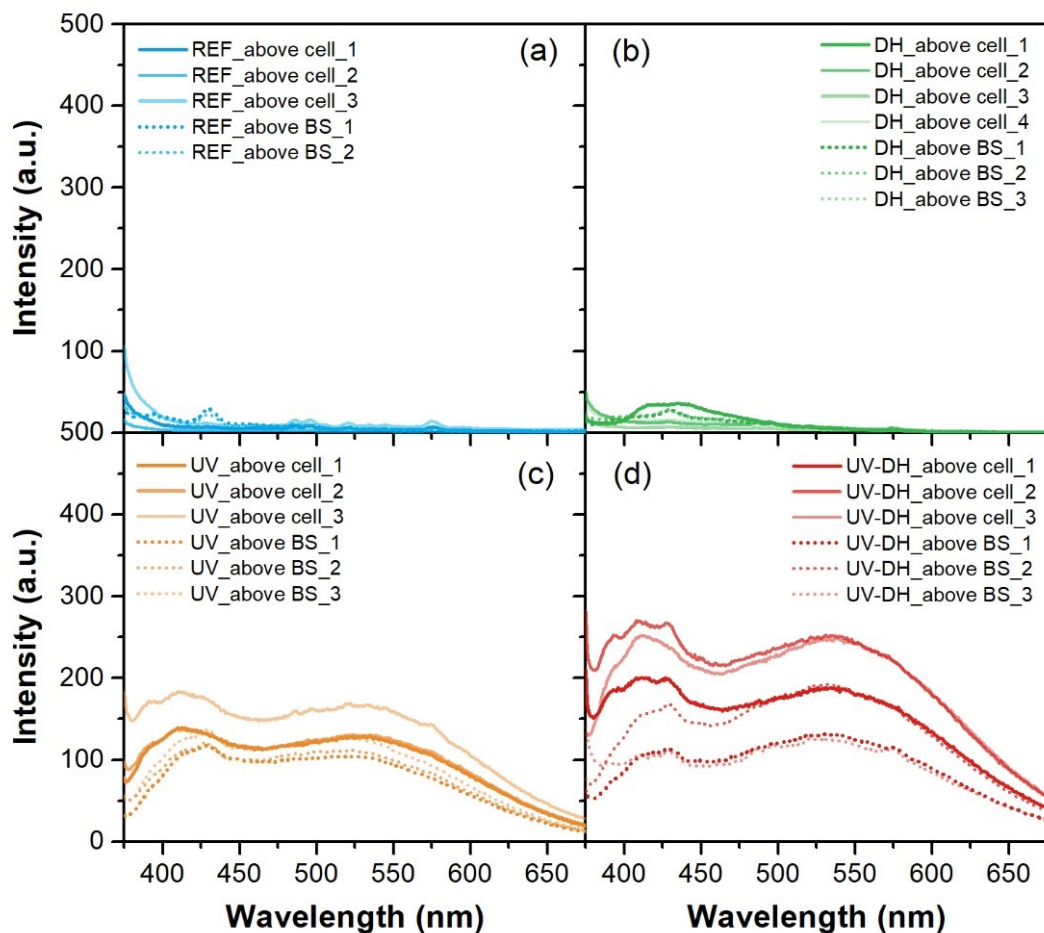

Figure 5.23: Fluorescence spectroscopy measurements on mini-modules: reference (a), module exposed to DH test (b), module exposed to UV test (c), module exposed to UV-DH test (d). Full lines represent spectra of the sample measured through the glass above the backsheet, whereas dotted lines represent spectra of the sample measured through the glass above the cell.

The images displayed in Figure 5.24 (a) to (d) further allow to visualize the different fluorescent behavior of the encapsulant material laminated within the

PV mini-modules. The images corresponding to the reference module and to the module exposed to DH test appear dark, whereas the modules exposed to UV and UV-DH combined test glow in the dark when exposed to UV light. The sample exposed to UV-DH combined test shows additional fluorescence when looking at the inner side of the backsheet that was uncovered by the glass and therefore directly exposed to the radiation during the UV-DH combined test. It is possible to notice that the inner side of the backsheet cracked, this exposing the PET core layer, which shows an intense fluorescence as well as the encapsulant material. The embrittlement of the backsheet directly exposed to the radiation was so severe that some small pieces of the backsheet fell apart
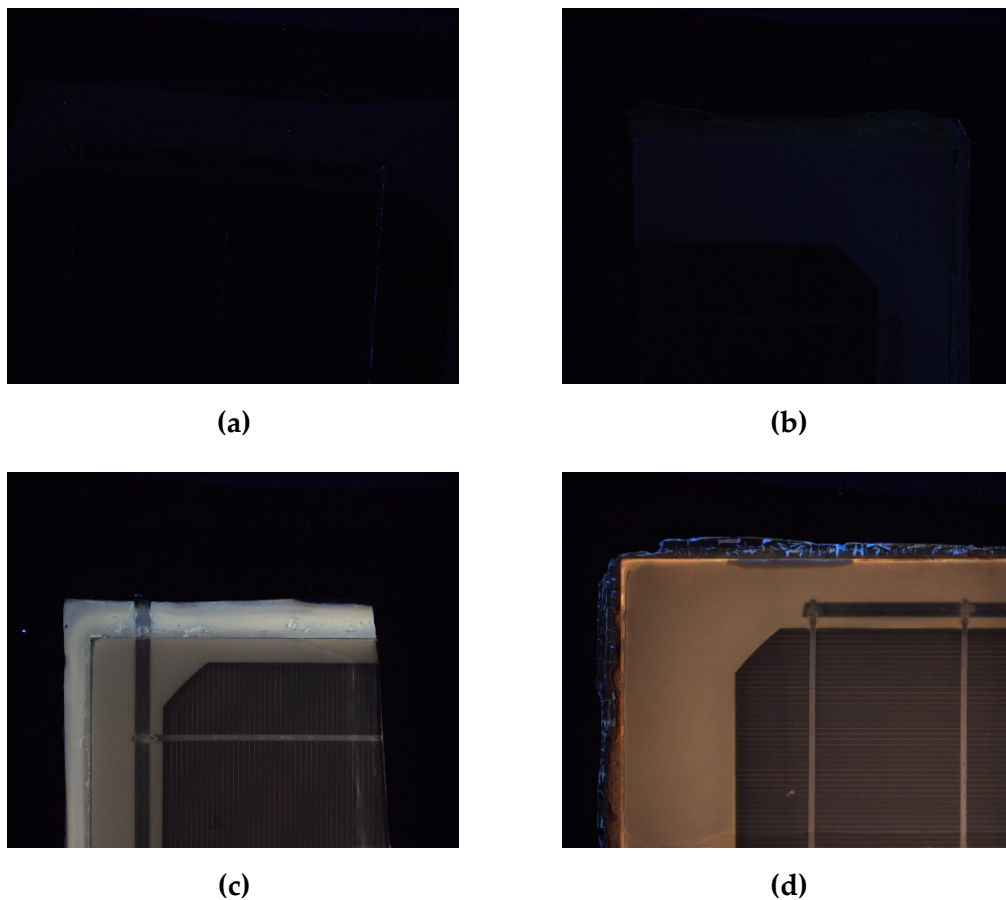

Figure 5.24: Fluorescence spectroscopy images taken using UV LED light source with 365 nm peak. The PV mini-modules displayed are the reference sample (a), module exposed to UV for 2000 hours (b), module exposed to dry UV test with a UV dose of 500 kWh m^{-2}, module exposed to UV-DH combined test with a dose of 250 kWh m^{-2}.

5.3.6 DSC

Figure 5.25 and Figure 5.26 show the thermal behavior of the encapsulants withdrawn from above the backsheet. The first heating curves (full line) give information regarding morphology of the materials and show both reversible and irreversible changes due to physical and chemical ageing, respectively. The second heating curves (dotted lines), instead, give more information regarding occurrence of irreversible modifications (chemical ageing).
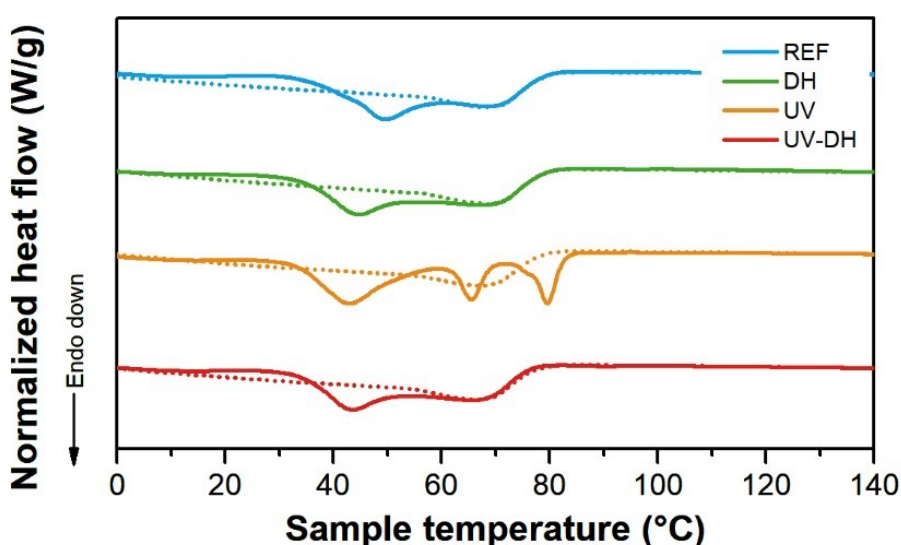

Figure 5.25: First (full lines) and second (dotted lines) heating curves of DSC measurements performed on EVA withdrawn from above the backsheet and exposed to different artificial ageing tests.

The first heating curve of the reference sample shows a melting process that takes place between 30 °C and 85 °C with two melting peaks at about 49 °C and 69 °C. Upon a second heating, the melting peak at lower temperature is no longer visible, whereas the main melting peak at 69 °C is left. This behavior is due to the rearrangements of crystalline structures upon melting. The cooling curve shows a crystallization process ongoing with a peak at about 47 °C. Upon the exposure to the artificial ageing tests, significant irreversible changes cannot be seen because the melting peak of the second heating curve remains substantially at the same temperature. On the other hand, morphological changes due to reversible (physical) processes are detected. The reversible effects disappear upon melting.

The samples exposed to DH shows a slight decrease of the lower temperature melting peak (from 49 °C to 44 °C), whereas the higher temperature melting

peak does not change its position. A further decrease of the lower temperature-melting peak towards 43 °C can be seen also for the samples exposed to UV irradiation. The higher temperature-melting peak, instead, does not show any changes for the samples exposed to UV-DH combined test. The samples exposed to dry UV test show the presence of populations with different crystal size, because they melt at different temperatures. Two melting peaks at 65.5 °C and 79.4 °C are identified. The crystallization peak slightly shifts from 47 °C of the reference sample to 48 °C of the sample exposed to UV test and to 46 °C of the samples exposed to dry UV and UV-DH combined test.
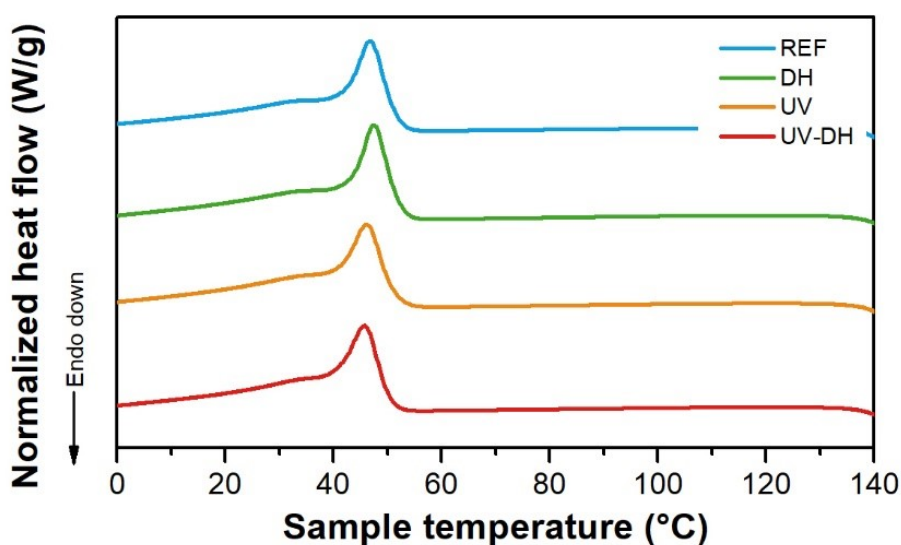

Figure 5.26: Cooling curves of DSC measurements performed on EVA withdrawn from above the backsheet and exposed to different artificial ageing.

A similar behavior to what has been described for the EVA extracted from above the backsheet can be seen for the encapsulant samples extracted from above the cell, Figure 5.27. The reference sample shows in the first heating the same melting peaks at 49 °C and at 69 °C. Similarly, the samples exposed to DH, dry UV and UV-DH combined tests shows a slight decrease towards about 45 °C. The sample exposed to dry UV, however, shows the presence of multiple melting peaks in the range between 35 °C and 90 °C, indicating the presence of crystals with different lamellar thicknesses and therefore different melting temperatures. The peculiar thermal behavior of the encapsulant material exposed to artificial ageing tests including UV radiation might be explained with the different temperature that the EVA reached during the tests. The EVA in contact with the cell in a module exposed to UV radiation might have had a

higher temperature than the EVA in contact with the backsheet. The second heating curves of the samples exposed to UV and UV-DH test showed a slight decrease of the melting peak temperature with respect to the reference sample regardless the position where the materials were extracted from (above the backsheet or above the cell). A slight drop in the melting enthalpy might be due to the recrystallization of the low-molecular degradation products generated upon exposure [36]. The results would been in good agreement with the increase of fluorescence intensity and yellowness index due to material degradation and chromophore formation [5, 36]
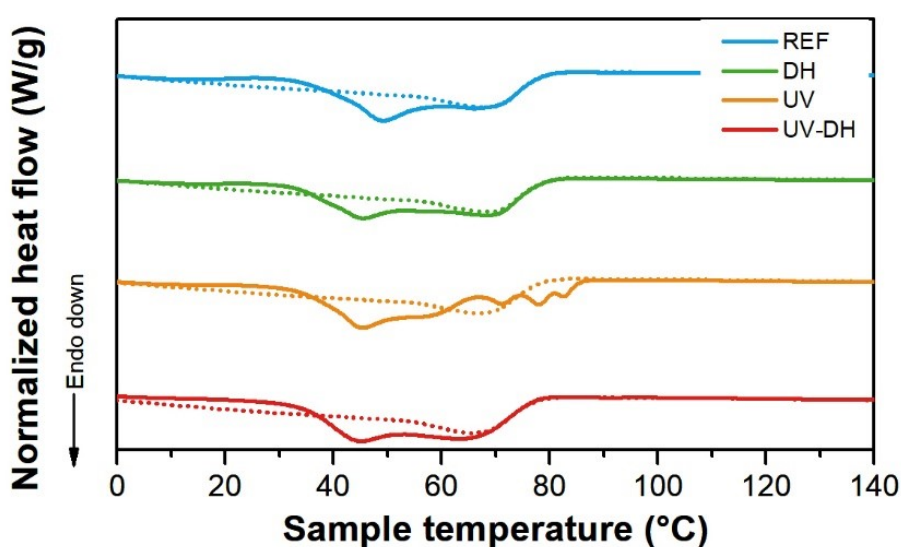

Figure 5.27: First (full lines) and second (dotted lines) heating curves of DSC measurements performed on EVA withdrawn from above the cell and exposed to different artificial ageing.

The cooling curve of the reference sample, Figure 5.28, shows a crystallization process with a peak at about 47 °C. The sample exposed to UV and UV-DH tests show a decrease of the crystallization temperature to about 45.5 °C.

The samples taken from "outside" are displayed in Figure 5.29 and Figure 5.30. The reference sample in this position shows some differences with respect to the same material above the backsheet and above the cell. The main melting peak remains stable at 69 °C in both first and second heating curve. Additionally, the first heating curve shows one peak at 50.3 °C and a shoulder at 42 °C. The cooling curve shows a crystallization peak at about 47 °C. The sample exposed to DH shows a slight increase of the high melting temperature-peak from 69 °C to about 71 °C in the first and second heating curve and a

secondary melting peak is present at about 45 °C. The cooling curve, instead, shows an increase of the crystallization temperature to 50 °C with respect to the reference material. The sample exposed to dry UV test shows two melting peaks in the first heating curve at about 42 °C, at about 80 °C and a shoulder is detected at 73.3 °C. The second heating curve shows a melting peak at about 75 °C.
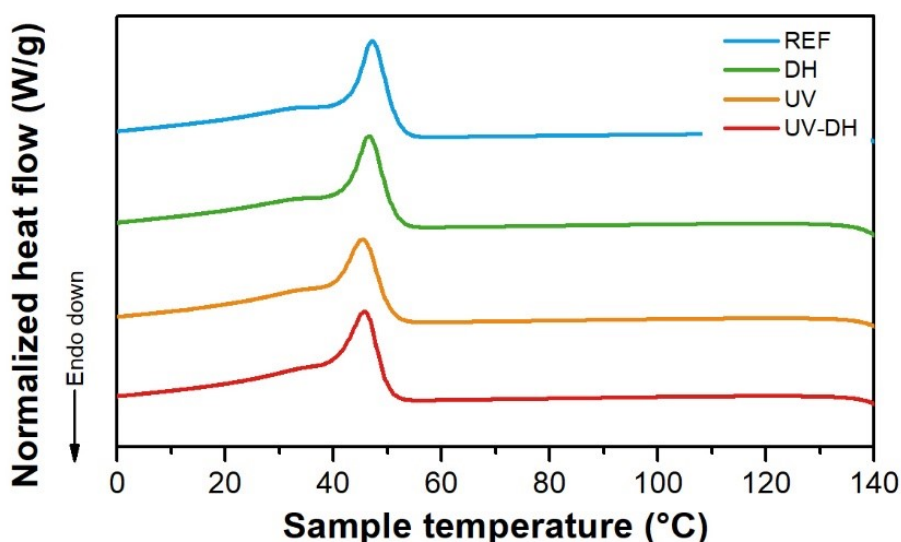

Figure 5.28: Cooling curves of DSC measurements performed on EVA withdrawn from above the cell and exposed to different artificial ageing.
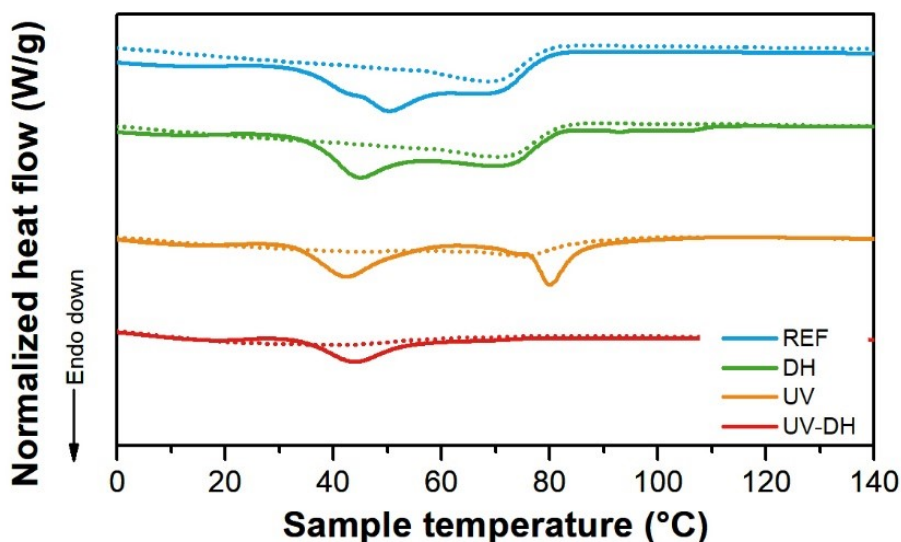

Figure 5.29: First (full lines) and second (dotted lines) heating curves of DSC measurements performed on EVA withdrawn from "outside", directly exposed.

The cooling curves of the sample exposed to UV irradiation show the most relevant differences with respect to the reference sample, Figure 5.30. The

sample shows a crystallization peak at about 47 °C in the cooling curve and an additional peak at about 25 °C. The cooling curve of the sample exposed to UV-DH combined test shows that the higher temperature crystallization-peak (about 48 °C) almost disappears, whereas a crystallization area can be observed starting from about 35 °C and going to lower temperatures.
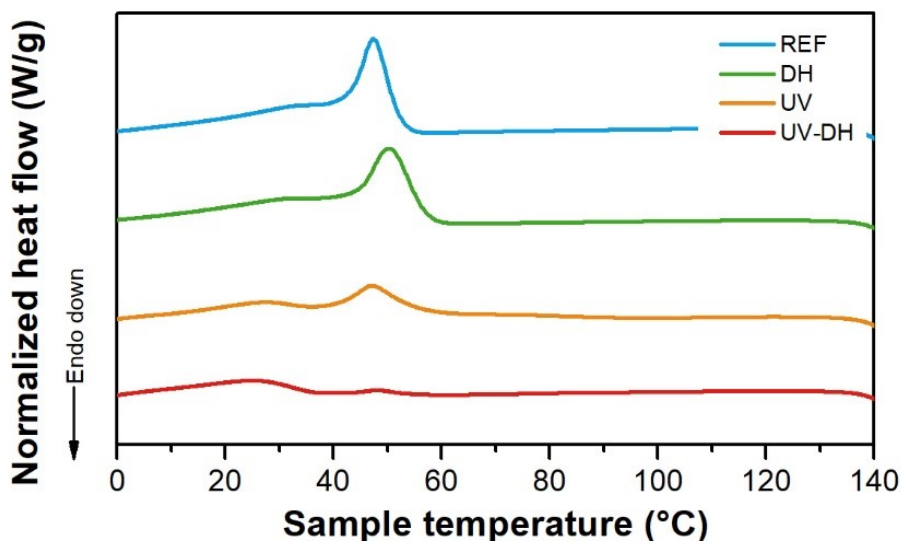

Figure 5.30: Cooling curves of DSC measurements performed on EVA withdrawn from "outside", directly exposed.

The crystallinity, calculated based on the melting enthalpy of the second heating curve, shows a decrease from ~22% of the reference sample to ~12% of the sample exposed to UV-DH combined tests. The decrease of the melting enthalpy of the second heating curve, associated to a decrease of the crystallization temperature and crystallinity are a clear sign of occurrence of chain scission processes for polyolefines [37].

5.3.7 TGA

Thermogravimetric analysis has been performed to determine changes in thermal stability of the exposed samples. The thermograms show the typical EVA behavior with two significant weight loss steps:

- First step between about 300 °C and 390 °C, meaning loss of vinyl acetate moieties (deacetylation);
- Second step between 390 °C and about 510 °C, meaning decomposition of polymer backbone [38].

Thermograms of EVA encapsulant withdrawn from above the backsheet, Figure 5.31, did not show significant material changes due to artificial ageing and the same conclusion can be drawn when looking at the encapsulant withdrawn from above the cell, Figure 5.32.
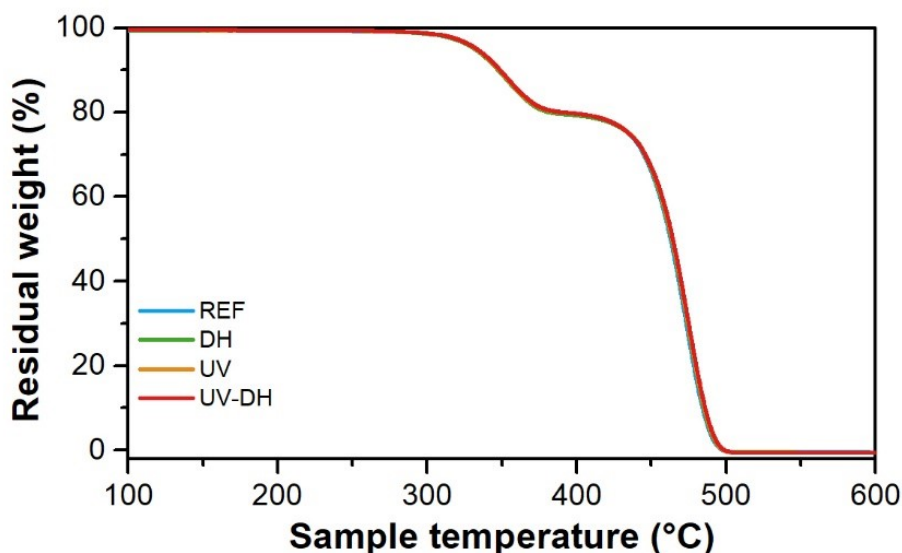
Figure 5.31: TGA thermograms of encapsulant samples withdrawn from above the backsheet.

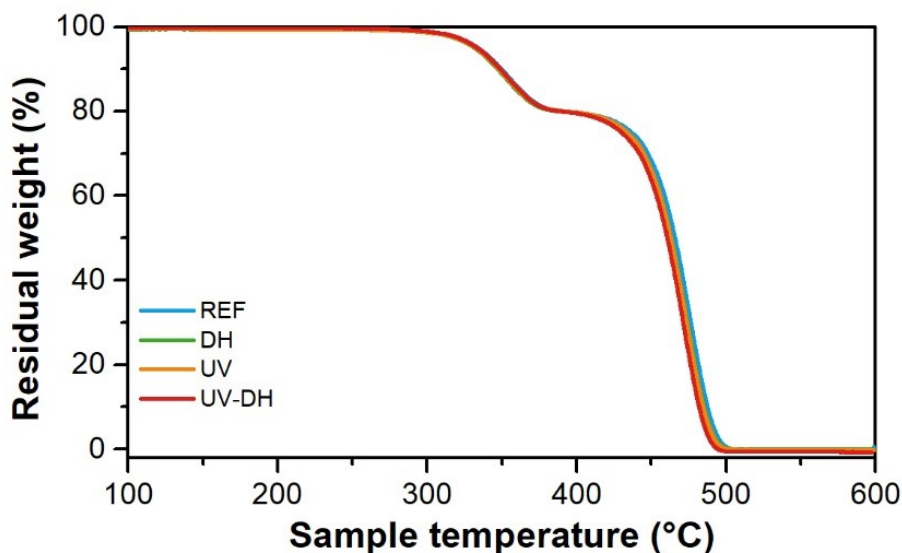**Figure 5.32: TGA thermograms of encapsulant samples withdrawn from above the cell.**

The excess encapsulant directly exposed showed, instead, signs of material degradation, Figure 5.33. The values of T_5 (temperature corresponding to 5% weight loss) and T_{40} (temperature corresponding to 40% weight loss) showed a shift towards lower temperatures for the samples exposed to UV and the effect

was even more pronounced for the sample exposed to UV-DH combined test, Figure 5.34. The sample exposed to DH, instead, did not show a significant change of thermal stability behavior with respect to the reference material
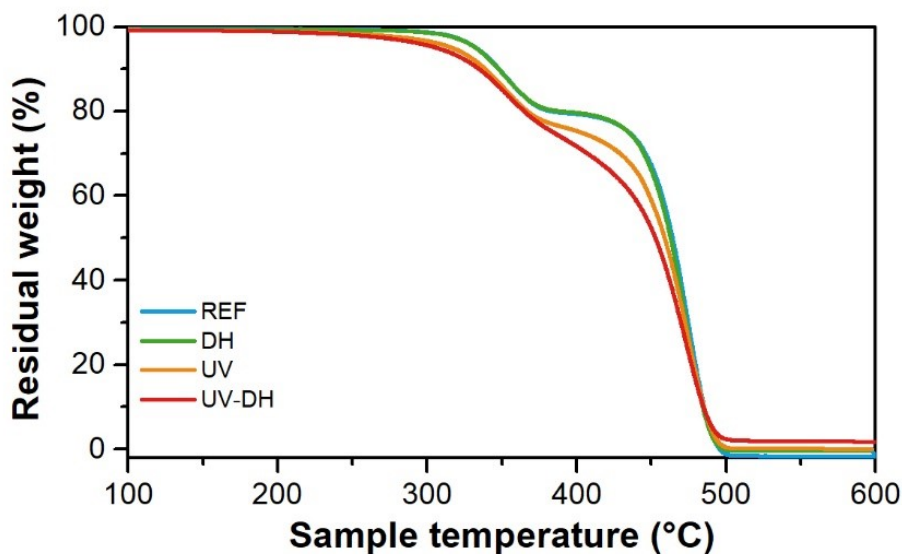
Figure 5.33: TGA thermograms of excess "outside" encapsulant samples.
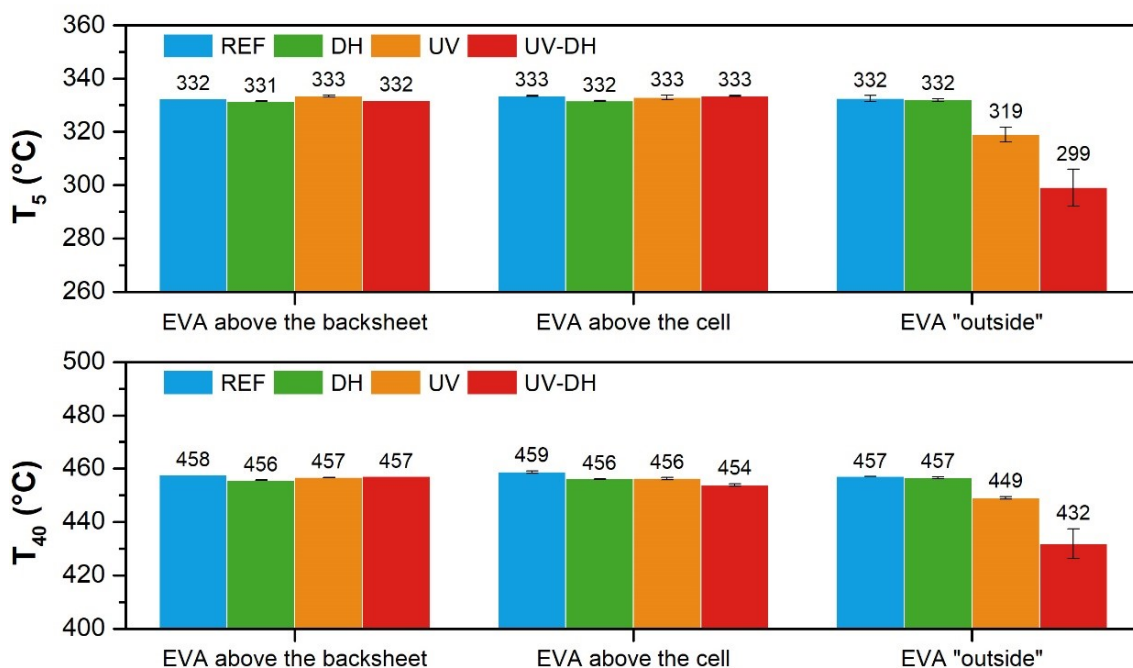

Figure 5.34: T_5 (temperature corresponding at 5% weight loss) and T_{40} (temperature corresponding at 40% weight loss) values from TGA of EVA samples taken from different positions.

The change of the shape of the curve in the first step for the more "severe" ageing tests, and the reduction of T_5 and T_{40}, is a confirmation of the worsening

of the thermal stability of the material. The occurrence of chain scission as well as the formation of many reactive species are produced upon UV exposure has been already proved my means of DSC analysis and FT-IR ATR spectroscopy, respectively. Therefore, with increasing temperature up to 400 °C, not only the deacetylation process takes place, but also the pyrolysis of the reactive species and the shorter chains [39], confirmed by GC/MS analysis.

5.4 How do polymer changes correlate to PV power degradation?

As expected, the results presented in this study showed that samples with the same bill of materials behaved differently upon the exposure to different artificial ageing tests, corresponding to different microclimates. The UV-DH combined test showed the strongest influence on power output among the used tests. This means that the combination of the stresses, rather than the single one, is decisive in causing material degradation and consequent power losses. The decrease in power output was mainly associated to a decrease in I_{SC}, which could be correlated with worsening of optical properties of the encapsulant, i.e. yellowing. Significant production of acetic acid upon exposure might be excluded as root cause, because a decrease of the carbonyl peak intensities in the FT-IR spectra could not be detected and no relevant changes could be seen in TGA measurements. Additionally, no significant changes of FF could be detected, often indirectly associated to corrosion of metallization and interconnections acetic acid production [20].

Color changes could not be correlated with any relevant change in functional groups detected by means of FT-IR spectroscopy measurements. The encapsulant above the cell and above the backsheet of the exposed samples, indeed, did not show significant differences with respect to the reference mini-module. The hypothesis is that the observed yellowing was caused by products of the antioxidant degradation, which was no longer detectable after the exposure to UV-DH combined test. However, the mentioned degradation products were not detected with FT-IR spectroscopy measurements. Therefore, power loss seems to not be directly related to degradation of the EVA polymer chain molecules, but rather to additive degradation [27].

FT-IR spectroscopy can be useful to understand the chemical changes taking place in the encapsulant, but it is not sensitive enough when the changes involve the stabilizers. When the material itself begins to degrade, by means of photo-oxidation reaction, it is then possible to additionally observe the formation of new functional groups. Degradation of the main polymer chain also results in reduced thermal stability.

Nevertheless, the increase of fluorescence intensity showed a good correlation with the increase of yellowness index of materials exposed to UV and UV-DH combined tests. The mini-module exposed to DH, although showing an increase of YI, did not show an increase of EVA's fluorescence, thus indicating that the origin of the discoloration might be, in this case, due to an unfavorable interaction between encapsulant and backsheet or to the reaction of unreacted peroxides with EVA's degradation products. Additionally, the increase of fluorescence intensity is well correlated with the decrease of melting temperature in the second heating curve for the materials exposed to artificial ageing tests including UV exposure. In this case, the increase of module temperature due to radiative heat combined with the UV radiation itself might have accelerated formation of unsaturation.

When comparing the behavior of the material directly exposed to the material encapsulated in the mini-module configuration, the importance of the shielding effect of the glass itself is obvious. The stabilization of the EVA encapsulant is crucial to the reliability of the material. The development of a special glass, which is not only highly transparent in the visible range of the solar spectrum, but is also able to filter the UV radiation out, might improve the whole module's reliability [40]. A summary of the changes that PV polymer experience and their effect on module electrical performances can be seen in Table 5.5.

Table 5.5: Polymer changes and correlation to electrical performances.

Polymer change	Causes	Effects on PV module performances
Encapsulant discoloration	• Additives degradation • Encapsulant degradation	• Reduction of power • Reduction of I_{sc}

Polymer change	Causes	Effects on PV module performances
Backsheet discoloration	• Inner layer degradation • Negative interaction with encapsulant	• No effect
Acetic acid production	• EVA degradation	• Reduction of power • Reduction of I_{sc} • Increase R_s • Decrease FF

5.5 Summary and conclusions

Mini-modules have been produced with EVA encapsulant and PET/PET/primer backsheets to investigate the influence of different artificial ageing tests on the degradation mechanisms taking place and finally on the influence on power output. Additionally, the interaction between the encapsulant and glass/solar cells has been the object of the investigation.

The encapsulant materials have been comprehensively analyzed with the objective to investigate changes in additive composition, chemical structure, morphology and thermal stability due to different environmental stress factors, microclimates and material interactions.

Results of electrical measurements showed that a slight decrease of power output has taken pace regardless of the artificial ageing test performed. However, the highest and most significant impact was achieved upon the exposure to UV-DH test. In all cases, the decrease in power output was associated to a decrease in short circuit current, probably due to yellowing. By evaluating the optical properties through the glass of the EVA above the backsheet, it was possible to observe an increase of the yellowness index for all the exposed modules and especially for the module exposed to UV-DH test. This result well correlates with the electrical measurements performed.

The degradation mechanism behind the formation of chromophores and discoloration of EVA encapsulant seems to be different. In the samples exposed to DH test, residues of crosslinking accelerators were detected. If the

crosslinking reaction has not taken place completely, it is possible that the unreacted peroxides created and oxidative environment and therefore chromophores were formed. The presence of UV irradiation, instead, caused not uniform consumption of antioxidant, whose degradation products might have caused the discoloration. However, the encapsulants withdrawn from above the backsheet and above the cell did not show significant formation of oxidation products at the surface in contact with the glass, and thermal properties did not change significantly. This indicates that no significant chain scission processes have occurred within the mini-module upon UV exposure.

The encapsulant withdrawn from "outside", namely the excess encapsulant directly in contact with the environment, showed extreme signs of degradation upon UV exposure, and especially upon UV-DH combined test. In this case, she browning of the encapsulant was due to photo-oxidative degradation reactions. Significant indications of chain scission could be detected with TD-GC/MS analysis, FT-IR ATR spectroscopy, DSC and TGA.

5.6 References

[1] F.J. Pern, "Factors that affect the EVA encapsulant discoloration rate upon accelerated exposure," *Solar Energy Materials and Solar Cells*, 41/42, pp. 587–615, 1996.

[2] A. W. Czanderna and F. J. Pern, "Encapsulation of PV modules using ethylene vinyl acetate copolymer as a pottant: A critical review," *Solar Energy Materials and Solar Cells*, vol. 43, no. 43, pp. 101–181, 1996, doi: 10.1016/0927-0248(95)00150-6.

[3] F.J. Pern and S.H. Glick, "Photothermal stability of encapsulated Si solar cells and encapsulation materials upon accelerated exposures," *Solar Energy Materials & Solar Cells*, no. 61, pp. 153–188, 1999.

[4] J. C. Schlothauer, K. Grabmayer, G. M. Wallner, and B. Röder, "Correlation of spatially resolved photoluminescence and viscoelastic mechanical properties of encapsulating EVA in differently aged PV modules," *Prog. Photovolt: Res. Appl.*, vol. 24, no. 6, pp. 855–870, 2016, doi: 10.1002/pip.2734.

[5] J. C. Schlothauer, K. Grabmayer, I. Hintersteiner, G. M. Wallner, and B. Röder, "Non-destructive 2D-luminescence detection of EVA in aged PV modules: Correlation to calorimetric properties, additive distribution and a clue to aging parameters," *Solar Energy Materials and Solar Cells*, vol. 159, pp. 307–317, 2017, doi: 10.1016/j.solmat.2016.09.011.

[6] Gernot Oreski, "Accelerated indoor durability testing of polymeric photovoltaic encapsulation materials," in *Reliability of Photovoltaic Cells, Modules, Components, and Systems III*, 2010, pp. 96–106.

[7] G. Oreski, A. Rauschenbach, C. Hirschl, M. Kraft, G. C. Eder, and G. Pinter, "Crosslinking and post-crosslinking of ethylene vinyl acetate in photovoltaic modules," *J. Appl. Polym. Sci.*, vol. 134, no. 23, p. 101, 2017, doi: 10.1002/app.44912.

[8] B. Ottersböck, G. Oreski, and G. Pinter, "Comparison of different microclimate effects on the aging behavior of encapsulation materials used in photovoltaic modules," *Polymer Degradation and Stability*, pp. 182–191, 2017, doi: 10.1016/j.polymdegradstab.2017.03.010.

[9] H. Han *et al.*, "Analysis of the degradation of encapsulant materials used in photovoltaic modules exposed to different climates in China," *Solar Energy*, vol. 194, pp. 177–188, 2019, doi: 10.1016/j.solener.2019.10.014.

[10] N. H. Phillips and K. P. Scott, "Quantifying PV module microclimates and translation into accelerated weathering protocols," in *SPIE Solar Energy + Technology*, San Diego, California, United States, 2014, 91790L.

[11] N. Bosco, T. J. Silverman, and S. Kurtz, "Climate specific thermomechanical fatigue of flat plate photovoltaic module solder joints," *Microelectronics Reliability*, vol. 62, pp. 124–129, 2016, doi: 10.1016/j.microrel.2016.03.024.

[12] R. Meier, M. Pander, S. Großer, and S. Dietrich, "Microstructural Optimization Approach of Solar Cell Interconnectors Fatigue Behavior for Enhanced Module Lifetime in Extreme Climates," *Energy Procedia*, vol. 92, pp. 560–568, 2016, doi: 10.1016/j.egypro.2016.07.020.

[13] D. E. Mansour *et al.,* "Effect of Backsheet Properties on PV Encapsulant Degradation during Combined Accelerated Aging Tests," *Sustainability*, vol. 12, no. 12, p. 5208, 2020, doi: 10.3390/su12125208.

[14] Y. Lyu, J. Hyun Kim, X. Gu, "Developing methodology for service life prediction of PV materials: quantitative effects of light intensity and wavelength on discoloration of a glass/EVA/PPE laminate," *Solar Energy*, vol. 174, pp. 515–526, 2018, doi: 10.1016/j.solener.2018.08.067.

[15] A. Borne, K. R. Choudhury, W. Gambogi, and K.-A. Weiss, "Novel Accelerated Testing Methods for Faster Evaluation of PV modules and Materials," in *37th European Photovoltaic Conference and Exhibition*, pp. 900–903.

[16] M. Owen-Bellini *et al.,* "Advancing reliability assessments of photovoltaic modules and materials using combined-accelerated stress testing," *Prog Photovolt Res Appl*, vol. 29, no. 1, pp. 64–82, 2021, doi: 10.1002/pip.3342.

[17] P. Hacke *et al.,* "Combined and Sequential Accelerated Stress Testing for Derisking Photovoltaic Modules," in *Advanced Micro- and Nanomaterials for Photovoltaics*, pp. 279–313.

[18] D. Wu, "Investigation of the Reliability of the Encapsulation System of Photovoltaic Modules," Loughborough University, Loughborough, UK, 2015.

[19] M. Bliss, "Measurement system for fast power and energy rating of photovoltaic devices," Loughborough University, Loughborough, UK, 2011.

[20] M. Koentges *et al.,* "IEA Task 13 - Review on Failures of PV," Report IEA-PVPS T13-01:2013, IEA - International Energy Agency, Nov. 2013.

[21] R. Yang, J. Zhao, and Y. Liu, "Oxidative degradation products analysis of polymer materials by pyrolysis gas chromatography–mass spectrometry," *Polymer Degradation and Stability*, vol. 98, no. 12, pp. 2466–2472, 2013, doi: 10.1016/j.polymdegradstab.2013.05.018.

[22] K. Harata, S. Kitagawa, Y. Iiguni, and H. Ohtani, "Identification of polymer species in a complex mixture by pyrolysis-gas chromatography-atmospheric pressure chemical ionization-high resolution time-of-flight mass spectrometry as a basis for environmental microplastic analysis," *Journal of Analytical and Applied Pyrolysis*, vol. 148, p. 104828, 2020, doi: 10.1016/j.jaap.2020.104828.

[23] C. Schwarzinger, I. Hintersteiner, B. Schwarzinger, W. BUCHBERGER, and B. Moser, "Analytical pyrolysis in the determination of the aging of polyethylene," *Journal of Analytical and Applied Pyrolysis*, vol. 113, pp. 315–322, 2015, doi: 10.1016/j.jaap.2015.02.005.

[24] Chitec, *Product Data Sheet: Chiguard PB-12: Ultraviolet light absorber for plastics, and adhesives.* [Online]. Available: http://file.yizimg.com/352101/2010080521360907.pdf (accessed: Nov. 22 2020).

[25] D. C. Miller *et al.,* "Degradation in photovoltaic encapsulant transmittance: Results of the first PVQAT TG5 artificial weathering study," *Prog Photovolt Res Appl*, vol. 27, no. 5, pp. 391–409, 2019, doi: 10.1002/pip.3103.

[26] *Standard Practice for Calculating Yellowness and Whiteness Indices from Instrumentally Measured Color Coordinates*, ASTM E313 - 05, ASTM International. [Online]. Available: http://www.astm.org/cgi-bin/resolver.cgi?E313-05

[27] N. S. Allen and M. Edge, "Perspectives on additives for polymers. 1. Aspects of stabilization," *J Vinyl Addit Technol*, pp. 1–23, 2020, doi: 10.1002/vnl.21807.

[28] G. Socrates, *Infrared and Raman Characteristic Group Frequencies: Tables and Charts,* 3rd ed. Chichester, West Sussex, England: John Wiley & Sons, Ltd, 2001.

[29] N. S. Allen, M. Edge, M. Rodriguez, C. M. Liauw, and E. Fontan, "Aspects of the thermal oxidation, yellowing and stabilisation of ethylene vinyl acetate copolymer," *Polymer Degradation and Stability*, no. 71, pp. 1–14, 2001.

[30] G. Oreski, G. M. Wallner, and R. W. Lang, "Ageing characterization of commercial ethylene copolymer greenhouse films by analytical and mechanical methods," *Biosystems Engineering*, vol. 103, no. 4, pp. 489–496, 2009, doi: 10.1016/j.biosystemseng.2009.05.003.

[31] K. Grabmayer *et al.,* "Accelerated aging of polyethylene materials at high oxygen pressure characterized by photoluminescence spectroscopy and established aging characterization methods," *Polymer Degradation and Stability*, vol. 109, pp. 40–49, 2014, doi: 10.1016/j.polymdegradstab.2014.06.021.

[32] K. Hara, S. Jonai, and A. Masuda, "Crystalline Si photovoltaic modules functionalized by a thin polyethylene film against potential and damp-heat-induced degradation," *RSC Adv.*, vol. 5, no. 20, pp. 15017–15023, 2015, doi: 10.1039/C4RA13360A.

[33] K. Hara and Y. Chiba, "Spectroscopic investigation of long-term outdoor-exposed crystalline silicon photovoltaic modules," *Journal of Photochemistry and Photobiology A: Chemistry*, vol. 404, p. 112891, 2021, doi: 10.1016/j.jphotochem.2020.112891.

[34] W. Yagoubi, A. Abdelhafidi, M. Sebaa, and S. F. Chabira, "Identification of carbonyl species of weathered LDPE films by curve fitting and derivative analysis of IR spectra," *Polymer Testing*, vol. 44, pp. 37–48, 2015, doi: 10.1016/j.polymertesting.2015.03.008.

[35] A. Abdelhafidi *et al.,* "Sun radiation and temperature impact at different periods of the year on the photooxidation of polyethylene films," *IJHT*, vol. 35, no. 2, pp. 255–261, 2017, doi: 10.18280/ijht.350204.

[36] Y. Lyu *et al.,* "Fluorescence imaging analysis of depth-dependent degradation in photovoltaic laminates: insights to the failure," *Prog Photovolt Res Appl*, vol. 28, no. 2, pp. 122–134, 2020, doi: 10.1002/pip.3212.

[37] G. W. Ehrenstein, G. Riedel, and P. Trawiel, *Thermal analysis of plastics: Theory and practice*. Munich: Carl Hanser Verlag, 2004.

[38] B. Rimez, H. Rahier, G. van Assche, T. Artoos, M. Biesemans, and B. van Mele, "The thermal degradation of poly(vinyl acetate) and poly(ethylene-co-vinyl acetate), Part I: Experimental study of the degradation mechanism," *Polymer Degradation and Stability*, vol. 93, no. 4, pp. 800–810, 2008, doi: 10.1016/j.polymdegradstab.2008.01.010.

[39] Z. Liu, J. Jin, S. Chen, and J. Zhang, "Effect of crystal form and particle size of titanium dioxide on the photodegradation behaviour of ethylene-vinyl acetate copolymer/low

density polyethylene composite," *Polymer Degradation and Stability*, vol. 96, no. 1, pp. 43–50, 2011, doi: 10.1016/j.polymdegradstab.2010.11.010.

[40] B. L. Allsopp *et al.,* "Towards improved cover glasses for photovoltaic devices," *Prog Photovolt Res Appl*, vol. 28, no. 11, pp. 1187–1206, 2020, doi: 10.1002/pip.3334.

6 Analysis of degradation of EVA encapsulant in PV modules operating in different climates

Parts of this work were presented as conference contributions:

- *"Effects of climate and microclimate on EVA degradation from field aged PV modules"*, oral presentation, 38th European PV Solar Energy Conference and Exhibition (EU PVSEC), 6th-10th of September 2021, virtual event.
- *"Degradation of Crystalline Silicon Photovoltaic Modules Installed in Different Climates"*, oral presentation, 49th IEEE Photovoltaic Specialists Conference (PVSC), 5th-10th June 2022, Philadelphia (USA).

I would like to thank Julian Ascencio-Vásquez for the contribution in providing the data for the climate analysis and Mark Köntges for providing the results of the electrical characterization of the modules exposed in the Caribbean, electroluminescence images and the measurements of acetic acid concentration.

6.1 Motivation

The importance of testing materials and modules in different climates has become more and more significant in recent years. The concept of "one fits all", namely one type of module fits all climates, was proven wrong in literature and new concepts of climate specific module design as well as artificial ageing tests were brought to the attention of the PV community [1].

In recent years, more and more attention has been given to the importance of testing PV modules in different climates as well as to provide guidelines about climate specific PV module design. Jordan et al. [2] first published a literature review regarding changes in power output of PV systems all over the world, trying to identify and correlate power losses to specific climate-related degradation modes. The impact of climate on PV performance was addressed as a potential problem, but the lack of data did not allow to draw precise conclusion in regard [2]. However, over the last decade many studies dealing with monitoring of PV systems' performances in different climate zones were published and more clear correlations between climatic conditions and PV degradation were found [3].

Omazic et al. [4] reviewed literature regarding field aged PV modules and identified the main degradation modes according to 5 different climate zones. Hot and humid conditions in tropical climates result as the most harmful for PV modules and encapsulant discoloration, extensive delamination at different interfaces and corrosion are the most relevant degradation modes. Production of acetic acid is favored by high humidity and high temperature conditions and all the acetic acid-related degradation modes occur with higher rates compared to other climates. In colder climates, the thermal degradation processes are slowed down. Degradation modes related to mechanical stresses are more relevant in snow and polar climates, where, besides snowfalls and wind, low temperatures (below $-15\,°C$) can cause EVA embrittlement and further mechanical stress on the cells and interconnections.

Ascencio-Vásquez et al. [5] developed a worldwide map of degradation mechanisms and degradation rates (%/year) for c-Si PV modules based on three mechanisms: EVA hydrolysis, thermomechanical and photo-degradation. Hydrolysis is temperature and humidity driven, photo-degradation is influenced by temperature, humidity and UV irradiation and thermo-mechanical degradation is mainly affected by temperature and temperature differences [6]. In their study, the most un-favorable climate zones for c-Si PV modules are, once again, tropical because of the high humidity and high temperature conditions.

New models able to predict power degradation and to make lifetime estimations were developed in recent studies [6, 7] and worldwide mapping of degradation rates were presented [5]. These studies show how the tropical climates, i.e. high irradiation, high temperature and high humidity values, strongly affect the performances of the PV modules. In these cases, the most relevant power losses were detected and correlated to failure modes such as yellowing of the encapsulant, corrosion of metallic interconnections and silver grids, delamination at different interfaces or backsheet cracks, just to name a few. However, most of the published studies include investigations of electrical performances [8–14] of field aged PV modules or characterization via non-destructive methods [15–17]. Only few studies report destructive investigations on PV materials to better understand the degradation mechanisms that took place over the years [18–21].

The objective of the work described in this chapter was to investigate the implication of using modules with the same bill of materials in different climates and to assess the impact of the different environmental stresses on material degradation. An investigation of chemical and thermal properties was carried out to correlate their changes to power degradation. Additionally, an analysis of the different climate where the PV modules were located was performed to assess the entity of the environmental stress factors.

6.2 Experimental

Four PV modules with the same bill of materials were object of the investigations described in this chapter. One module, considered as reference, was kept in the dark while the other three modules were exposed outdoor and operated in two different locations for about 7 years. The modules operated in Germany, classified as moderate climate, and in the Caribbean, considered as tropical climate. All modules were characterized by the same configuration and bill of materials: PV glass, encapsulant (EVA), poly-crystalline Silicon solar cells, encapsulant (EVA) and polymer backsheet. Encapsulant material was withdrawn from four full-size PV modules named as follows:

- M1, reference module, kept in the dark;
- M2, module exposed in moderate climate (Germany) for about 7 years;
- M3 and M4, modules exposed in tropical climate (the Caribbean) for about 7 years.

The difference between M3 and M4 lies in the different electrical performances as well as in the concentration of the acetic acid produced upon exposure, details will be discussed in the next sections.

Characterization of the electrical performances of the PV modules were carried out at the Institute für Solerenergieforschung GmbH in Emerthal in Germany. I-V curves were measured to assess the extent and to investigate the causes of the power degradation of the modules exposed in the tropical climate with respect to the reference module. Electroluminescence images were taken to further investigate the reason for the changes in electrical performances. Moreover, EVA encapsulant material was extracted from the modules and quantitative acetic acid measurements were performed to assess its concentration by means of ion chromatography. For each module, encapsulant

samples were withdrawn from five different positions (Figure 6.1) to evaluate the influence of the microclimate on polymer behavior and to assess interactions between the encapsulant and the different PV module components:

- Back encapsulant, in contact with the cell and the backsheet, indirectly exposed to outdoor conditions (P1 and P2),
- Back encapsulant between cell and backsheet (P3), below the adhesive layer connecting the junction box,
- Back encapsulant between cell and backsheet (P4) in the area *inside* the junction box,
- Front encapsulant (P5), between glass and the solar cell approximatively in the center of the module.

The modules exposed in the tropical climate showed presence of darker areas in the middle of the cells in different positions in the central area of the module, as can be seen in bottom right hand side of Figure 6.1.

Figure 6.1: Positions of encapsulants' withdrawal. P1 and P2 (left): back encapsulant, in contact with the cell and the backsheet, indirectly exposed to outdoor conditions. P3 (top right): back encapsulant between cell and backsheet, below the adhesive layer connecting the junction box. P4 (top right): back encapsulant between cell and

backsheet in the area "inside" the junction box. P5 (bottom right): front encapsulant, between glass and the solar cell in the center of the module.

The characterization methods applied to the withdrawn encapsulants were:

- TD-GC/MS for additive analysis,
- FT-IR ATR spectroscopy to highlight the changes in chemical structure,
- DSC to investigate chemical and morphological changes,
- TGA to assess changes in thermal stability.

6.3 Climate analysis

The exact location where the PV module were installed was not disclosed for confidential reasons. The climate data analysis presented in this section was carried out considering a general location in central Germany and in the Caribbean as locations. The analysis is therefore carried out not to describe in detail the exact climate where the PV modules are installed, but to give an insight of the stressors typical of each climate and their impact on the polymer behavior. The climate data were obtained from the ERA5 reanalysis dataset [22] and manipulated to obtain the variable of interest. The ERA5 reanalysis datasets are characterized by an hourly resolution, include values of ambient, and dew point temperatures, global horizontal irradiance, irradiance in plane of array, wind speed, wind direction and many more.

The ambient relative humidity RH values were calculated according to equation 6.1 using the WVP, Water Vapor Pressure at dew temperature (T_{dew}) and at ambient temperature (T_{amb}) .

$$RH[\%] = \frac{WVP(T_{dew})}{WVP(T_{amb})} \cdot 100 \qquad \text{(Equation 6.1)}$$

The WVP values were calculated using the Buck model [23], equation 6.2:

$$WVP =$$
$$\begin{cases} 0.61115 \cdot \exp\left(\left(23.036 - \frac{T}{330.70}\right) \cdot \left(\left(\frac{T}{279.82} + (T)\right)\right)\right), \ T < 0 \\ 0.61121 \cdot \exp\left(\left(18.678 - \frac{T}{234.84}\right) \cdot \left(\left(\frac{T}{257.14} + (T)\right)\right)\right), \ T \geq 0 \end{cases} \qquad \text{(Equation 6.2)}$$

Module temperature values are calculated according to the model developed by Ross (equation 6.3):

$$T_{mod} = T_{amb} + k_{Ross} \cdot E_{POA} \qquad \text{(Equation 6.3)}$$

where T_{mod} corresponds to the module temperature, T_{amb} to the ambient temperature, k_{Ross} to a coefficient related to the efficiency of the heat transfer between the PV module and the surrounding environment depending especially on the mounting configuration, and E_{POA} corresponds to the incident solar irradiance. However, in this case the global horizontal irradiance (GHI) was used, as the tilt angle of the installed modules was unknown. The value of k_{Ross} was set to 0.03, which corresponds to an intermediate value between a well cooled and a not so well cooled module [24], being unknown the configuration of the PV modules exposed.

The UV fraction (UV_{total}) of the solar spectrum that includes UVA and UVB radiation can be estimated, as a first approximation, according to a linear model (equation 6.4) [25]:

$$UV_{total} = c_1 \cdot E_{POA} + c_2 \qquad \text{(Equation 6.4)}$$

The coefficient c_1 is typically set to 0.5, whereas the coefficient c_2 can be neglected. As well as for the calculation of the module temperature, also in this case the GHI values are used instead of E_{POA}.

The data calculated as described above were then grouped into daily values according to the following criteria:

- Maximum and minimum daily ambient temperature,
- Maximum and minimum daily module temperature,
- Mean daily relative humidity,
- Maximum daily global horizontal irradiance.

The UV dose is calculated as the integral of the global horizontal irradiance values over the timeframe considered, from the beginning of 2010 until the end of 2018.

Figure 6.2 and Figure 6.3 describe the values of maximum and minimum daily ambient temperatures in the Caribbean and in Germany from 2010 until 2018. From the boxplot, Figure 6.2, it is interesting to notice how the maximum and minimum daily temperature values are quite stable. The median value for the maximum daily ambient temperature is about 26.9 °C, whereas the value for minimum daily ambient temperature is about 25.4 °C. The corresponding values for Germany are 12.2 °C and 5.3 °C, respectively. However, the range of

ambient temperature is much larger for Germany with respect to the Caribbean. The variation for Germany is between 35.2 °C (absolute maximum) and −14.2 °C (absolute minimum, with some outliers going down to −21.4 °C), whereas the variation for the Caribbean is between 29.3 °C (absolute maximum) and 22.2 °C (absolute minimum).
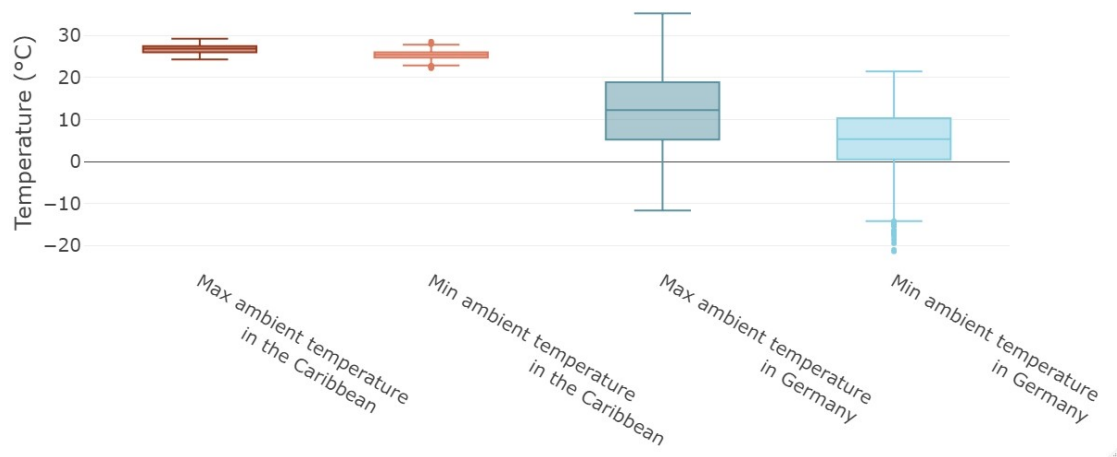

Figure 6.2: Maximum and minimum daily ambient temperature from 2010 to 2018 in the Caribbean and in Germany, box plot.
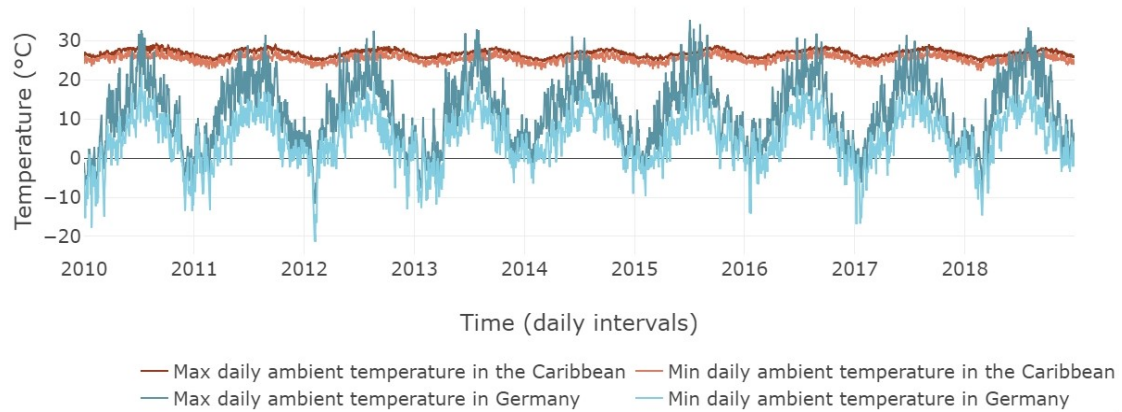

Figure 6.3: Maximum and minimum daily ambient temperature from 2010 to 2018 in the Caribbean and in Germany, time series.

Even though the ambient temperature values in the Caribbean do not seem extreme, it is important to notice how the microclimate influences very much the conditions that the modules experience. The estimated module temperatures, which consider the increase of temperature due to irradiation, show how the actual module operating temperature might be very different from the surrounding environment, especially the maximum values.

The maximum module temperature estimated for the modules operating in the Caribbean, Figure 6.4 and Figure 6.5, ranges between 58 °C and 42 °C, with a median value of about 52 °C, whereas the minimum module temperature varies between 28.6 °C and 22.2 °C, with a median value of 25.5 °C.
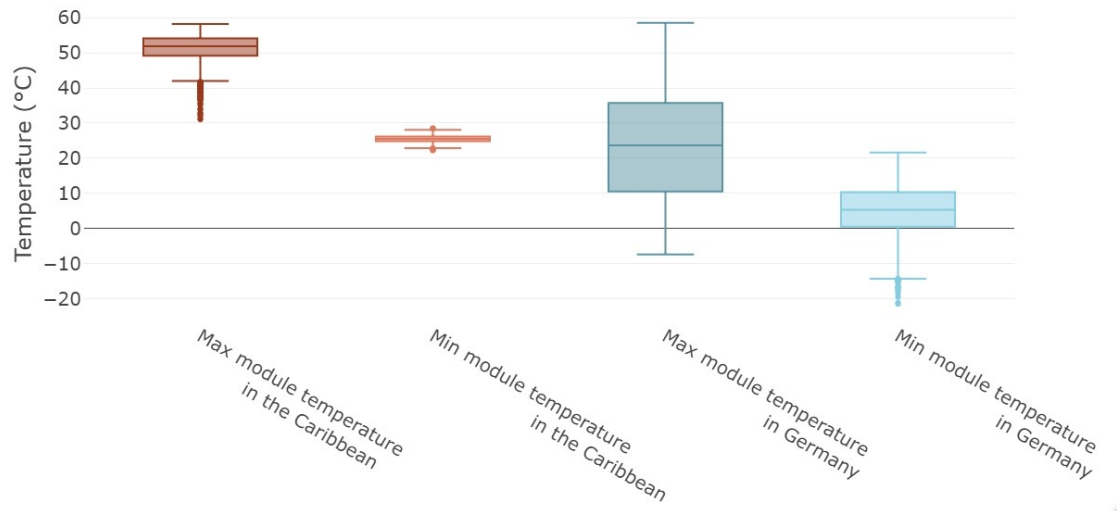

Figure 6.4: Maximum and minimum daily module temperature from 2010 to 2018 in the Caribbean and in Germany, box plot.
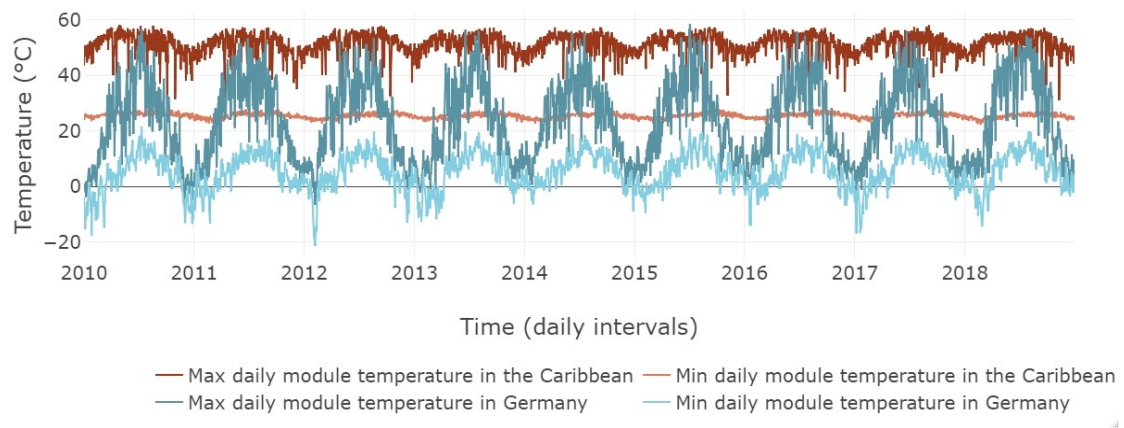

Figure 6.5: Maximum and minimum daily module temperature from 2010 to 2018 in the Caribbean and in Germany, time series.

As well as for the ambient temperature, the module exposed in Germany can experience more significant temperature variations throughout their lifetime. The module temperatures, indeed, can vary between about 58.5 °C and -14.2 °C. However, the operating temperatures of the modules exposed in Germany are generally lower than the module temperature in the Caribbean. Figure 6.5 shows the evolution of module temperature over time for both locations. It is

possible to observe how the difference between maximum and minimum values is quite constant in the Caribbean, whereas it changes quite significantly for Germany showing very strong seasonality. It is noticeable how the temperature difference decreases during winter times and how it increases during summer seasons. The mean daily relative humidity values are represented in Figure 6.6 and Figure 6.7. The mean daily relative humidity in the Caribbean varies between about 90% and 70%, whereas the mean daily relative humidity in Germany varies between 99.5% and 44.5%. The median value for both locations is about 82%. Once again, the variations that can be achieved in Germany are much more pronounced than the variations that might take place in the Caribbean.
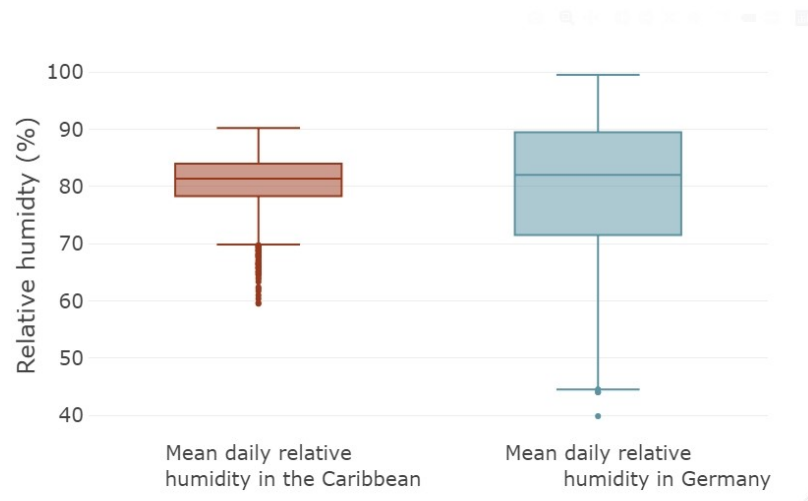

Figure 6.6: Mean daily relative humidity from 2010 to 2018 in the Caribbean and in Germany, box plot.
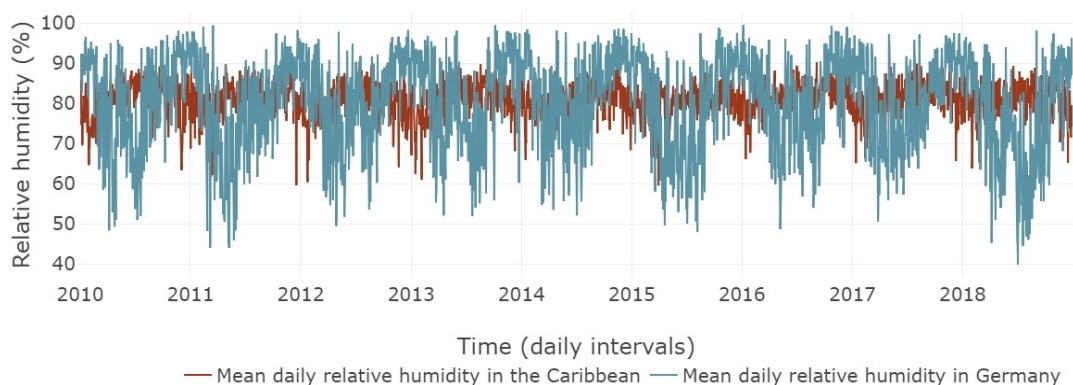

Figure 6.7: Mean daily relative humidity from 2010 to 2018 in the Caribbean and in Germany, time series.

The global irradiance values for Germany and the Caribbean are shown in Figure 6.8 and Figure 6.9. The irradiance values for the Caribbean are very high compared to Germany. The median value for the maximum irradiance in the Caribbean is about 845 W m^{-2}, whereas it is about 419 W m^{-2} in Germany. Additionally, the estimated UV dose accumulated in the two locations in the 9 years of the PV module operation is about 505 kWh m^{-2} for Germany and almost double for the Caribbean, about 968 kWh m^{-2}.
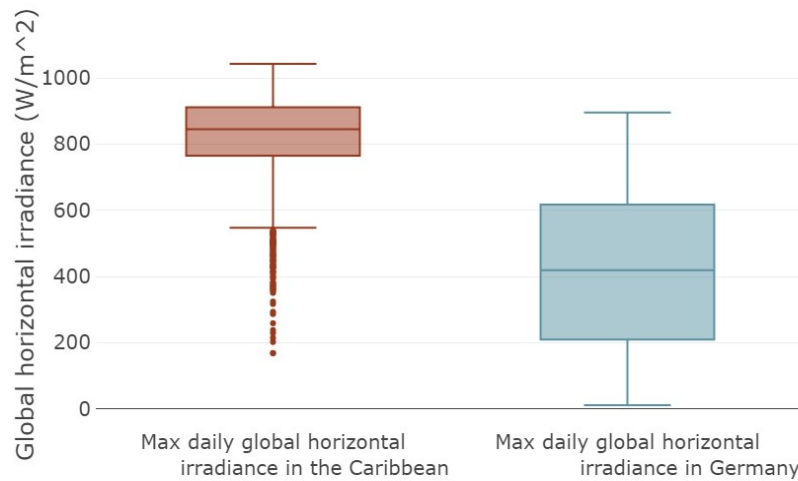

Figure 6.8: Maximum daily global horizontal irradiance from 2010 to 2018 in the Caribbean and in Germany, box plot.
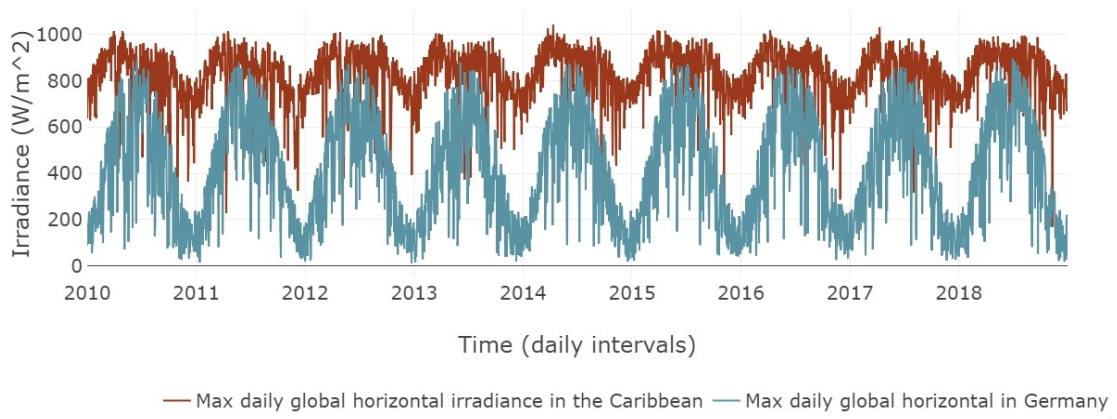

Figure 6.9: Maximum daily global horizontal irradiance from 2010 to 2018 in the Caribbean and in Germany, time series.

In summary, the modules operating in the Caribbean might experience conditions that are not significantly affected from seasonality. Values of module temperature, relative humidity and irradiance are less variable over the years, but typically higher than the corresponding values in Germany. Modules

operating in Germany are more subject to seasonality and especially to thermal cycling with respect to the modules exposed in the Caribbean.

The significant difference between the climate and especially the microclimate that the modules experience in the two locations would make them prone to different behavior upon exposure. The modules exposed in Germany, that experience thermal cycles especially during the summer, would be particularly sensitive towards mechanical stresses due to encapsulants thermal expansion. However, the more overall mild environmental conditions should not cause a significant material degradation for a well-designed configuration. On the other hand, the higher stresses that the modules exposed in the Caribbean might experience persistently during their lifetime might lead to severe material and performances degradation.

6.4 Results

6.4.1 PV modules performances and acetic acid concentrations

The modules exposed to the tropical climate in the Caribbean showed a significant power degradation with respect to the reference module. The reference module did not show power decrease with respect to the nameplate value and the other relevant parameters did not show significant deviations. M3 and M4 showed 45% and 10% power loss, respectively, that was mainly associated with a drop in fill factor. The measured fill factor for M3 was 43.6% instead of 73.7% (nameplate value) and 68.3% for M4. Additionally, M3 and M4 showed a decrease in short circuit current. The measured value was 7.77 A for M3 and 8.05 A for M4 instead of 8.27 A (nameplate value). No significant decrease in performance was reported from the PV system owner for the module exposed in the moderate climate (Germany). The electroluminescence images, displayed in Figure 6.10, showed evidence of acetic acid corrosion on the cells, characterized by a typical pattern with dark areas on the cells.

The acetic acid concentration measurements were performed on EVA extracted from the reference module M1 and on EVA extracted from other two modules (not described in this study). The modules were the same as M3 and M4, were exposed in the same location of the tropical climate and were characterized by power loss values of 31% and 53%, respectively. Also, the degradation mechanisms observed for these additional two modules were the same as

described for M3 and M4, namely power loss associated with drop of fill factor, decrease of short circuit current and presence of typical acetic acid corrosion pattern on the electroluminescence images.
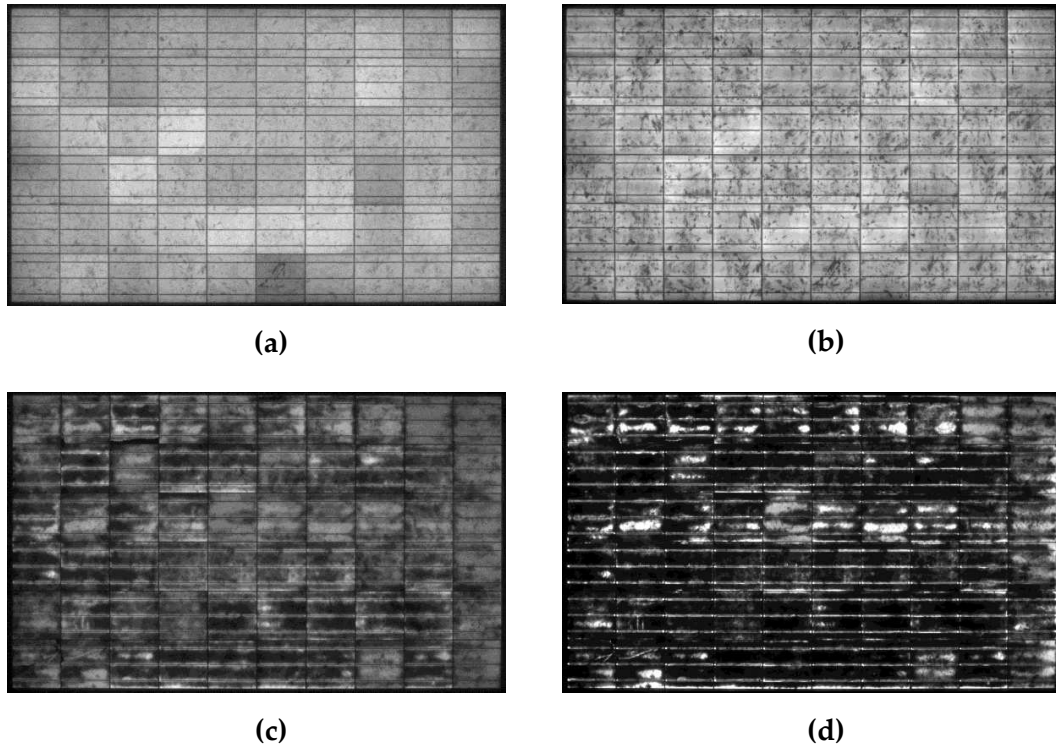

Figure 6.10: Electroluminescence images of reference module (M1) taken at 1/10 I_{SC} (a) and I_{SC} (b) forward current and module exposed in the Caribbean with 45% power loss (M3) taken at 1/10 I_{SC} (c) and I_{SC} (d) forward current.

The concentration of acetic acid was equal to 82±14 µg/g$_{EVA}$ for the reference module (M1), to 498±87 µg/g$_{EVA}$ for the module with 31% power loss and to 827±144 µg/g$_{EVA}$ for the module with 53% power loss. It is reasonable to assume that the values for M3 and M4 would have been included within the range mentioned above. These results are particularly interesting because they show how the acetic acid production upon exposure was severe for the EVA extracted from modules exposed in the tropical climate.

6.4.2 Backsheet material identification

As a preliminary procedure, the backsheets were cut and embedded in an acrylic resin to look at the cross section for further analysis. The so prepared samples were characterized by means of optical microscopy and FT-IR microscopy. The objective of the investigations was to determine the thickness of the different polymer layers constituting the backsheets and to identify the

polymers, respectively. The device used for the measurements mentioned above was an Olympus Microscope BX51 reflecting microscope.

The materials constituting the backsheet were proven to be the same for each PV module. The identified structure for each backsheet can be seen in Figure 6.11. Six layers were identified. Layer 1 corresponds to the outer layer of the backsheet, which is directly in contact with the environment, and was identified as PET.
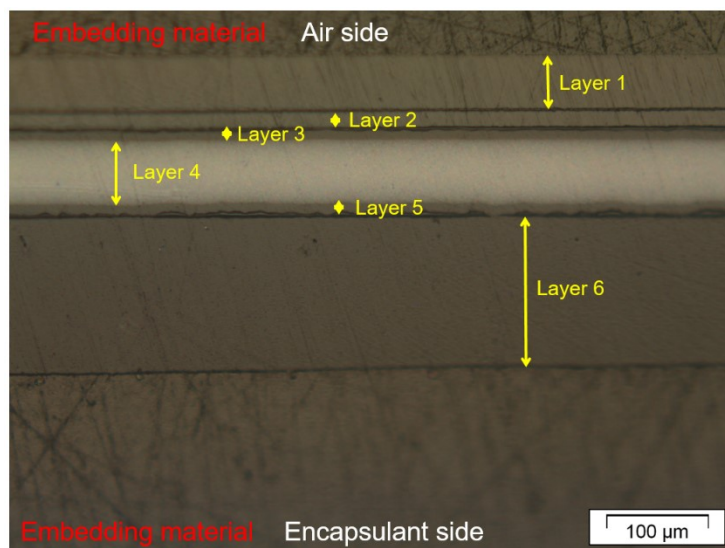

Figure 6.11: Microscope image of the cross section of a backsheet sample.

Layers 2 and 3 are possibly an adhesive layer used to connect the outer layer with the core layer of the backsheet and from FT-IR analysis, it seems to be acrylate-based. Layer 4 is the core layer of the backsheet and it is PET based. Differently from the other layers, which appear to be transparent, the core layer is white looking due to the presence of whitening agents, presumably TiO_2. Layer 5 is an additional adhesive layer and layer 6 is the inner layer in contact with the encapsulant material. The inner layer is based on polypropylene. All the backsheets analyzed are characterized by the same overall thickness that is about 300 μm.

6.4.3 TD GC/MS

The results of the TD-GC/MS measurements of EVA extracted from M1 (reference module) are showed in Figure 6.12. The same additive composition was identified for materials extracted from all positions. A 2,6-bis(1,1-dimethylethyl)-4-methyl phenol (also known as butylated hydrohytoluene,

BHT) was detected as primary antioxidant at a retention time of about 15 min. Additionally, a phosphoric acid, tris(2-ethylhexyl) ester was detected at about 24.5 min and identified as a secondary antioxidant. Finally, a [2-hydroxy-4-(octyloxy)phenyl]phenyl methanone was detected at about 27 min and it corresponds to an UV absorber. Interestingly, the primary antioxidant could not be detected in the front encapsulant, although no difference was reported in the bill of materials between front and back encapsulant. The same stabilizers detected in M1 could be detected also in M2. Once again, the primary antioxidant could not be in the front encapsulant, Figure 6.13.
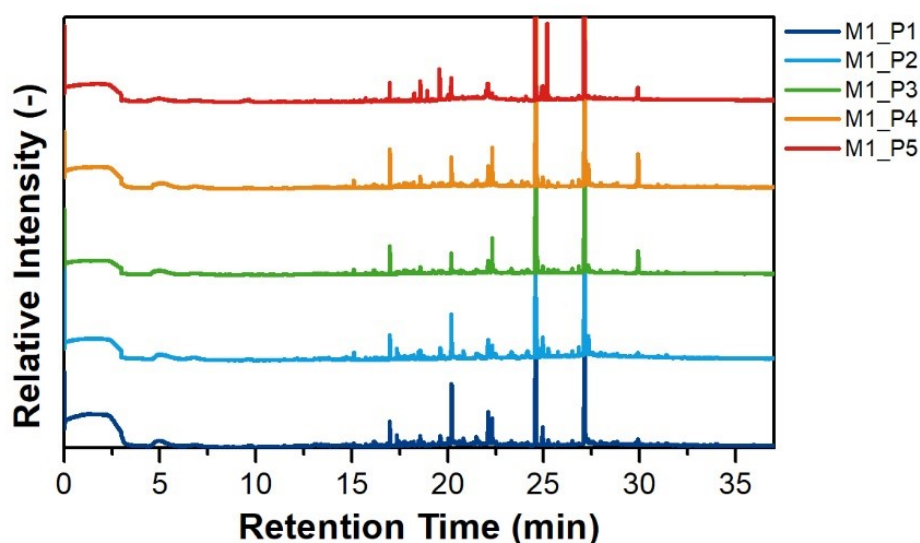

Figure 6.12: Chromatograms of EVA encapsulant withdrawn from different positions (P1-P2 back encapsulant, P3-P4 back encapsulant junction box, P5 front encapsulant in the middle of the module) from the reference module.

The qualitative additive analysis performed on M3, Figure 6.14, revealed the presence of the secondary antioxidant in the EVA samples withdrawn from each area of the PV module. The primary antioxidant was detected in the back encapsulant (P1, P2), not homogenously in the back encapsulant underneath the junction box (P3 but not in P4) and not detected in the front encapsulant. The UV absorber could be detected in the back encapsulant and could not be detected in the front encapsulant.

The EVA withdrawn from M4, Figure 6.15, showed the same additive distribution as in M3. The back encapsulant was characterized by the presence of primary and secondary antioxidant and UV absorber. The back encapsulant underneath the junction box showed the secondary antioxidant and the UV

absorber, the primary antioxidant was not homogenously distributed. The front encapsulant showed only the secondary antioxidant.

Figure 6.13: Chromatograms of EVA encapsulant withdrawn from different positions (P1-P2 back encapsulant, P3-P4 back encapsulant junction box, P5 front encapsulant in the middle of the module) from the module exposed in Germany.

Figure 6.14: Chromatograms of EVA encapsulant withdrawn from different positions (P1-P2 back encapsulant, P3-P4 back encapsulant junction box, P5 front encapsulant in the middle of the module) from the first module exposed in the Caribbean.
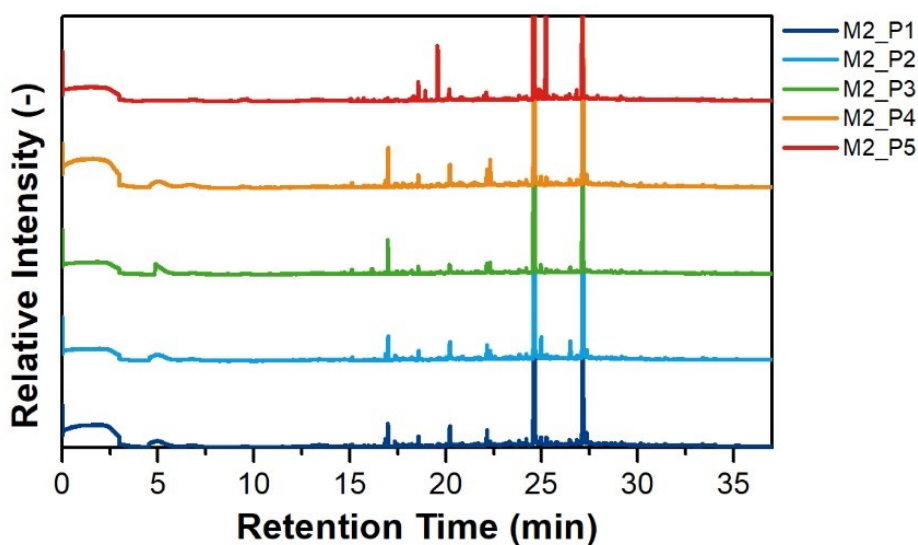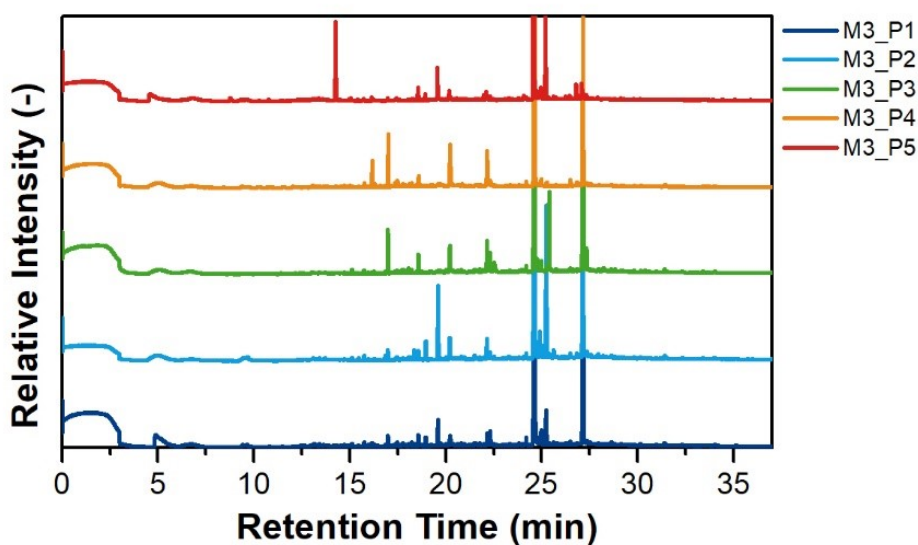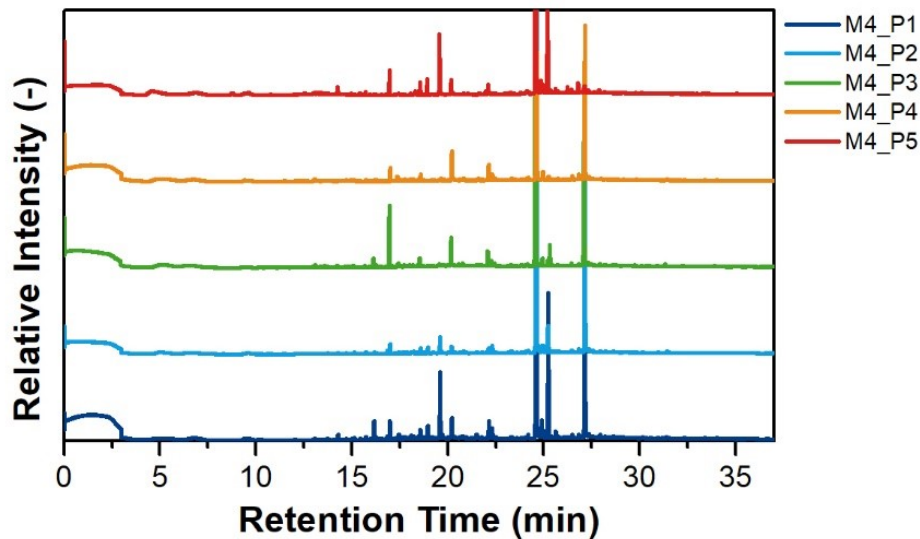
Figure 6.15: Chromatograms of EVA encapsulant withdrawn from different positions (P1-P2 back encapsulant, P3-P4 back encapsulant junction box, P5 front encapsulant in the middle of the module) from the second module exposed in the Caribbean.

To summarize, the primary antioxidant could not be detected in the front encapsulant regardless the location of exposure, namely Germany or the Caribbean. The reference sample did not show presence of primary antioxidant in encapsulant as well as the other modules. Though the composition of front and back encapsulant should have been the same according to the information available in the bill of materials, the results showed a discrepancy. The back encapsulant, indeed, requires a more effective stabilization recipe towards oxidative reactions, as oxygen molecules might penetrate from the polymer backsheet in the first place. The encapsulant samples, withdrawn from M1 and M2, between the cell and the backsheet showed, indeed, presence of primary and secondary antioxidants. The modules exposed in the Caribbean, however, showed an inhomogeneous distribution of the primary antioxidant, which is missing in correspondence of the junction box. Higher temperatures developed near the junction box [26] might be the main cause of the stabilizer's consumption in that area of the module. Additionally, the UV absorber could be detected in the front encapsulant of M1 and M2, but not in M3 and M4. Possibly, the higher levels of radiation that the modules experienced during exposure in tropical climate were too high and the stabilizer was no longer

effective after about 7 years of operation. A summary of the results can be seen in Table 6.1.

Table 6.1: Summary of TD-GC/MS measurements of the encapsulants.

	Additive	Back EVA (P1)	Back EVA (P2)	Back EVA J-Box (P3)	Back EVA J-Box (P4)	Front EVA (P5)
M1	Primary antioxidant	✓	✓	✓	✓	n. d.
	UV absorber	✓	✓	✓	✓	✓
	Secondary antioxidant	✓	✓	✓	✓	✓
M2	Primary antioxidant	✓	✓	✓	✓	n. d.
	UV absorber	✓	✓	✓	✓	✓
	Secondary antioxidant	✓	✓	✓	✓	✓
M3	Primary antioxidant	✓	✓	✓	n. d.	n. d.
	UV absorber	✓	✓	✓	✓	n. d.
	Secondary antioxidant	✓	✓	✓	✓	✓
M4	Primary antioxidant	✓	✓	n. d.	✓	n. d.
	UV absorber	✓	✓	✓	✓	n. d.
	Secondary antioxidant	✓	✓	✓	✓	✓

✓= detected, n. d. = not detected

6.4.4 FT-IR ATR Spectroscopy

EVA encapsulant samples were withdrawn from the modules in different areas to and FT-IR ATR spectroscopy measurements were performed to investigate possible changes in the chemical structure of the EVA's surface in contact with different module's materials. In particular, the measured side of the EVA samples taken from the backside was the one directly in contact with the backsheet, possibly more susceptible to oxidation, due to the shorter oxygen

transport pathway. For the EVA withdrawn from the front side, the side directly in contact with the glass corresponds to the surface object of the investigation. The characteristic bands of EVA were extensively discussed in the previous chapters (Chapter 3 and Chapter 4) and the most relevant bands and their assignments are summarized in Table 6.2.

Table 6.2: FT-IR ATR spectroscopy bands of EVA and their assignments

Wavenumber [cm^{-1}]	Assignment	Remark
2920	Asymmetric stretching vibration of CH_2	Ethylene moieties
2850	Symmetric deformation vibration of CH_2	Ethylene moieties
1736	C=O stretching vibration	Vinyl acetate moieties
1465	Asymmetric deformation vibration of CH_2	Ethylene moieties
1370	Symmetric deformation of CH_3	Ethylene moieties
1238	C–O–C stretching vibration	Vinyl acetate moieties
1020	C–O–C stretching vibration	Vinyl acetate moieties
960-940	CH out-of-plane deformation vibration of vinyl ether	Degradation product
910	CH out-of-plane deformation vibration of vinyl	Degradation product
720	CH_2 skeleton rocking vibration	Ethylene moieties

The typical bands for ethylene units are visibe at 2920 cm^{-1}, 2850 cm^{-1}, 1465 cm^{-1}, 1370 cm^{-1} and 720 cm^{-1} (see Figure 6.16). The vinyl acetate related bands are located at 1736 cm^{-1}, 1238 cm^{-1} and 1020 cm^{-1}. The additional bands presents in the region between 1600 cm^{-1} and 1500 cm^{-1} might be related to additives and/or degradation products [27]. Looking at the spectra with a naked eye it seems that there are no significant differences between the materials extracted from different areas of the modules as well as from different modules.
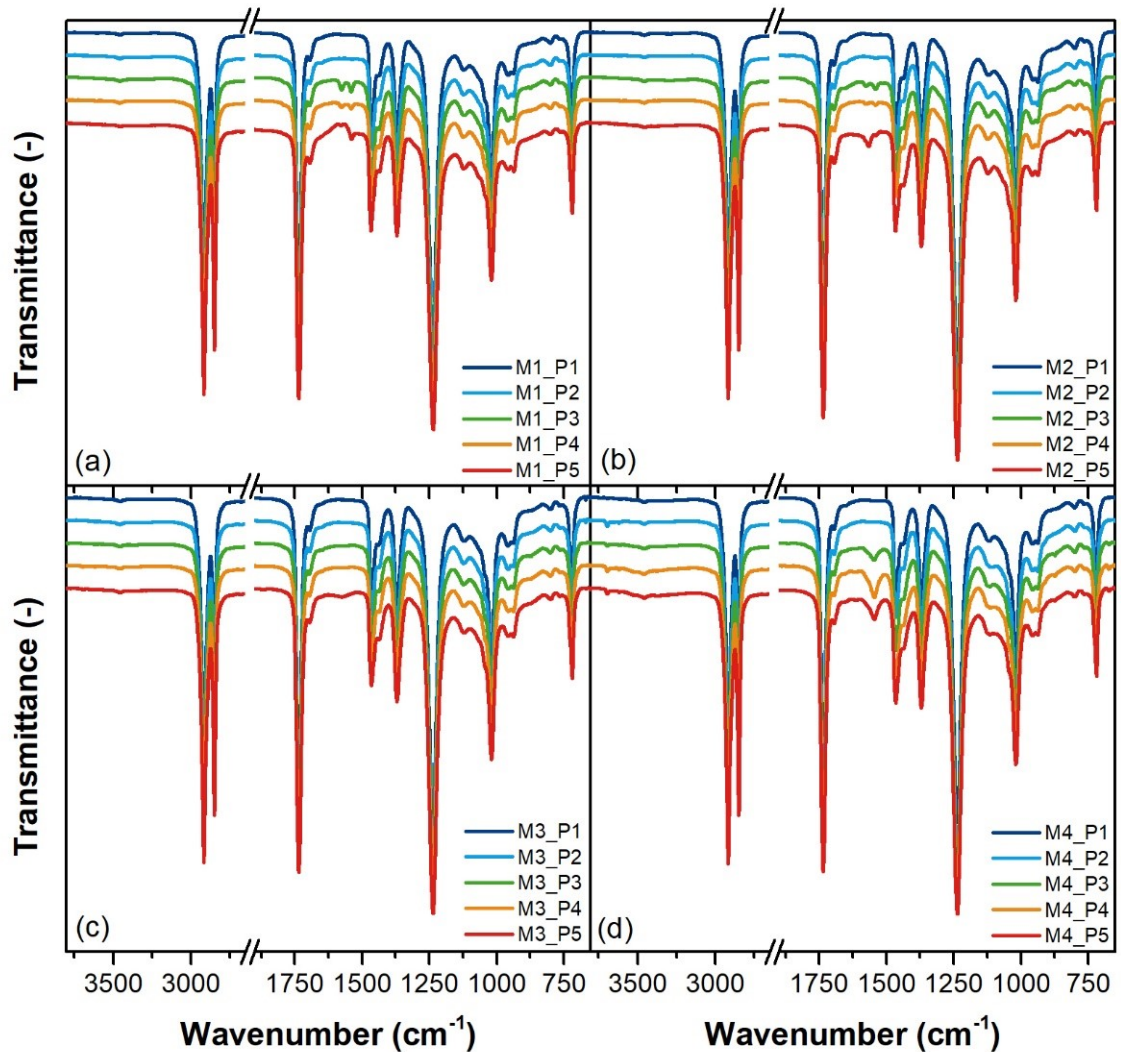
Figure 6.16: FT-IR ATR Spectra of EVA encapsulant withdrawn from different positions (P1-P2 back encapsulant, P3-P4 back encapsulant junction box, P5 front encapsulant in the middle of the module) from the reference module – M1 (a), from the module exposed in Germany – M2 (b), from the modules exposed in the Caribbean – M3 (c) and M4 (d).

It seems that there is a small reduction in the intensity of the bands zooming in the region between 1800 cm^{-1} and 650 cm^{-1} related to vinyl acetate units for the samples taken from the front encapsulant in the modules exposed in the tropical climate (M3 and M4) with respect to the materials taken in different positions (Figure 6.17). The decrease the intensity of the bands in the region mentioned above is often associated to the occurrence of the deacetylation process. However, the trend seems to be very limited and no clear conclusions regarding material degradation might be derived from these results.
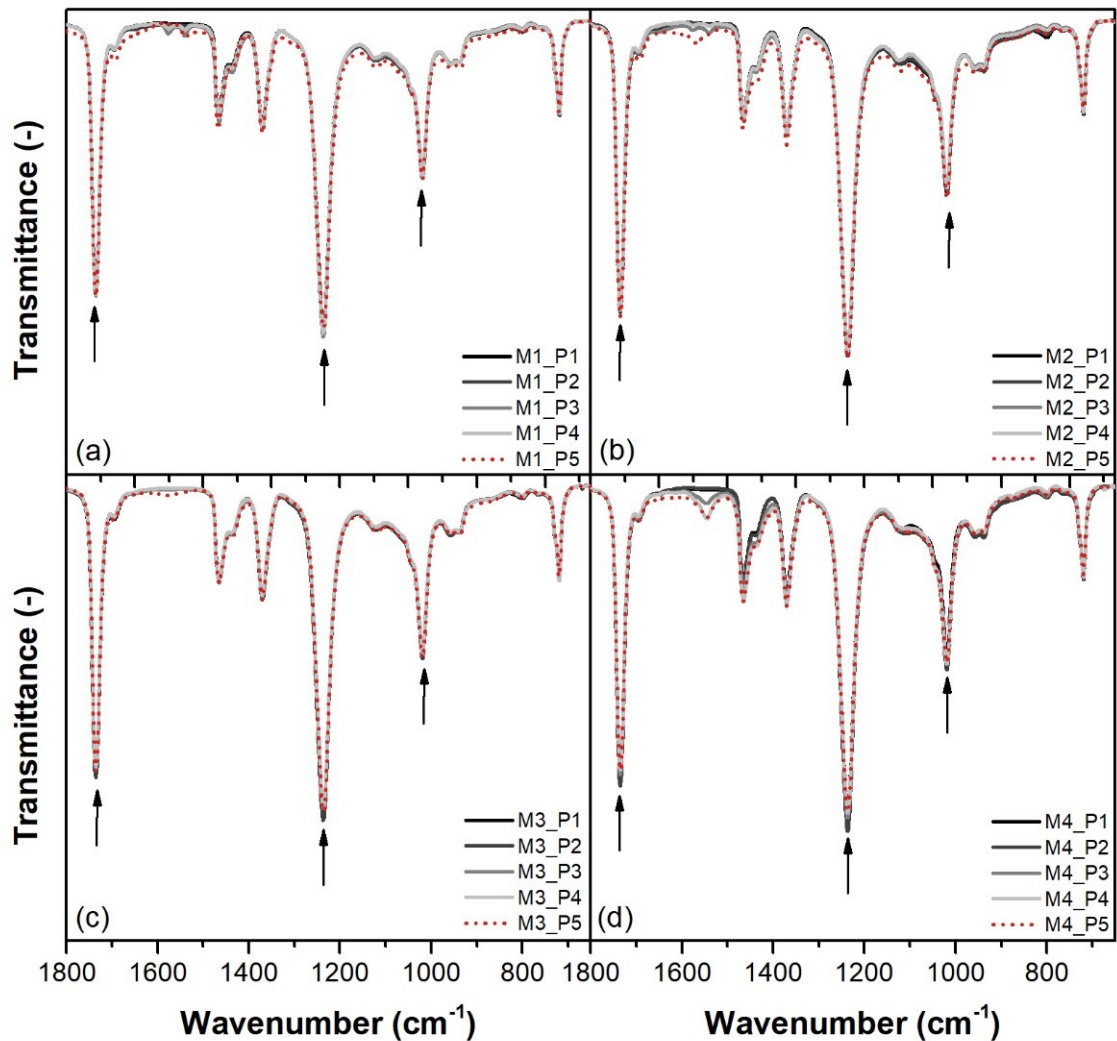
Figure 6.17: Zoom of FT-IR ATR spectra of EVA encapsulant withdrawn from different positions (P1-P2 back encapsulant, P3-P4 back encapsulant junction box, P5 front encapsulant in the middle of the module) from the reference module – M1 (a), from the module exposed in Germany – M2 (b), from the modules exposed in the Caribbean – M3 (c) and M4 (d).

Oxidation indices were calculated based on the measured spectra of all the extracted materials at least three measurements were performed for each sample and averaged. The results are showed in Figure 6.18 and the error bars correspond to the standard deviation between the measurements.

The samples extracted from the reference module (M1) showed similar OI values, regardless of the position of the module from where the sample was extracted. The OI values of the modules operating outdoor showed higher values compared to those of the reference module, although it was not possible to observe a clear trend between the different locations of exposure.
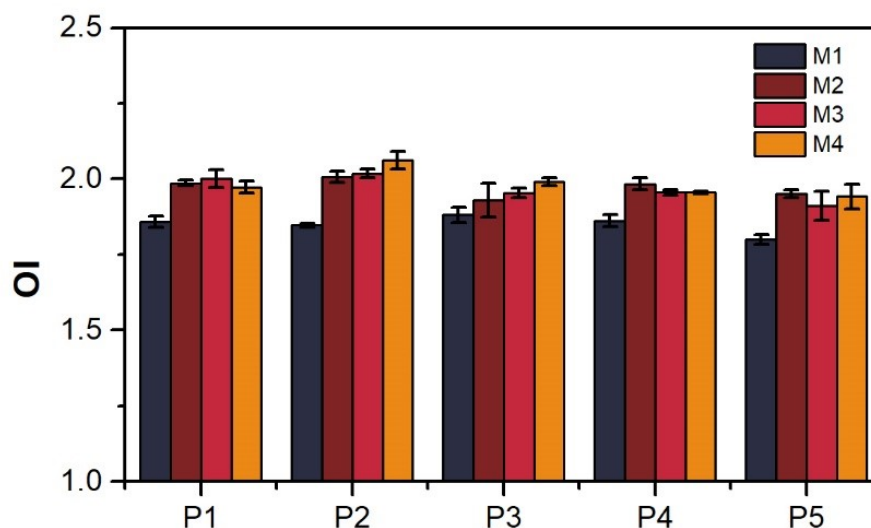
Figure 6.18: Oxidation indices measured from the ATR spectra of the encapsulants withdrawn from the four different module areas: back encapsulant (P1-P2), back encapsulant underneath the junction box (P3-P4), front encapsulant (P5).

6.4.5 DSC

Thermal properties of encapsulant extracted from the PV modules were characterized by means of DSC analysis and the results are shown in Figure 6.19. The thermographs representing the first heating step of the DSC analysis showed a melting peak area between 29 °C and 78 °C for the reference module (M1). The module exposed in Germany, showed a melting area between 26 °C and 85 °C with multiple peaks observable in this area due to rearrangements of the crystalline structures due to melting of crystals and recrystallization at lower temperatures. The modules exposed in the Caribbean (M3 and M4) showed melting regions similar to the one observed for M2. However, subtle differences can be seen between the modules exposed in Germany and in the Caribbean. The latter, indeed, showed a more relevant melting area within the temperature interval 26 °C – 60 °C, whereas the module exposed in Germany showed peaks with more pronounced intensity at higher temperatures. This behavior could be explained with the different temperature that the polymers experienced during PV modules operation. As described in previous sections, Germany is characterized by more pronounced differences between maximum and minimum module temperature, especially during warm season. The temperature variation might have favored thermodynamic rearrangements of crystalline structures.

The melting peak temperatures extracted from the thermograms representing the second heating step of the DSC analysis are summarized in Figure 6.20. The melting peak of the materials extracted from the reference modules are, regardless the position, higher than the melting temperatures of the material extracted from modules exposed outdoor, regardless the location of exposure. The modules exposed in Germany and the Caribbean did not show a significant trend. The only relevant difference could be observed for the material extracted in P5 (front encapsulant between glass and solar cell). The samples extracted from the modules exposed in the Caribbean showed a melting peak temperature of about 55 °C, whereas the material taken from M2 showed a value of about 57 °C and the reference module a value of about 60.4 °C.
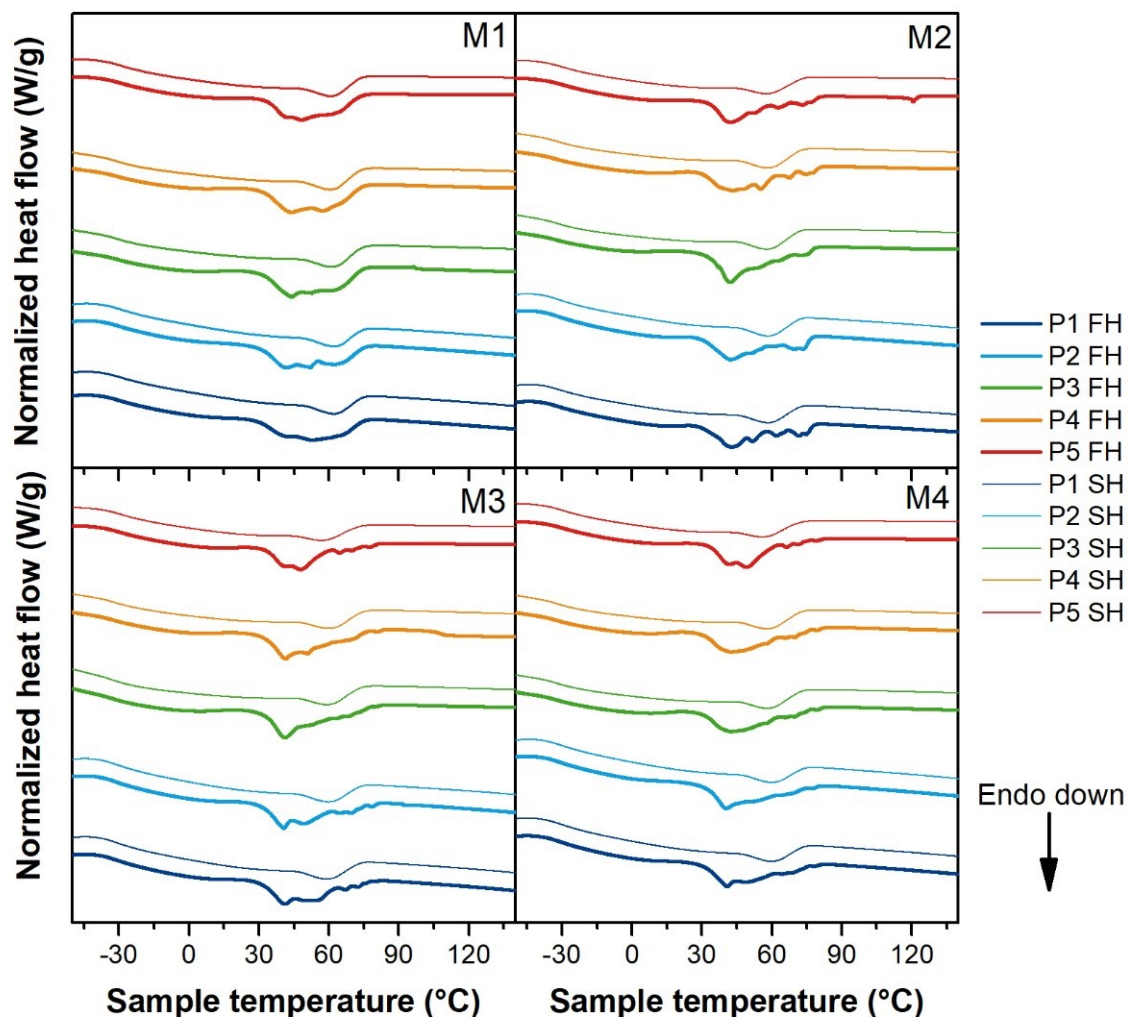

Figure 6.19: DSC thermograms of EVA encapsulant withdrawn from different positions (P1-P2 back encapsulant, P3-P4 back encapsulant junction box, P5 front encapsulant in the middle of the module) from four modules (M1 – Reference,

exposed in Germany, M3 and M4 – exposed in the Caribbean). Thick lines are referred to first heating curves (FH), thin lines to second heating curves (SH).

This behavior, once again, could be explained from the higher temperature reached by the encapsulant above the solar cell due to the effect of the solar radiation during the exposure time. The almost constantly higher module temperature experienced by the modules in the Caribbean most likely caused a reduction of the EVA molecular mass, resulting in a decrease of the melting temperature. Finally, the results of the crystallinity evaluation are displayed in Figure 6.21. The results did not show very significant differences. The samples extracted from the backside showed crystallinity values between 3% and 4%, without showing a particular trend. The samples extracted from the front side of the modules exposed in the Caribbean showed lower crystallinity values compared to the other modules.
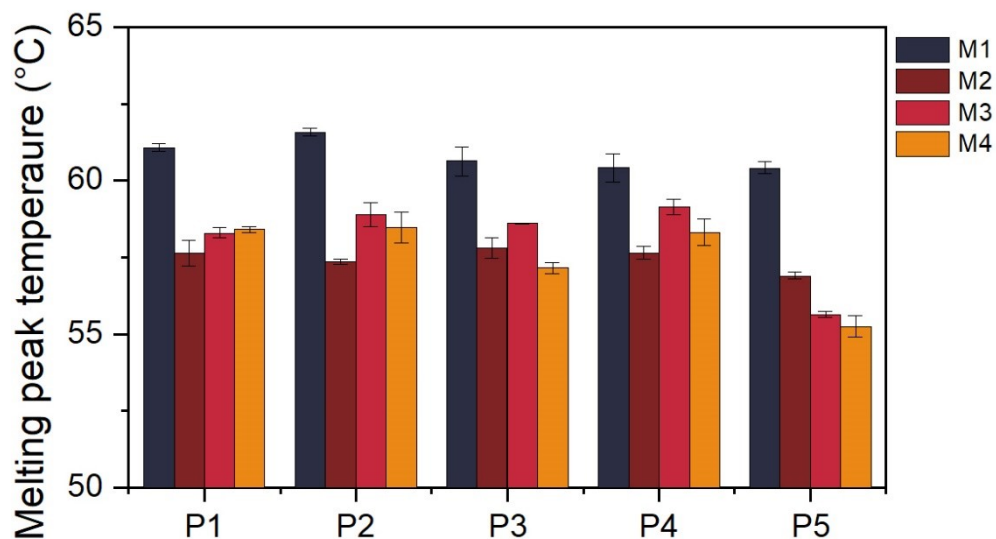

Figure 6.20: Melting peak temperatures extracted from the second heating curves of DSC thermograms for the EVA withdrawn from M1 to M4 in the areas: back encapsulant (P1-P2), back encapsulant underneath the junction box (P3-P4), front encapsulant (P5).
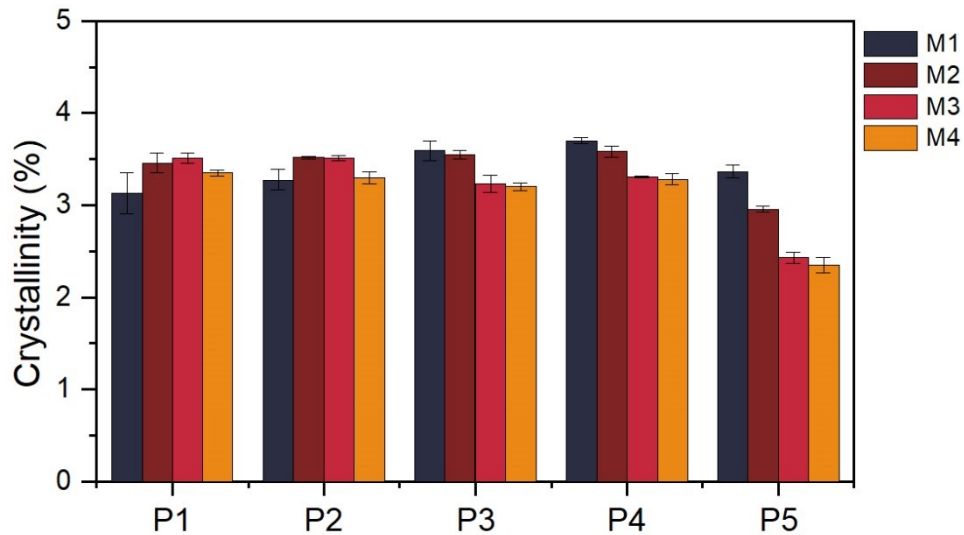
Figure 6.21: Crystallinity calculated from EVA melting peak in the second heating curves of DSC thermograms for the EVA withdrawn from M1 to M4 in the areas: back encapsulant (P1-P2), back encapsulant underneath the junction box (P3-P4), front encapsulant (P5).

6.4.6 TGA

The EVA encapsulant material extracted from the different areas of the PV modules was investigated by means of TGA and the results are shown in Figure 6.22. The curves are very similar to one another and no clear differences can be identified by naked eye when looking at them. The only noticeable difference is that the residue at 550 °C is higher for all the samples extracted from the front side with respect to the samples extracted in the different areas of the module. The samples extracted from P1 to P4 are encapsulant removed from the backside of the module, between the solar cell and the polymer backsheet, whereas the P5 samples were taken out from the front side of the module, between the solar cells and the glass. During the extraction procedure, it was easier to detach the encapsulant from the backside of the cell rather than from the front. Additionally, the residue of the solar cells present on the front EVA were scratched manually to remove as much material as possible, however it was not possible to remove completely all the residues. This discrepancy in the sample preparation procedure might have led to a difference in the residue at the end of the measurements. T_5 values were extracted from the thermograms of the extracted samples and the results are shown in Figure 6.23. Within the

same module, T_5 values did not show significant differences regarding to the area of the module from which the materials were extracted. However, little differences could be observed when looking at the EVA taken from the same position of different modules. In this case, indeed, the T_5 values of the thermograms related to EVA taken from the reference module are slightly higher that the T_5 values referred to the encapsulant material taken from modules operating in the field, regardless of the location and regardless of the area of extraction. The results are in good agreement with the trend of the OI values described in chapter 4, namely the slight reduction in the materials' thermal stability well correlates with an initial occurrence of materials' oxidation.
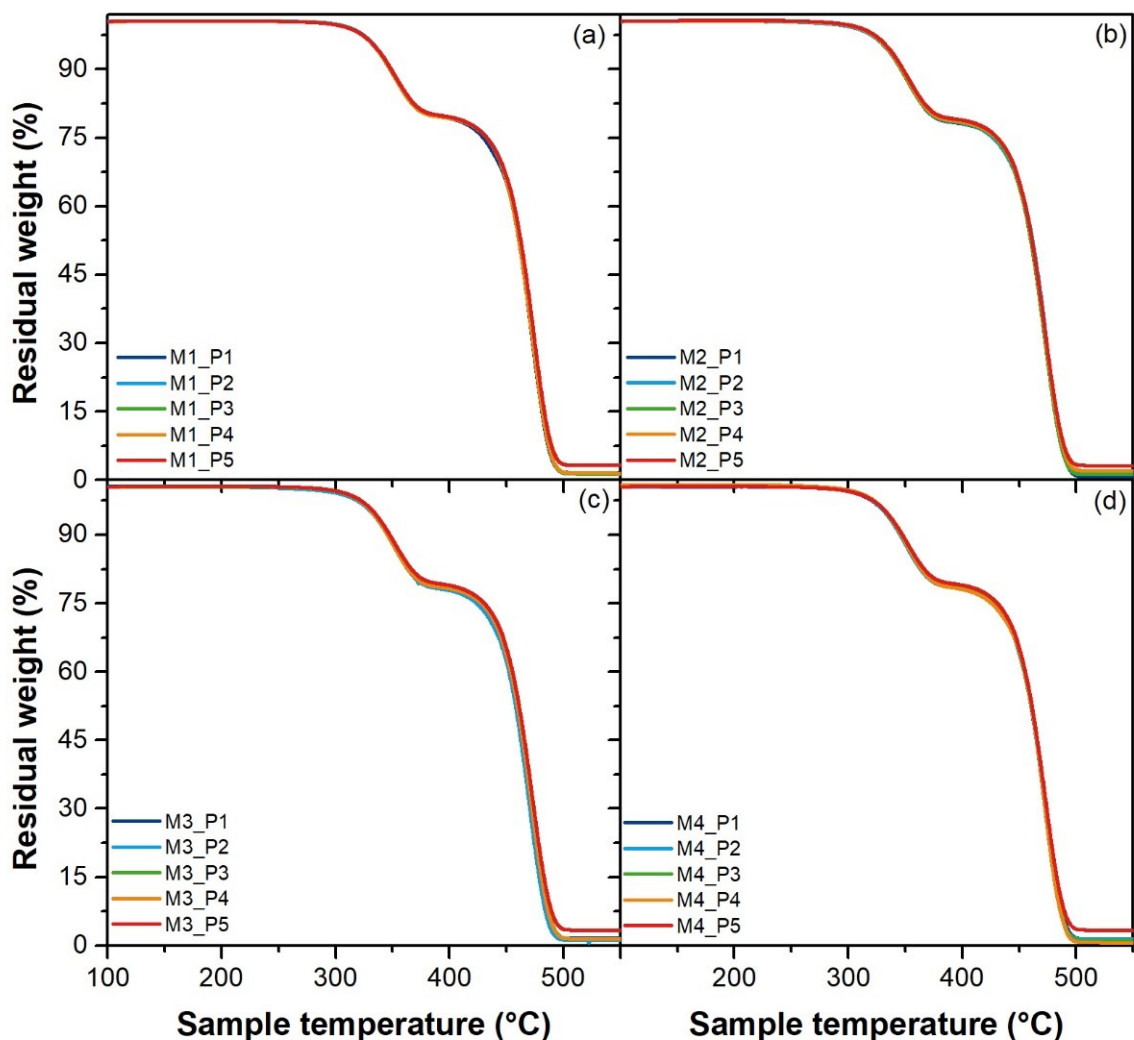

Figure 6.22: TGA thermograms of EVA encapsulant withdrawn from different positions (P1-P2 back encapsulant, P3-P4 back encapsulant junction box, P5 front

encapsulant in the middle of the module) from the M1 (a), M2 (b), M3 (c) and M4 (d).

However, it is important to notice that neither results from TGA nor results from FT-IR ATR measurements did show evidence of acetic acid production even though high acetic acid concentrations were detected by means of ion chromatography. It seems that even high concentrations of acetic acid are below the limit of detection for the deacetylation reaction using FT-IR ATR or TGA.
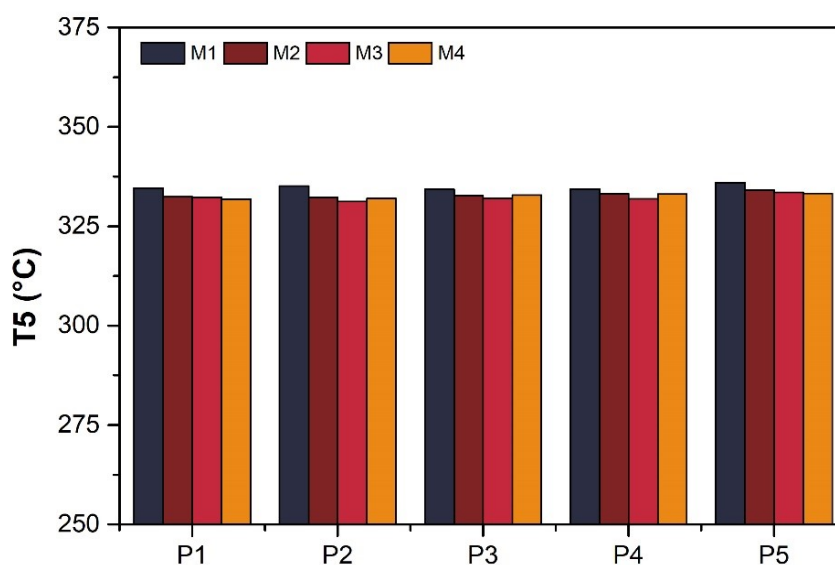

Figure 6.23: T_5 values extracted from TGA measurements performed on EVA encapsulant materials taken from different areas (P1 to P5) of the four PV modules (M1 to M4).

6.5 Influence of microclimate on polymer behavior

The modules exposed in tropical climate showed very strong power loss (about 45% for M3 and about 10% for M4) compared to the reference sample. No significant performance loss was reported from the PV system owner for the module operating in moderate climate (M2). The power loss was associated with a decrease of fill factor and short circuit current. The decrease in fill factor was associated with corrosion of metallization and cell degradation. The acetic acid measurements showed that the modules that experience power losses between 31% and 53% were characterized by acetic acid concentration 6-10 times higher than the reference module (M1). Interestingly, even though significant acetic acid amount was detected via ion chromatography and clear

evidences could be seen from electroluminescence images, no relevant signs of deacetylation could be determined via FT-IR ATR spectroscopy or TGA. The most significant difference that could be detected was related to the thermal properties when observing the melting peak of the second heating curve. The results showed a decrease of the temperature for all the field exposed modules with respect to the reference. In particular, the materials extracted from M3 and M4 in P5 showed a further decrease of the melting peak temperature, and about 5 °C of difference could be detected with respect to the reference module. Based on this evidence, it seems that DSC would be the most sensitive method, compared to FT-IR ATR spectroscopy and TGA, to detect changes in molar mass for EVA encapsulant. Ion chromatography remains the main characterization method able to provide quantitative values of acetic acid concentrations.

The estimated module temperature based on satellite data for the Caribbean was quite higher than the estimated module temperature for Germany. This is due to generally higher ambient temperature in the Caribbean and especially to high solar radiation, which is almost double than the radiation estimated for Germany. A high module temperature combined with a generally high humidity throughout the operating time favored the occurrence of deacetylation. This reaction caused the reduction of molecular mass of the EVA and could be seen from the decrease of its melting temperature detectable in the second heating curve. Additionally, from the methodology point of view, it is once again interesting to see how even a slight increase of the OI calculated using FT-IR ATR spectra well correlated with slight decrease of thermal stability for the materials object of the investigation.

6.6 Summary and conclusions

In this chapter, four PV modules characterized by the same bill of materials were object of the investigation. Three of the four modules were in field operation of two different locations, Germany and the Caribbean, for about 7 years. After this time, the performances of the module exposed in the Caribbean significantly degraded, whereas the module exposed in Germany did not experience significant and unexpected power losses. Additionally, the extent of the power loss was not homogeneous

From the analysis of the satellite-based climate, it resulted that the PV module exposed in the Caribbean experienced an almost double UV dose with respect to the module exposed in Germany during the operating timeframe. Additionally, the Caribbean climate is characterized by generally higher ambient temperature and humidity values than the one typical of the German climate. High ambient temperature and high solar radiation result in a much higher module temperature throughout the whole year. Those factors can be translated into very high stresses that PV materials have to withstand in the Caribbean during operation. The German climate is more subject to seasonality and it seems that the temperature differences (thermal cycles) might be the most relevant stress parameter for PV materials in this type of climate. The modules exposed in the Caribbean experienced the most relevant damage even though the extent of the damage was not homogeneous. The power loss could be correlated especially to the acetic acid production.

6.7 References

[1] G. C. Eder *et al.,* "Climate specific accelerated ageing tests and evaluation of ageing induced electrical, physical, and chemical changes," *Prog Photovolt Res Appl*, vol. 27, no. 11, pp. 934–949, 2019, doi: 10.1002/pip.3090.

[2] D. C. Jordan and S. R. Kurtz, "Photovoltaic Degradation Rates-an Analytical Review," *Prog. Photovolt: Res. Appl.*, vol. 21, no. 1, pp. 12–29, 2013, doi: 10.1002/pip.1182.

[3] M. Halwachs *et al.,* "Statistical evaluation of PV system performance and failure data among different climate zones," *Renewable Energy*, vol. 139, pp. 1040–1060, 2019, doi: 10.1016/j.renene.2019.02.135.

[4] A. Omazic *et al.,* "Relation between degradation of polymeric components in crystalline silicon PV module and climatic conditions: A literature review," *Solar Energy Materials and Solar Cells*, vol. 192, pp. 123–133, 2019, doi: 10.1016/j.solmat.2018.12.027.

[5] J. Ascencio-Vásquez, I. Kaaya, K. Brecl, K.-A. Weiss, and M. Topič, "Global Climate Data Processing and Mapping of Degradation Mechanisms and Degradation Rates of PV Modules," *Energies*, vol. 12, no. 24, p. 4749, 2019, doi: 10.3390/en12244749.

[6] I. Kaaya, M. Koehl, A. P. Mehilli, S. de Cardona Mariano, and K. A. Weiss, "Modeling Outdoor Service Lifetime Prediction of PV Modules: Effects of Combined Climatic Stressors on PV Module Power Degradation," *IEEE J. Photovoltaics*, vol. 9, no. 4, pp. 1105–1112, 2019, doi: 10.1109/JPHOTOV.2019.2916197.

[7] M. Gagliardi and M. Paggi, "Long-term EVA degradation simulation: Climatic zones comparison and possible revision of accelerated tests," *Solar Energy*, vol. 159, pp. 882–897, 2018, doi: 10.1016/j.solener.2017.10.081.

[8] A. Skoczek, T. Sample, and E. D. Dunlop, "The results of performance measurements of field-aged crystalline silicon photovoltaic modules," *Prog Photovolt Res Appl*, vol. 17, no. 4, pp. 227–240, 2009, doi: 10.1002/pip.874.

[9] A. Pozza and T. Sample, "Crystalline silicon PV module degradation after 20 years of field exposure studied by electrical tests, electroluminescence, and LBIC," *Progress in Photovoltaics: Research and Application*, pp. 368–378, 2016, doi: 10.1002/pip.2717.

[10] K.Yedidi, S.Tatapudi, J.Mallineni, B.Knisely, K.Kutiche, G.TamizhMani, "Failure and Degradation Modes and Rates of PV Modules in a Hot-Dry Climate: Results after 16 years of field exposure," in *Photovoltaic Specialist Conference (PVSC), 2014 IEEE 40th*, pp. 3245–3247.

[11] E. Urrejola *et al.,* "Effect of soiling and sunlight exposure on the performance ratio of photovoltaic technologies in Santiago, Chile," *Energy Conversion and Management*, vol. 114, pp. 338–347, 2016, doi: 10.1016/j.enconman.2016.02.016.

[12] F. Carigiet, C. J. Brabec, and F. P. Baumgartner, "Long-term power degradation analysis of crystalline silicon PV modules using indoor and outdoor measurement techniques," *Renewable and Sustainable Energy Reviews*, vol. 144, p. 111005, 2021, doi: 10.1016/j.rser.2021.111005.

[13] M. Chikh, S. Berkane, A. Mahrane, R. Sellami, and N. Yassaa, "Performance assessment of a 400 kWp multi- technology photovoltaic grid-connected pilot plant in arid region of Algeria," *Renewable Energy*, vol. 172, pp. 488–501, 2021, doi: 10.1016/j.renene.2021.02.168.

[14] S. W. Adler, M. S. Wiig, A. Skomedal, H. Haug, and E. S. Marstein, "Degradation Analysis of Utility-Scale PV Plants in Different Climate Zones," *IEEE J. Photovoltaics*, vol. 11, no. 2, pp. 513–518, 2021, doi: 10.1109/JPHOTOV.2020.3043120.

[15] N. Bansal, P. Pany, and G. Singh, "Visual degradation and performance evaluation of utility scale solar photovoltaic power plant in hot and dry climate in western India," *Case Studies in Thermal Engineering*, vol. 26, p. 101010, 2021, doi: 10.1016/j.csite.2021.101010.

[16] E. Annigoni, A. Virtuani, M. Caccivio, G. Friesen, D. Chianese, and C. Ballif, "35 years of photovoltaics: Analysis of the TISO-10-kW solar plant, lessons learnt in safety and performance—Part 2," vol. 27, no. 9, pp. 760–778, 2019, doi: 10.1002/PIP.3146.

[17] S. S. Chandel, M. Nagaraju Naik, V. Sharma, and R. Chandel, "Degradation analysis of 28 year field exposed mono-c-Si photovoltaic modules of a direct coupled solar water pumping system in western Himalayan region of India," *Renewable Energy*, vol. 78, pp. 193–202, 2015, doi: 10.1016/j.renene.2015.01.015.

[18] K. Hara and Y. Chiba, "Spectroscopic investigation of long-term outdoor-exposed crystalline silicon photovoltaic modules," *Journal of Photochemistry and Photobiology A: Chemistry*, vol. 404, p. 112891, 2021, doi: 10.1016/j.jphotochem.2020.112891.

[19] M. C. C. d. Oliveira *et al.*, "Comparison and analysis of performance and degradation differences of crystalline-Si photovoltaic modules after 15-years of field operation," *Solar Energy*, vol. 191, pp. 235–250, 2019, doi: 10.1016/j.solener.2019.08.051.

[20] H. Han *et al.*, "Aging behavior and degradation of different backsheets used in the field under various climates in China," *Solar Energy Materials and Solar Cells*, vol. 225, p. 111023, 2021, doi: 10.1016/j.solmat.2021.111023.

[21] H. Han *et al.*, "Analysis of the degradation of encapsulant materials used in photovoltaic modules exposed to different climates in China," *Solar Energy*, vol. 194, pp. 177–188, 2019, doi: 10.1016/j.solener.2019.10.014.

[22] European Centre For Medium-Range Weather Forecasts, "ERA5 Reanalysis," 2017.

[23] A. L. Buck, "New Equations for Computing Vapor Pressure and Enhancement Factor," *J. Appl. Meteor.*, vol. 20, no. 12, pp. 1527–1532, 1981, doi: 10.1175/1520-0450(1981)020<1527:NEFCVP>2.0.CO;2.

[24] E. Skoplaki and J. A. Palyvos, "Operating temperature of photovoltaic modules: A survey of pertinent correlations," *Renewable Energy*, vol. 34, no. 1, pp. 23–29, 2009, doi: 10.1016/j.renene.2008.04.009.

[25] I. Kaaya, J. Ascencio-Vásquez, K.-A. Weiss, and M. Topič, "Assessment of uncertainties and variations in PV modules degradation rates and lifetime predictions using physical models," *Solar Energy*, vol. 218, pp. 354–367, 2021, doi: 10.1016/j.solener.2021.01.071.

[26] R. J Wieser *et al.*, "*Spatiotemporal modeling of realworld backsheets degradation data*," NREL 2022 PV Reliability Workshop [conference presentation], Online event

[27] A. P. Patel, A. Sinha and G. Tamizhmani, "Field-Aged Glass/Backsheet and Glass/Glass PV Modules: Encapsulant Degradation Comparison," in *IEEE Journal of Photovoltaics*, vol. 10, no. 2, pp. 607-615, March 2020, doi: 10.1109/JPHOTOV.2019.2958516.

7 Summary

The lifetime of polymeric materials exposed in the environment is affected by several factors such as intrinsic stability, additives and stabilizers, climatic conditions, microclimate and so on. Polymers used as encapsulant materials are supposed to last in the environment for at least 25 years and it is very important that they are able to withstand the conditions that they will face. Additionally, the understanding of the degradation mechanisms taking place during operation is everything but an easy task especially when multiple stressors are acting simultaneously.

Even though EVA is still the most widely used encapsulant, its degradation mechanisms taking place during operation are not yet completely understood, this is also because of the variety of formulations available on the market. Each stabilization package and combination with different PV module components might potentially lead to different degradation pathways. New materials are continuously developed and offered as a potential replacement for EVA to overcome the issues associated with its use. For this reason, it is necessary to evaluate the stability of the alternative materials and to investigate their behavior under the effect of typical environmental stress factors.

A comparison of the performances of POE and TPO encapsulants with respect to EVA was presented in the first part of the thesis. The materials were exposed to different artificial ageing tests (with and without UV irradiation). All the encapsulant did not show significant changes after the exposure to DH test. Among the tested materials, TPO showed the worst behavior upon UV exposure ant that was characterized by strong presence of oxidation products, significant discoloration, embrittlement and severe decrease of thermal stability. The antioxidant present in the reference TPO was depleted already in the early stages of exposure, thus leaving the material unprotected from the action of the irradiation. EVA and POE were characterized by a different stabilization recipe, which proved to be more effective in protecting the polymers from degradation up to higher UV doses. However, the materials showed evidence of consumption of stabilizers, signs of oxidation, decrease of thermal stability and discoloration in correspondence of the highest UV dose applied. From the methodological point of view, a good correlation was found

between increase of oxidation indices calculated from FT-IR ATR spectroscopy measurements and decrease of T_5 values calculated from TGA in correspondence of depletion/consumption of stabilizers, in particular antioxidants.

The second and third part of the thesis dealt with further investigation of EVA degradation behavior considering different microclimates, corresponding to sample configurations, exposure to artificial ageing and natural weathering in different climates. An additional topic of interest was the change of materials properties and characteristics and the effect on changes of PV module performances. Mini-modules exposed to different artificial ageing tests were considered in the second part of the thesis, whereas full scale modules operating in different climates were object of investigation for the third and final part. In particular, the second part of the thesis showed that the exposure of mini-modules to UV and especially UV-DH combined test causes the most relevant changes in electrical performances and encapsulant properties. The power losses were more relevant for modules exposed to UV-DH combined test and associated especially with decrease in short circuit current, due to yellowing of the encapsulant. The mini-modules were laminated so that excess of EVA encapsulant was present on the outer perimeter of the glass. In presence of oxygen (excess of encapsulant material directly exposed to the environment) it was possible to observe at the end of the exposure consumption of stabilizers (especially BHT antioxidant) with consequent yellowing, formation of oxidation products, chain scission phenomena with effect on thermal properties and thermal stability. A similar behavior could be seen for the EVA directly exposed in the first part. The illuminated samples, instead, showed. The same trend, with different impacts depending on the artificial ageing procedure applied (dry UV test or UV-DH combined test) could be seen also in the laminated EVA.

Bare EVA samples exposed to DH test did not show significant changes in thermal stability, chemical composition and presence of stabilizers, in accordance to what was showed in the first part of the thesis. The same trend could be seen in this chapter for the laminated encapsulant between cell and glass and between backsheet and glass. The PV module stack including solar cells, glass and backsheet were proven to have a significant effect of changes in

polymer properties upon UV and UV-DH combined exposure, thus substantiating how the microclimate can affect polymer behavior.

The final part of the thesis showed how the climate and especially the microclimate that the polymers see during the operation of the PV modules has a tremendous impact on the performances and the degradation phenomena taking place. Three PV modules with EVA as encapsulant and with the same bill of materials have been in operation in for about 8 years in moderate (Germany) and tropical climate (the Caribbean). A fourth module was stored as a reference during the same period. The results showed that the modules exposed in the tropical climate experienced the most severe power degradation, associated especially with corrosion phenomena due to acetic acid production. The acetic acid concentration was detectable by means if ion chromatography and electroluminescence images, but evidence of deacetylation reaction could not be detected by means of FT-IR ATR spectroscopy or TGA, possibly because below of the limit of detection for these methods. Chain scission processes could be detected observing the T_m values of the DSC second heating run. Moreover, the qualitative additive analysis showed that a consumption of the antioxidant took place for the encapsulants in the area of the PV module beneath the junction box for the modules exposed in tropical climates. Additionally, the UV absorber was no longer detectable in the front encapsulant of the modules exposed to tropical climates.

The results presented in this thesis showed how the microclimate has a fundamental effect in determining how the materials behave upon the exposure to environmental stress factors. The work additionally showed that the degradation mechanisms taking place follow complex pathways interacting with each other. From the methodology point of view, good correlation was found between consumption of antioxidants, increase of OI and decrease of T_5 values. The outcomes of this work can be useful to the PV community to better understand the interactions between materials upon exposure. Additionally, this work showed hot it is necessary to look not only at the overall properties of the encapsulants but also to the changes in the additives present in the polymers, to better understand degradation mechanisms and their effects.

Further work and effort should be focused on making the additive analysis not only qualitative, but also quantitative, which might be particularly challenging

in case of strongly degraded polymers. Furthermore, the presented methodology could be applied to test the reliability of PV modules with alternative encapsulants such as POEs and TPOs. As in the future more and more modules with different encapsulants will be on the market, possibly new degradation modes will be observed. Having a known portfolio of characterization methods able to describe polymer ageing in PV application is already a good starting point to analyze and understand the causes of possible damages. A graphical summary of the main findings of the thesis can be seen in Figure 7.1.
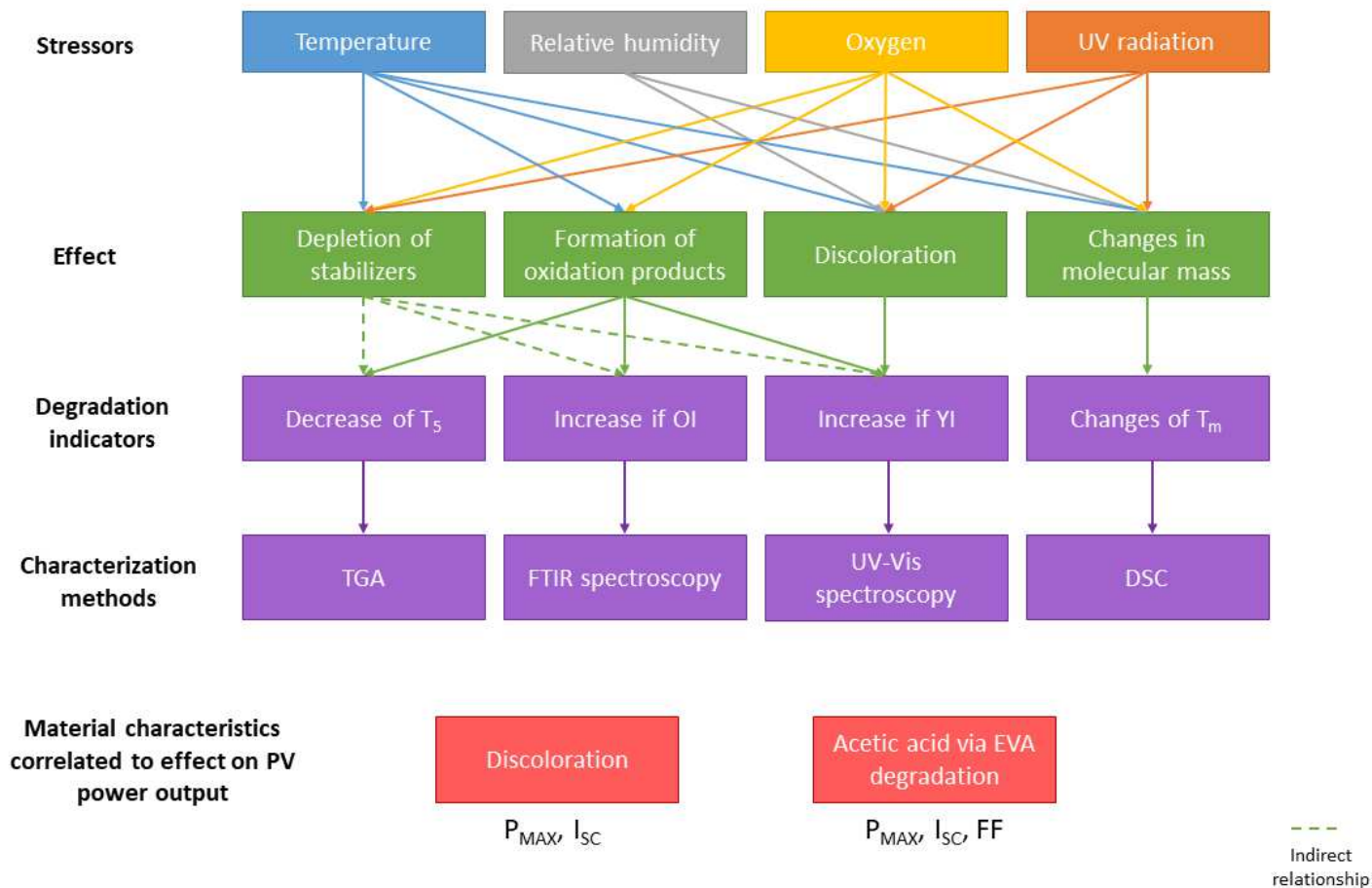
Figure 7.1: Summary of stress factor, effects on material properties and PV power output.